2012

Corrosion of Post-Tensioned Tendons Repaired with Dissimilar Grout

Juan Carlos Rafols
University of North Florida

CORROSION OF POST-TENSIONED TENDONS REPAIRED WITH DISSIMILAR GROUT

by

Juan Carlos Rafols

A thesis submitted to the Department of Civil Engineering
in partial fulfillment of the requirements for the degree of

Masters of Science in Civil Engineering

UNIVERSITY OF NORTH FLORIDA

COLLEGE OF COMPUTING, ENGINEERING AND CONSTRUCTION

July 2012

CERTIFICATE OF APPROVAL

The thesis of Juan Carlos Rafols is approved: (Date)

Signature Deleted

7/11/12

Dr. Nathaniel M. Jackson, Ph.D., PE

Signature Deleted

7/10/12

Dr. Kingsley Lau, Ph.D.

Signature Deleted

7/9/2012

Dr. Adel ElSafty, Ph.D., PE, Chair

Accepted for the Civil Engineering Department:

Signature Deleted

7/25/2012

Murat M. Tiryakioglu, Ph.D., CQE
Director, School of Engineering

Accepted for the College of Computing, Engineering and Construction:

Signature Deleted

7/25/12

Dr. Mark A. Tumeo, Ph.D., JD, PE
Dean

Accepted for the University:

Signature Deleted

8/6/12

Dr. Len Roberson, Ph.D.
Dean of the Graduate School

ACKNOWLEDGEMENTS

First, I want to thank my family for the unconditional support and encouragement to pursue my master's degree.

Second, I want to thank my advisor Dr. Adel ElSafty. It has been an honor being one of his M.S.C.E. students at the University of North Florida. He has encouraged me to pursue knowledge in new fields and to keep growing both academically and professionally. With his constant challenges, he has been able to continually keep the interest and knowledge growth in me, as well as in my fellow students.

Third, I want to thank Dr. Kingsley Lau from the State Materials Office of the Florida Department of Transportation in Gainesville, FL. He has taken me under his wing and helping me in imaginable and countless ways over this journey, while making this experience productive and stimulating. The joy, knowledge, and enthusiasm he shares for his job is immeasurable. Thanks for the patience, knowledge, guidance, motivation, and ideas shared throughout this process.

Special thanks are due to all employees at the State Materials Office of the Florida Department of Transportation in Gainesville, FL. in the Corrosion and Chemical Laboratories. Special thanks to Mario Paredes and Ivan Lasa for opening their doors, not only to me, but to the University of North Florida as well. Thanks to Paul Bradateanu for his contribution to the work. Thanks to Ashley Pole, Steve Schein, Dennis Baldi, Richard Nalli, Thomas Frank, Awilda Merced, Jason Burchfield, Beth Miller, Ron Simmons, Barbara Beatty and all other employees for the help provided when needed, whether it was helping to build samples, testing, answering questions, sharing ideas or jokes, thanks. Thanks to all of you for making part of your family.

Thanks to Matt Brosman from the University of Florida.

TABLE OF CONTENTS

LIST OF FIGURES

LIST OF TABLES

ABSTRACT

A failure associated with steel corrosion was identified in early 2011 in a bridge external post-tensioned tendon, approximately eight years after construction. Large voids in the grout and pockets of non-homogeneous material were identified. The non-homogeneous grout was characterized by high moisture content, and in most cases, the chloride content was lower than conservative threshold values. The non-homogeneous grout also had high pH and high content of sulfates (approximately in the range of 10,000-ppm). As a result, there was an interest in the study of possible corrosion development in repaired systems in which the affected tendons have been re-grouted with dissimilar grouts.

The presence of two distinct grouting materials, manifested by the existing/simulated base grout and a newly introduced repair grout, provided the dissimilar grout condition studied. Corrosion activity was monitored in un-stressed mock up assemblies, in sections retrieved from the failed tendon, and in samples immersed in simulated pore solution. Corrosion activity was monitored through macrocell current, linear polarization resistance, open circuit potential, potentiodynamic scans, and electrochemical impedance spectroscopy. Samples in simulated pore solutions were studied at various pH levels and constituent concentrations. All samples were repaired or built with commercially available grouts.

After analysis, no evidence of corrosion development was found when both existing and repair grout were free of material deficiencies. Corrosion activity was noted in the presence of non-homogeneous grout and an increase in rate was observed due to macrocell coupling with sections containing normal grout. Results suggest that early exposure to sulfate to hydroxyl ion ratio as low 0.35 may prevent steel passivation and result in early high corrosion rates. Otherwise, sulfate to hydroxyl ratios as high as three may not be sufficient to initiate corrosion after formation of passive layer.

CHAPTER 1 - INTRODUCTION

1.1 GROUTED POST-TENSIONED TENDONS

1.1.1 USE: ADVANTAGES AND DISADVANTAGES

Prestressing is a state prior to service loading and can be subdivided into prestressed and post-tensioned construction depending on the sequence of stress application to the steel reinforcement and casting of the concrete member. In this introduction, the term prestressing refers to both prestressed and post-tensioned structural members; however, the thesis topic has specific reference to post-tensioned tendons. Furthermore, there is distinction in post-tensioned construction between grouted and un-grouted tendons[1]. The work presented in the thesis refers to grouted tendons. One of the principal advantages of prestressed concrete members is that they are usually in compression during their service life, helping avoid development of flexural cracks during early stages of loading (Segunpta & Devdas, Prestressed Concrete Structures, 2012; Methods of Prestressing in Concrete, 2011; Salas, Schokker, West, Breen, & Kreger, 2004). This compressive force provided by the prestressing steel prevents the cracks from developing by eliminating or considerably reducing the tensile stresses at the midspan of the section at service loads, which provides for higher bending, shear, and torsional capacities of the section. In the case for post-tensioned tendons, application of tension to the steel strands is done after the hardening of the concrete. Because of the added capacity gained by the prestressing, the sections are able to behave elastically, and almost all of the concrete capacity in compression is used across the entire cross section when applying all loads to the structure.

At the same time and because the concrete section remains un-cracked under service loads, corrosion is reduced, thus increasing the durability of the structure. Prestressing also provides improved performance

[1] Bonded tendons refer to post-tensioned tendons grouted after stressing. In unbounded tendons, each strand is free to move relative to the concrete. Steel strands are typically protected from aggressive environments by a grease coating and/or plastic sheathing.

(resilience) under dynamic and fatigue loading and higher span-to-depth ratios, which allows for larger spans and reduction of self-weight, thus providing a more economical section.

In spite of its advantages, the need for skilled personnel for inspection and construction, quality control, and cost of high strength materials, must be properly addressed.

1.1.2 EXTERNAL TENDONS

When the prestressing of the member is achieved with tendons located outside the concrete, the members are called external tendons. In the case of beams, these tendons usually lie outside the member. For box girders, the tendons lie within the hollow space of the section. This type of prestressing simplifies construction of the members by reducing the presence of ducts within webs/flanges, reducing the required web thickness, simplifying tendon layout, facilitating grouting due to better access, and reducing other construction deficiencies such as grout leakage. In addition, external tendons are easier to inspect during construction and maintenance, and are replaceable in the future. Disadvantages of external tendons include the added cost of construction associated with ducts, anchorages, and deviators; limitation to straight or harped profiles; exposure to deleterious chemicals; vandalism; and in case of total loss of structural integrity of the tendon, the prestressing force disappears over the complete length of the tendon. For protection against corrosion (FDOT, 2002a), this type of tendon relies on being fully grouted, having impervious plastic pipe, concrete cover and enclosure within the surrounding hollow box.

1.1.3 INTERNAL TENDONS

When the prestressing of the member is achieved with tendons located inside the concrete, they are called internal tendons. This type of tendon has the advantage of possibly allowing redevelopment of the strands in case of failures. In addition, because draped tendons can be constructed, design that is more elaborate can be achieved with lower production costs. However, tendons are difficult to inspect and replace, because they are completely embedded in the member.

1.1.4 CONSTRUCTION OF GROUTED TENDONS

As described by the "Post-Tensioned Tendon Installation and Grouting Manual" (Corven & Moreton, 2004) from the Federal Highway Administration, a grouting procedure should be developed and implemented for construction. The recommended procedure is presented in this section.

In general, the contractor should prepare and submit a grouting plan according to the requirements of the project specifications. The Inspection Agency should record and review submittals, and notify the contractor of the acceptability of the plan.

Prior to grouting, tendon ducts, grout inlets and outlets, and anchors should be examined and all debris and water should be removed to avoid blockages or dilution of the grout. Prior to the installation of the steel strands, it is recommended that the ducts be proved free of blockages by passing a suitable size torpedo through the duct. Inlets, outlets, and connections should be proved airtight and free from dirt. Inlets and outlets should be provided with positive shut-off valves capable of withstanding the maximum grouting pressure and the system should be tested with compressed air to verify if any connection, joint or fitting requires sealing or repair. After initial pressurizing, the pressure loss after five minutes should be less than ten percent. This test can be done, depending on the type and complexity of the project: 1) before placement of concrete around ducts, 2) after concrete has been placed but before a girder has been shipped from a yard, 3) after a girder has been erected and continuity splices made with adjacent girders, 4) after precast segments have been erected, or 5) after post-tensioning strands have been installed.

The grout mixer should be capable of producing a homogeneous and stable grout, free of lumps. Either vane-paddle or high-speed shear mixers with a speed of about 1,000 or 1,500 rpm respectively, should be used although high-speed shear mixers distribute cement more uniformly, improve bleed characteristics, and minimize cement lumps. The use of high-speed mixers is recommended when using pre-packaged grouts.

Most mixers are equipped with a mixing tank that discharges through a screen into a storage tank mounted over the grout pump. The screen should contain openings of 1/8 inch (3mm) maximum size to screen lumps from the mix. When thixotropic grouts are used, two identical mixing/storage tanks

are needed that alternate between blending and storage so a new mix can be started while the other is pumped. The screen between the tank and the pump may have openings of 3/16 inch (5mm). The mixer should have the ability to keep the grout agitated for continuous use.

Grout pumps should be a positive displacement type (fluid is moved by trapping a fixed amount of it and then forcing the trapped volume into the discharge pipe) and be able to maintain an outlet pressure of at least 145 psi (1 MPa). In addition, they should have a system of recirculating the grout when pumping is not in progress.

A pressure gage with a full-scale reading of not more than 300 psi (2 MPa) should be installed between the pump outlet and the duct inlet to monitor pressure built up in the hoses. Diameter and pressure between pumps and hoses should be compatible.

For on-site testing of production grouts, daily sampling of production of fluid grout should be performed. The following equipment should be available for grout sampling: 1) clean containers, 2) flow-cone, 3) one liter container and stopwatch for fluidity (ASTM C393), 4) American Petroleum Institute Mud-Balance for density tests, 5) 2 inch (50 mm) molds for making strength test cubes, 6) graduated cylinder and strand sample for Wick Induced Bleed Test (ASTM C940), and 6) for thixotropic grout - Schupack Pressure Grout Test Kit.

If the project requires vacuum grouting, all necessary equipment should be available at the job site at all times. The equipment should be of volumetric measuring type with the ability to measure the volume of a void and supply a measured volume of grout to fill the void.

A standby grout mixer and pump should be available at all times during grouting operations and an air compressor must be available to provide oil free compressed air for checking ducts and to blow out any water in the ducts.

Adequate flushing equipment and potable water should be available in the event it is necessary to remove grout from a duct. However, the practice of completely removing grout from a duct should be avoided, as the vacuum grouting method is preferred for repair of partially filled ducts, in most cases.

It is recommended to base the mixing proportions on the approved mix design, and should be batched by weight to an accuracy of +2%. Grout should be continuously mixed until pumped. Water must not be added to increase fluidity if it has decreased by a delay in the use of the grout. Discharged and tested grout should be properly discarded. It is recommended that daily production be monitored by the following test: 1) Production Bleed Test - either wick induced bleed test (non-thixotropic grout) or Schupack pressure bleed test (thixotropic or pre-bagged grouts), 2) Normal, Non-Thixotropic, grout (prior to injection at inlet) - consistency test according to ASTM C-939, 3) Thixotropic Grout - the modified ASTM C939 or "mud-balanced" test of the American Petroleum Institute, 4) Normal, Non-Thixotropic, grout (Discharge at final Outlet) - fluidity test according to ASTM C-939 or Wet Density Method for field samples according to ASTM C138, 5) Thixotropic Grout (Discharge at final Outlet) - fluidity test according to the modified ASTM C-939 or "mud-balanced" test of the American Petroleum Institute.

Prior to grouting, all outlets should be opened and checked to ensure are clear from any debris or water.

Pumping should ensure complete filling of the tendon and it should be a continuous operation. Grout should be ejected from the first, and subsequent outlets, until all entrained air and slugs of water have been removed prior to closing the outlet. At each outlet and final grout cap, pumping should continue until the consistency of the discharged grout is the same as the injected grout. At least two gallons (1.7 L) of grout should be discharged through the final cap before closing it. In normal cases, grout should be injected at a pressure not higher than 75 psi (0.2 Mpa) at the inlet. Pumping pressure should not exceed 145 psi (1 MPa) and the flow rate should be injected at a rate of 16 feet to 50 feet of duct per minute under normal conditions.

1.1.5 MATERIALS

As described in the "Post-Tensioning Tendon Installation and Grouting Manual" (Corven & Moreton, 2004), the satisfactory performance of this systems depends on the appropriate selection of material that make the components of the post-tensioning system.

The steel strands are made of high tensile steel strands comprised of seven individual wires. Six wires are wrapped around a center wire. All strands should be Grade 270 ksi (1860 Mpa) low relaxation

steel conforming to the requirements of ASTM A-416 "Standard Specification for Steel Strand, Uncoated Seven Wire Strand for Prestressed Concrete". Although steel strand is mostly available in two nominal sizes, 0.5 in (13mm) and 0.6 in (15 mm), Grade 270 is available in sizes as small as 0.25 in (6.35 mm). Due to the cold forming process, strand conforming to ASTM A-416 has been reported to be relatively resistant to stress corrosion and hydrogen embrittlement (Corven & Moreton, 2004).

The grout serves the dual purpose of providing alkaline environment around the post-tensioning reinforcement and bonds the tendon to the structure. Historically the use of Type I or II cement has been evident and compliant with specifications, but recently, the requirement for pre-bagged grouts based on performance requirements has gained momentum and is a requirement in many jurisdictions. These pre-bagged grouts are made of cementitious materials, filler, water and admixtures that help improve workability, lower water requirements, meet low bleed requirements, and improve pumping.

The ducts are available in different materials for different applications and type of tendons, but recently the use of high-density polyethylene (HDPE) has become more common in most states with galvanized steel (SCH 40) sections used when deviation of tendons is necessary.

1.2 PROBLEM DEFINITION

Corrosion protection of post-tensioned (PT) steel strand has typically consisted of embedding strand in highly alkaline grout material within a high-density polyethylene (HDPE) duct. The grout environment ideally would promote steel passivation and the HDPE duct would prevent intrusion of moisture and aggressive chemicals into the tendon. However, corrosion development of PT tendons has occurred in several bridges. In early tendon failures in Florida, corrosion had partially been attributed to formation of void spaces in the PT duct due to bleed water accumulation or improper grouting procedures among other material degradation (Powers, 1999; Hartt & Venugopalan, 2002; Corven J. , 2001; FDOT, 2002; Sagües A. , 2005; Sprinkel, 2009). Subsequently, new grout material requirements for PT systems specify minimal bleed water to mitigate corrosion development. Still, recently, corrosion problems have occurred with these newly formulated grouts.

The Ringling Causeway Bridge was among the first PT bridges to be constructed in Florida with the low bleed water grouts. Severe material deficiencies have been observed recently in the external

post-tensioned tendons, where tendon failure due to corrosion had occurred after approximately 8 years of construction. The deficient grout there was typically characterized as having high moisture content, high pore water pH, low total chloride concentrations, and high sulfate concentrations. In cases where up to half of the tendon length was not filled with grout, large voids were sometimes also associated with corrosion. Accelerated corrosion occurred in regions with severe grout segregation, and was aggravated by macrocell formation between regions of dissimilar aerated conditions caused by varying moisture content, distance from vent ports, and strand interstitial crevice environments.

The deficient grout with varying extent of segregation showed characteristics like having different properties and chemistry, which may maintain corrosion activity. Although early repair procedures have been implemented to remove the most severe segregated grout from some locations of the deficient tendons, some concerns on future corrosion progression after initial repairs have been raised.

There is an interest in gauging the extent to which corrosion may develop for repaired PT systems in which void spaces have been re-grouted with dissimilar grouting materials. There is also an interest in corrosion investigation where differences in pore water chemistry may contribute to corrosion development. This study aims at determining the extent to which corrosion macrocell of strand in dissimilar grout materials can form.

1.3 OBJECTIVES AND APPROACH

The objective of this research was to identify the propensity for corrosion in PT tendons repaired with dissimilar grouts. The research was to identify corrosion mechanisms that may occur in tendons with ideal and deficient/partial repair conditions. This study has particular emphasis on conditions found at the Ringling Causeway Bridge due to the discovery of severely segregated grout and corrosion failure. This study also provides implications for repair of other PT bridges that may have similar deficiencies.

The research approach included the following tasks:

Task 1 Identify Corrosion Mechanism

The first task of the research described in this thesis included the identification of the corrosion mechanisms of recent tendon corrosion failures including the Ringling Causeway Bridge.

Task 2 Establish Corrosion Baseline for Repair of Tendon Void Spaces.

The second task was to establish baseline results for corrosion propensity of tendons with void spaces filled with dissimilar repair grout. Test setup was developed to measure corrosion in extracted tendon sections from the Ringling Bridge that had preexisting large void spaces filled with repair grout products.

Task 3 Elucidate Material Corrosion Parameters.

The third task was to prepare laboratory samples based on the findings in Task 1 and to elucidate possible parameters of the corrosion failure at the Ringling Bridge including presence of voids and presence of aggressive chemical species.

Task 4 Elucidate Corrosion Parameters in Repair Conditions.

The fourth task was to prepare laboratory samples to elucidate parameters that may be involved in corrosion formation after introduction of the repair grout, including simulating ideal and deficient/partial repair conditions.

CHAPTER 2 - LITERATURE REVIEW

2.1 BLEED WATER/VOID FORMATION

In the past, void formation inside post-tensioned ducts has been associated with incomplete or improper grouting, air pockets and evaporation of water from bleed water pockets (Schokker, Koester, Breen, & Kreger, 1999). In the case of improper grouting, the void is formed by spaces that are not completely filled with grout during the construction process and air pocket formation through the length of the tendon. Voids due to bleed water result from the separation of water from the cement. In post-tensioned strands, bleed water formation is thought to be accentuated by the interstitial spaces between the strand wires because it provides easy passage for the water but not the concrete (Trejo, et al., 2009). This type of void usually forms near the high intermediate points in the ducts. The bleed water accumulated and associated void space formation has been identified as one of the major causes of corrosion in post-tensioned tendons in many research reports (Powers, 1999; Corven Engineering, Inc., 2001; Parsons Brinckerhoff Quade and Douglas, Inc., 2001). In the presence of these type of voids, it has been identified that dissimilar metallic materials, grout class, oxygen availability, cementitious pore solution pH, carbon dioxide concentration, moisture content, precipitation, time of wetness, relative humidity, chloride concentration, and temperature are among the factors that may influence corrosion (Trejo, et al., 2009). Additional information of corrosion processes are detailed later. In the following, case studies of deficient tendons are presented.

2.2 CASE STUDIES

Bob Graham Sunshine Skyway Bridge: The original bridge that was a steel truss structure that stretched across Tampa Bay. In May 9, 1980, a freight ship hit and destroyed part of the bridge (Trejo, et al., 2009). To replace the bridge and at a cost of $244 million, the Bob Graham Sunshine Skyway Bridge was commissioned and constructed. Eight years after construction, the FDOT found a failed tendon in

a pier. At that time, the top and bottom anchorage zones of the vertical tendons also showed sign of severe corrosion damaged (Trejo, et al., 2009; Brown, 2002).

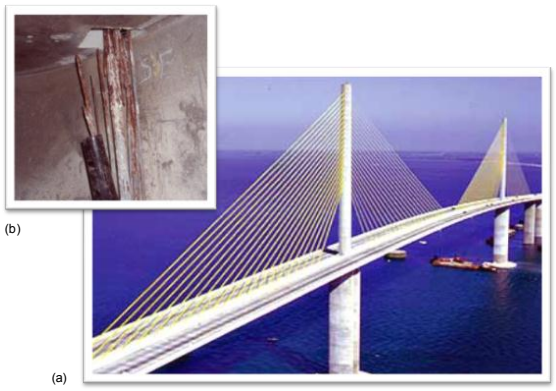

Figure 2.1 Sunshine Skyway Bridge
(a) Bob Graham Sunshine Skyway Bridge, Tampa, FL. (www.pbs.org), (b) Tendon Corrosion in the Sunshine Skyway Bridge (FDOT, 2002).

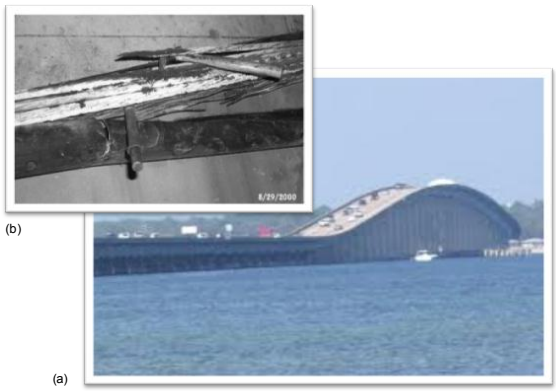

Figure 2.2 Mid-Bay Bridge
(a) Mid-Bay Bridge, Choctawhatchee Bay, FL. (www.travel.emeraldcoast.com), (b) Failure of a tendon on the Mid-Bay Bridge (FDOT, 2002a).

Mid-Bay Bridge: The Mid-Bay Bridge is a low-level precast segmental bridge. During an inspection in the year 2000, corrosion failures were detected in two external tendons. In this case, exposed strand was observed along a bleed water trail and cracked ducts were identified. In total, eleven out of 846 tendons were replaced (FDOT, 2002a). In its final report, FDOT includes the following findings regarding the found damages: a) severe corrosion near anchorages zones, b) large amount of voids close to anchorage zones and midspans, c) variations in grout color, e) low pH near void regions due to carbonation, and f) cracked HDPE ducts.

Niles Channel Bridge: The Niles Channel Bridge is part of the Overseas Highway of the Florida Keys and is a seven miles long, segmental bridge with 234 external grouted tendons (Trejo, et al., 2009). The bridge was constructed in 1983, and after approximately sixteen years of service one of the tendons failed. Damage found in shown in figure 2.3. The failure was attributed to chloride infiltration into a tendon anchorage with voids. The failure at this bridge was responsible for the initiation of efforts to better understand the condition of post-tensioning in Florida bridges (FDOT, 2002a). As a result of this investigation, important steps were taken to improve design requirements and specifications. This include: 1) consideration and encouragement to use pre-bagged grouts, 2) bottom-up grouting was

specified to minimize void development, 3) requirement to show vent locations on construction plans and 4) enhanced training for construction personnel.

Figure 2.3 Advanced Corrosion of Strands within Niles Channel Bridge Tendons (FDOT, 2002a).

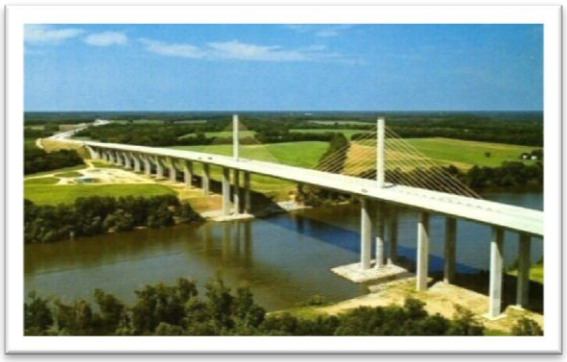

Figure 2.4 Varina Enon Bridge in Virginia (Trejo, et al., 2009a).

Varina Enon Bridge: The Varina Enon is a cable stay, post-tensioned, segmental bridge over the James River in Virginia. In this bridge, one the external tendon failed in 2007 after approximately seventeen years of service (Trejo, et al., 2009).

This tendon failure had the particularity that it occurred approximately three to four years after the repair of identified voids. This repair was performed using newer high-performance repair grouts and the failure was identified to have taken place at the interface between the existing and the new repair grout. This prompted the need for research to study the influence of new repair grouts on tendon corrosion, especially at the interface between grouts (Trejo, et al., 2009). In addition, because of the lack of completely sealed tendons, intrusion of moisture from the environment into the ducts was identified as a possible factor that accelerated the corrosion of the exposed tendons. The Varina Enon final report also identified that approximately 55% of the repaired voids using vacuum machines were not always properly filled (Sprinkel, 2009).

San Francisco Oakland Bay Bridge: The San Francisco Oakland Bay Bridge brought into consideration the effect of delayed grouting time during construction and possible early corrosion development. Due to construction constraints, numerous internal tendon ducts were left un-grouted after post-tensioning for periods up to fifteen months. After the discovery of rust-colored water at vent ports

and anchorage heads in some locations, an extensive investigation was conducted to assess the corrosion condition and evaluation of possible loss of strength in the affected strands. Although extensive testing and assessment of conditions were studied in the identified strands, actual failure was found only on one strand and it was associated with a mechanical distress. The assessment concluded that for this particular bridge, exposure conditions and the delayed grouting apparently had limited corrosion effects. The final report emphasizes that the limited effects seen in this case, in no way was to be viewed as dismissing the adverse consequences of delayed grouting in future construction projects (Sagües, Karins, & Lau, Corrosion Characteristics of Post-Tensioned Strands in Ungrouted Ducts, 2011).

2.3 PT GROUTS

Most pre-bagged grouts, including the ones listed in the FDOT Qualified Product List, are known as thixotropic grouts. This type of grout is one that begins to gel and stiffen in a relatively short time while at rest after mixing. Yet when mechanically agitated, returns to a fluid state with much lower viscosity. Most grouts made with cementitious materials, admixtures and water are non-thixotropic. Thixotropy may be exhibited by some, but not necessarily all, pre-bagged grouts.

A critical feature of a grout is that it should remain pump-able for the anticipated time required to fully inject the tendon. This may be significant for long tendons or where a group of several tendons is to be injected in one continuous operation. Some thixotropic grouts can have very low viscosity after agitation, becoming easy to pump (Corven & Moreton, 2004).

2.3.1 MATERIALS EVALUATION

2.3.1.1 Time to Grout

As required and stated in the FDOT Standard Specification 462, section 6.2, for all bar and strands located in superstructures, the time between the initiation, completion of prestressing, and grouting shall not exceed fourteen calendar days. Any light surface corrosion forming during this period will not be cause for rejection of the prestressing steel (FDOT, 2011).

2.3.1.2 Wick Induced Bleed Test and Schupack Bleed Test

The Wick Induced Bleed Test has the purpose of determining the bleed properties of a grout (VSL International, Inc., 2002). It involves completely immersing a 20 in. (0.5 m) length of strand in a cylinder of grout following a modified version of the ASTM C940 to quantify the amount of water accumulation above the grout (Corven & Moreton, 2004). The test simulates the filtering effects of the strands but does not take into account the pressure to which the grout is subject during grouting procedures. The Schupack bleed test has been created to directly measure the bleed resistance under pressure, as it reproduces the pressure head and some filtering effects in post-tensioned tendons (Hamilton, et al., 2006).

2.3.1.3 Inclined Tube Grout Bleed Test

The inclined tube grout test is used to determine properties and stability of the grouts using a large-scale model and the proposed grouting procedures. One of the major benefits of this test is that the filtering effect of the strands is considered along with the equipment specified for construction. The inclined tube grout bleed test has been specified in Europe and recently established by PTI in the US.

2.3.1.4 Sedimentation Test

The sedimentation test measures the homogeneity of a grout through the measurement of the grout density. This test is performed using transparent PVC tubes and the grout and equipment specified for construction.

2.3.2 FDOT SPECIFICATIONS

Requirements for post-tensioning grout are stated in section 938 of the "Standard Specifications for Road and Bridge Construction", 2010 Edition (FDOT, Specification 938 POST-TENSIONING GROUT, 2009). It covers all grouts used to protect post-tensioning steel differentiated in three applications: horizontal, vertical and repair.

It establishes the general requirements for grouts and states that only grouts listed on the Department's Qualified Product List (QPL) can be used. It recommends that mixing should be done following manufacturer recommendations (FDOT, Specification 938 POST-TENSIONING GROUT, 2009).

For the physical properties of the grout, the FDOT specifications establishes the following requirements (938-4): 1) grout shall not contain aluminum or other components which produce hydrogen, carbon dioxide or oxygen gas (938-4.1), 2) the grout shall meet or exceed the properties in Table 2.1 (testing must comply with the standards and modified ASTM or FM (Florida Method) test methods at normal laboratory temperatures) (938-4.2) and, 3) perform an accelerated corrosion test as outlined in Appendix B of the "Specification for Grouting of Post-Tensioning Structures" published by the Post-Tensioning Institute (938-5).

Variations in testing depending on specific application (horizontal, vertical or repair) is stipulated in section 983-6 (938-6.1, 6.2 and 6.3). Following, in Table 2.1, is a complete list of properties, values, and applicable test method for grouts.

2.3.3 CURRENT CORROSION PROBLEMS

Due to the excess water added to achieve the desired viscosity for grout injection, the cement particles may form lumps that settle, causing water to move upward and collect at the top surface (particularly when water content is significantly greater than needed for the cement hydration). This sedimentation or segregation has been associated with an apparent reduction of grout density (VSL International, Inc., 2002). In addition, this water movement may increase the segregation as it may wash out components and admixtures.

Although this effect was intended to be minimized with the use of the pre-bagged grouts in compliance with the new specifications, severe material irregularities or deficiencies have been observed in recent constructions of PT tendons in Florida Bridges. In recent cases, the deficient grout was characterized by sections with high moisture, wet-plastic, and white chalky material. The main concern is that these sections of segregated grout can create environments with different pore solution chemistry and physical properties, where development of corrosion can occur.

Property	Test Value	Test Method
Total Chloride Ions	Max. 0.4 lbs/yd^3	FM 5-516
Fine Aggregate (if utilized)	99% passing the No. 50 Sieve (300 micron)	ASTM C 136*
Hardened Height Change @ 24 hours and 28 days	0.0% to +0.2%	ASTM C 1090**
Expansion	$\leq$ 2.0% for up to 3 hours	ASTM C940
Wet Density - Laboratory	Report maximum and minimum obtained test value lbs/ft^3	ASTM C 185
Wet Density - Field	Report maximum and minimum obtained test value lbs/ft^3	ASTM C 138
Compressive Strength 28 day (Average 3 cubes)	$\geq$ 7,000 psi	ASTM C 942
Initial Set of Grout	Min. 3 hours Max. 12 hours	ASTM C 953
Time of Efflux	***	***
(a) Immediately after mixing	Min. 20 Sec. Max. 30 Sec.	ASTM C 953
	or Min. 9 Sec. Max. 20 Sec.	ASTM C 939****
(b) 30 minutes after mixing with remixing for 30 sec.	Max. 30 Sec.	ASTM C 939
	or Max. 30 Sec.	ASTM C 939****
Bleeding @ 3 hours	Max. 0.0 percent	ASTM C 940*****
Permeability @ 28 days	Max. 2,500 coulombs at 30 V for 6 hours	ASTM C 1202

*Use ASTM C 117 procedure modified to use a #50 sieve. Determine the percent passing the #50 sieve after washing the sieve.
**Modify ASTM C 1090 to include verification at both 24 hours and 28 days.
***Adjustments to flow rates will be achieved by strict compliance with the manufacturer's recommendations. The time of efflux is the time to fill a one liter container placed directly under the flow cone.
****Modify the ASTM C 939 test by filling the cone to the top instead of to the standard level.
*****Modify ASTM C 940 to conform with the wick induced bleed test as follows:
(a) Use a wick made of a 20 inch length of ASTM A 416 seven wire 0.5 inch diameter strand. Wrap the strand with 2 inch wide duct or electrical tape at each end prior to cutting to avoid splaying of the wires when it is cut. Degrease (with acetone or hexane solvent) and wire brush to remove any surface rust on the strand before temperature conditioning.
(b) Condition the dry ingredients, mixing water, prestressing strand and test apparatus overnight at 65 to 75°F.
(c) Mix the conditioned dry ingredients with the conditioned mixing water and place 800 ml of the resulting grout into the 1,000 ml graduate cylinder. Measure and record the level of the top of the grout.
(d) Completely insert the strand into the graduated cylinder. Center and fasten the strand so it remains essentially parallel to the vertical axis of the cylinder. Measure and record the level of the top of the grout.
(e) Store the mixed grout at the temperature range listed above in (b).
(f) Measure the level of the bleed water every 15 minutes for the first hour and hourly for two successive readings thereafter.
(g) Calculate the bleed water, if any, at the end of the 3 hour test period and the resulting expansion per the procedures outlined in ASTM C940, with the quantity of bleed water expressed as a percent of the initial grout volume. Note if the bleed water remains above or below the top of the original grout height. Note if any bleed water is absorbed into the specimen during the test.

Table 2.1 FDOT Specifications for Grout (FDOT, Specification 938 POST-TENSIONING GROUT, 2009).

2.4 CORROSION BASICS

2.4.1 ELECTROCHEMISTRY

2.4.1.1 Oxidation/Reduction Reaction

As the basis of the mixed potential theory, is the hypothesis that separates any electrochemical reaction into two or more partial oxidation and reduction reactions. In addition, there can be no net accumulation of electric charge during these electrochemical reactions (Popov, 2002). Corrosion involves the destructive dissolution of metals by an electrochemical reaction with its environment, described as a set of redox reactions.

Reaction relevant to corrosion of steel in cementitious material, metal (iron) is oxidized at the anodic sites and electrons are liberated. The metal cation can move into the surrounding concrete as ferrous ions. The oxidation reaction for iron can be described by the anodic reaction,

$$2Fe \rightarrow 2Fe^{+2} + 4e^{-} \quad (1)$$

The electrons flow to the local cathodic site where the reduction reaction takes place. In conditions relevant to corrosion of steel in cementitious materials, the cathodic reaction involves oxygen being reduced at the cathodic sites and consumption of electrons. The reduction can be described by the cathodic reaction,

$$2H_2O + O_2 + 4e^{-} \rightarrow 4OH^{-} \quad (2)$$

To maintain electrical neutrality, the ferrous ions migrate through the concrete pore solution to the cathodic sites where they combine to form iron hydroxides and oxides, commonly known as rust (3) (Portland Cement Association, 2012).

$$2Fe^{2+} + 4OH^{-} \rightarrow 2Fe(OH)_2 \quad (3)$$

A graphical representation of the describe process is shown in Figure 2.5.

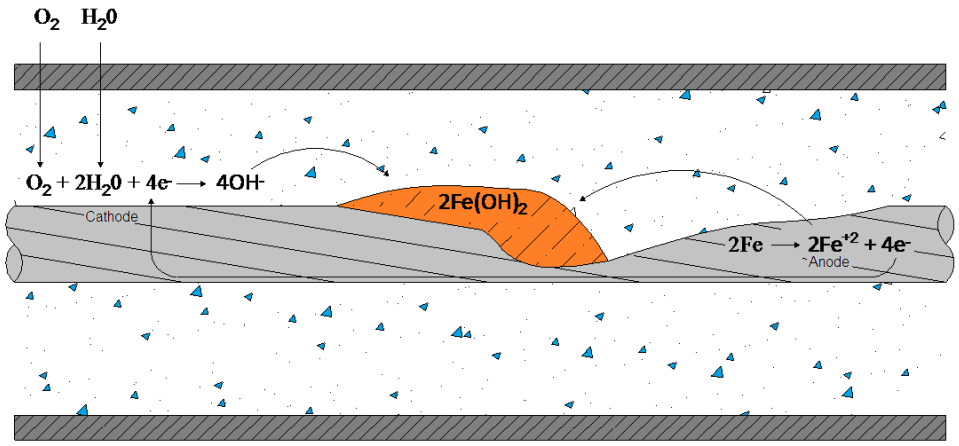

Figure 2.5 Corrosion of embedded metals in cementitious materials.

2.4.1.2 Galvanic Cell

A traditional galvanic cell is an electrochemical cell that derives energy from the redox reactions that takes place inside the cell. It generally consists of two different metals, one that acts as an anode, one that acts as a cathode, a salt bridge or porous membrane, and a wire connecting the electrodes. The salt bridge or porous membrane facilitates the exchange of ions between the metals. An electric current is measured through the switch. The anode is the electrode at which the oxidation occurs. The cathode is the electrode at which the reduction occurs and the salt bridge is the electrolyte. The salt bridge contains the ions involved in the redox reaction.

For the case of post tensioned tendons, corroding sections of the strand will act as an anode while the rest of the strand will act as the cathode. The wet concrete or grout will act as the electrolyte and the metallic connection is provided the strands itself.

2.4.1.3 Passivity

Passivity results when the metal forms a very thin, oxidized, protective film on their surface in corrosive solutions. It is defined as a condition of corrosion resistance due to the formation of a thin surface film under oxidizing conditions.

In iron, the corrosion rate decreases above some critical potential E_p. This corrosion resistance above E_p (Figure 2.6) is define a passivity.

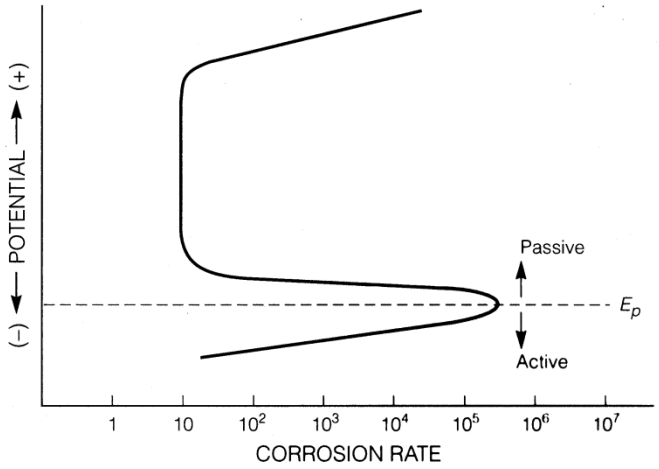

Figure 2.6 Passivity at oxidizing potentials above Ep (Jones, 1996).

Passive corrosion rates are very low, a reduction of 10^3 to 10^6 times below the corrosion rate in the active state is not usual. This film acts a barrier to the anodic dissolution reaction, and because of its fragility, its breakdown can result in unpredictable localized forms of corrosion (Jones, 1996).

In addition, the effectiveness of the passivation film is a function of the pH of the pore solution in contact with the steel. If the pH is generally greater than 11.5 the passivation film in normally maintained and corrosion rates should be very low (Bentur, Diamond, & Berke, 1997). The effectiveness of this film is diminished at pH level below 11.5 or when chloride ions are present.

2.4.2 CORROSION OF STEEL IN CEMENTITIOUS SYSTEMS

2.4.2.1 Oxygen Reduction

The anodic reaction for active corrosion of iron in a cementitious system can be described by reaction (1), but the corrosion rate varies due to changes in the cathodic reduction reaction, given in reaction (2). Manifestation of corrosion in iron near ambient temperatures requires dissolved oxygen in alkaline solutions. Any factors affecting the dissolved oxygen will affect the corrosion rate proportionally

(Jones, 1996). As a result, any event that increases the amount of available oxygen for reaction (2) will cause an increase in the corrosion rate of the steel.

2.4.2.2 Pore Solution

Not only composition of the pore solution in the cementitious material is important, but changes in composition between adjacent or along the steel can have an effect in corrosion development or corrosion rate (Verma & Balasubramanian, 2007). Factors that may affect corrosion development or rate include the amount of water in the grout (moisture content), dry-wet cycles, and the components that can be introduced in the grout with the cycles (ex. ingress of chlorides, chloride diffusion, oxygen availability and pH level).

Pore solutions always contain dissolved ions derived from the cement and usually contain alkali (K^+ and Na^+) and hydroxide ions in relatively high concentrations. In addition, smaller concentrations of calcium and sulfate ions can be found. The OH^- concentration is quite high and is responsible for the high pH values in the pore solution. This high pH (alkalinity) is directly responsible of promoting the passivation of the steel (Bentur, Diamond, & Berke, 1997). Destabilization of the passive film due to reduced pH result in general corrosion.

2.4.2.3 Chloride

The ion of most concern is the chloride ion (Cl^-). This ion has the effect of destabilizing the passive film if present in sufficient concentration. Sources of this ion most commonly include seawater spray, deicing salts, salt contaminated aggregates, and calcium chloride from accelerating admixtures. This destabilization will most commonly occur at discrete locations and result in pitting corrosion.

It has been previously suggested, that there is a minimum chloride concentration, which must be exceeded before depassivation can take place. This concentration is a function of the pH (Bentur, Diamond, & Berke, 1997). The relationship between critical chloride ion concentration in pore solution, and pH has been suggested by Hausman and Gouda from data obtained from experiments and is shown in Figure 2.7.

In practice, most specifications and guidelines, do not refer to the $[Cl^-]/[OH^-]$ ratio as found in pore solutions, but rather refer to total content of chloride in concrete (Bentur, Diamond, & Berke, 1997). Content is usually specified in terms of the percentage by weight of the cement, usually 0.2% of the cement content of the concrete. When assessment of current structures is made, usually critical chloride levels will be specified per unit volume of concrete. As per FDOT specifications, chloride content is limited to a maximum of 0.4 lb/yd^3. As recommended by the American Concrete Institute, chloride content may vary from 0.06 to 0.15 % weight of cement to no limit, depending on the application. Lower limits are required for prestressed systems, as a failure in this type of structures is more severe than in regular reinforced concrete.

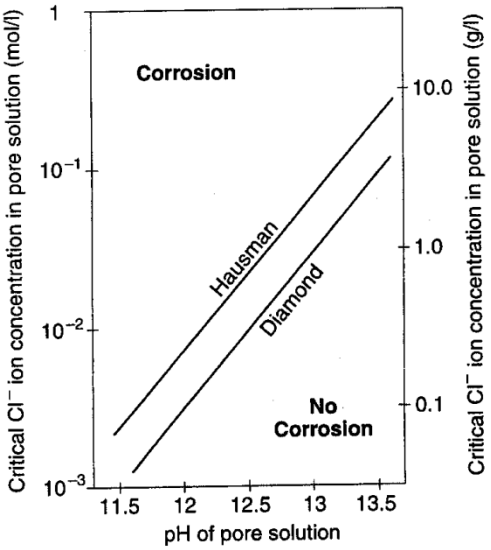

Figure 2.7 Relation between threshold chloride ion concentration and pH (Bentur, Diamond, & Berke, 1997).

Although efforts have been made to establish this limit, effect of chloride content can vary by other variables like mix proportion, water-cement ratio, curing conditions, environmental conditions, degree of carbonation, temperature, relative humidity, and extent of polarization among others.

2.4.2.4 Sulfates

Recently, corrosion in post-tensioned tendons has been associated with pockets of whitish unhardened grout characterized by alkaline pH and high content of sulfate ions (Bertolini & Carsana,

2011) (Kingsley Lau, Ivan Lasa, Mario Paredes, 2011). Corrosion attack has been found at these locations, which has led to failure of the tendon in relatively short periods, similar to recent findings in the Ringling Causeway Bridge in Sarasota, FL. Corrosion has been associated with low levels of oxygen in the interstices space of the tendon strand (Bertolini & Carsana, 2011).

2.4.3 CORROSION TESTING

2.4.3.1 Reference Cell

Any electrochemical cell consists of two half-cells. By making one of the half cell known (reference cell), we are able to isolate the second one for measurement and study. The reference cell is commonly known as the reference electrode, and the potential of the second, or unknown, is called the electrode potential. Measurement of the second is made in particular reference to the reference electrode in the cell (Jones, 1996).

The saturated calomel electrode is one of the most common reference electrode used in laboratories and the most convenient for corrosion purposes (Jones, 1996). It consists of mercurous chloride, Hg_2Cl_2, mixed with a mercury paste on a pool of liquid mercury in contact with a saturated KCl solution. For the measurement taken as part of this project, a standard Saturated Calomel Electrode (SCE) was used.

2.4.3.2 Open Circuit Potential (OCP)

The principle of this technique is essentially taking measurements of the corrosion potential in the strand (unknown potential) with respect to a standard reference electrode (known potential). A schematic of the setup used to make this type of measurement is shown on Figure 2.8.

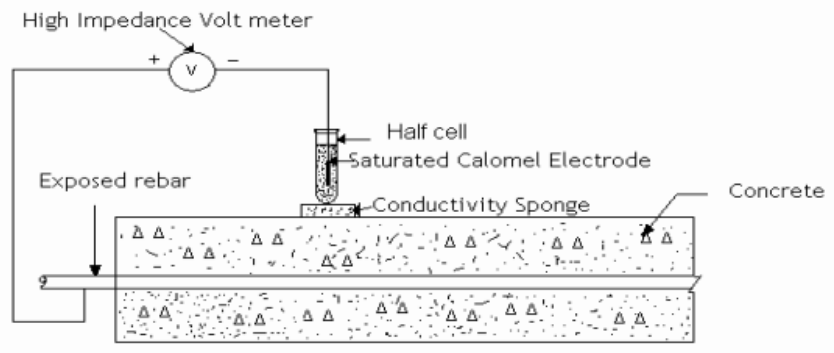

Figure 2.8 Schematic of Setup for Open Circuit Potential measurement (Song & Saraswathy, 2007).

Open Circuit Potential value (mV vs. SCE)	Corrosion Condition
< -456	Severe Corrosion
< -276	High (<90% risk of corrosion)
-126 to -275	Intermediate corrosion risk
> -125	Low (10% risk of corrosion)

Table 2.2 Corrosion condition (risk) related with half-cell potential (SCE only) measurements.

As per ASTM C876 standard (Standard Method for Half-Cell Potential of Reinforcing Steel in Concrete), the probability of corrosion reinforcement for measurements taken using a Saturated Calomel Electrode are presented in Table 2.2.

Although, monitoring of OCP is the most typical procedure for routine inspection of reinforced concrete structures, special care must be taken as a number of factors affect measurements. Among these factors are polarization by limited diffusion of oxygen, concrete porosity, the presence of resistive layers and others. It is suggested that OCP measurements be complemented by other methods (Videm, 1998), as this test will only provide information of corrosion probability and does not indicate corrosion rates. OCP is a very useful technique to identify anodic and cathodic sites in structures when potential maps are developed as per ASTM C-876-91.

2.4.3.3 Macrocell

Macrocell currents measure the current (Amp) passing between discrete embedded metal members (Hansson, Poursaee, & Jaffer, 2007). In general, Macrocell corrosion can occur when an actively corroding metal (anode) is coupled to an inactive metal (cathode), either because of its different composition or environment. The macrocell current is defined as the current between the anodic and cathodic areas and measured currents are good indication of corrosion activity. The current can be measured by connecting a zero-impedance ammeter connected between the anodic and cathodic bars and measuring the current directly (Bentur, Diamond, & Berke, 1997).

This is a fast, non-destructive technique that allows identification of corrosion initiation. Measured corrosion current can be easily related to corrosion rate or mass loss using Faraday's Law by integrating the current along time to determine total charge (coulombs) for a given period.

Special care must be taken, if the resistivity of the material through which the current is being measured is very high, as the macrocell might not occur (Bentur, Diamond, & Berke, 1997) or may be affected by the solution resistance development of the material.

2.4.3.4 Linear Polarization Resistance (LPR)

LPR is a method of determining instantaneous corrosion rate in reinforcing steel in concrete. This technique is fast, non-intrusive, and requires only a connection to the steel (working electrode). The data provides valuable insight of the instantaneous corrosion rates, giving more detailed information than OCP (Song & Saraswathy, 2007).

In LPR measurement, the steel is perturbed by a small overvoltage from its equilibrium potential. This can be accomplished potentiostatically by changing the potential of the steel by a fixed amount, ΔE, and monitoring the current decay, ΔI, after a fixed period. Conditions are selected such that the change in potential, ΔE, falls within the linear Stern Geary range of 10-30 mV (Song & Saraswathy, 2007). This means, restricting the potential to be very close to the OCP. In this range, the current versus voltage curve approximates a straight line. The slope of this line has the units of resistance (ohms) and is called

the Polarization Resistance (Gamry Instruments, 2010). The Polarization Resistance, Rp, of the steel is then calculated from the equation,

$$\mathrm{Rp} = \Delta\mathrm{E}/\Delta\mathrm{I} \qquad \text{Eq. 1.1}$$

from which the corrosion current, $I_{corr,}$ can be calculated by,

$$\mathrm{I_{corr}} = \frac{\beta a \beta c}{2.3\ \mathrm{Rp}\ (\beta a + \beta c)} = \mathrm{B}/\mathrm{Rp} \qquad \text{Eq. 1.2}$$

where, B is the Stern-Geary constant. This constant has a value of 26 mV for active steel and 50 mV for passive steel (Song & Saraswathy, 2007). After obtaining the value for I_{corr}, and if the surface area being polarized is accurately known, the current density i_{corr} can be calculated by Equation 1.3.

$$\mathrm{i_{corr}} = \mathrm{I_{corr}}/\mathrm{A} \qquad \text{Eq. 1.3}$$

The criteria presented in Table 2.3 for corrosion has been developed from field and laboratory experiments to correlate the corrosion current density to the extent in corrosion damage (Song & Saraswathy, 2007).

Corrosion Current Density (μA*cm^{-2})	Extent of Corrosion
$i_{corr} < 0.10$	Passive Condition
$0.10 < i_{corr} < 0.50$	Low to Moderate Corrosion
$0.5 < i_{corr} < 1.0$	Moderate to High Corrosion
$i_{corr} > 1.0$	High Corrosion

Table 2.3 Corrosion current density vs. condition of steel (Song & Saraswathy, 2007).

2.4.3.5 Electrochemical Impedance Spectroscopy (EIS)

In the Electrochemical Impedance Spectroscopy (EIS) technique, an alternating potential is applied at varying frequencies and the resulting alternating current is measured. The impedance or alternating voltage divided by the alternating current are plotted against each other, as a function of frequency. In simple terms, the impedance is a measure of the ability of a circuit to resist the flow of electric current, but it is not limited by the simplifying properties of an ideal resistor (Gamry Instuments, 2009).

EIS is commonly analyzed by fitting the impedance spectrum data into a equivalent circuit analog composed of common electrical components as resistors, capacitors an inductors. The basic of this technique is that the steel in the concrete or grout behave like the circuit shown in Figure 2.9a.

The R_s resistor represents the concrete resistance and R_p the polarization resistance. The capacitance C is related to the double layer that forms in the electrochemical systems at the metal/solution interface (Bentur, Diamond, & Berke, 1997). The general equation to describe this equivalent analog circuit is as follows,

$$Z_t[\Omega] = R_s + \frac{1}{R_p + Y_o(j\omega)^n} \qquad \text{Eq. 1.4}$$

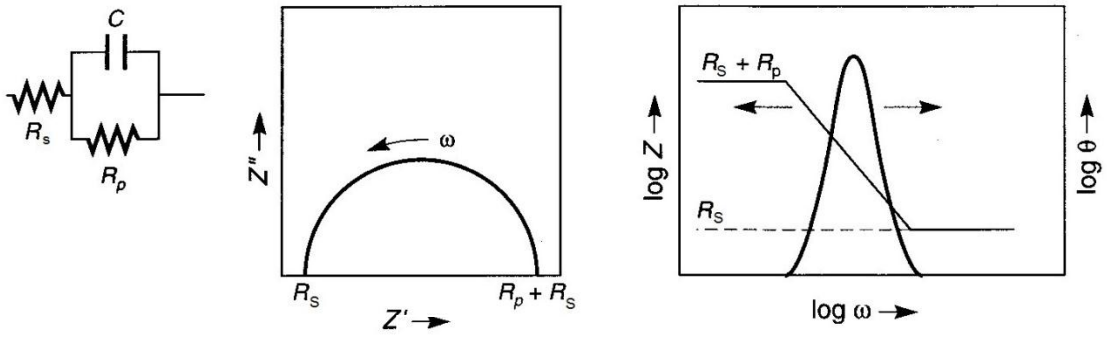

Figure 2.9 Data Display for EIS a) Equivalent analog circuit for a corroding electrode, b) Nyquist Plot, c) Bode Plot (Jones, 1996).

In Equation 1.4, the term $Y_o(j\omega)^n$ refers to the CPE's impedance. The EIS data can be plotted in a Nyquist plot or Bode plot (Figure 2.9b and 2.9c) from which values of R_s and R_p can easily obtained. The corrosion current, I_{corr} can be calculated by

$$I_{corr} = \frac{B}{R_p} \qquad \text{Eq. 1.5}$$

where B is the Stern-Geary coefficient and R_p is the polarization resistance.

CHAPTER 3 - METHODOLOGY

3.1 FIELD SAMPLES

3.1.1 DEFICIENT GROUT CONDITION (FS-SM / FS-LG)

To simulate the deficient grout conditions in field samples, samples using sections from a retrieved failed tendon were built. The tendon was 4 in. diameter with twenty-two wire strands, 1/2 in. diameter. The retrieved tendon was cut in 6 in. length sections. On the bottom side of the section, a #18 wire was attached to the king wire of each strand (all twenty-two strands will work as one working electrode). Each connection between the king wire and the wire cable were encapsulated in epoxy resin to protect the connection. After each connection was individually protected, the complete bottom part was encapsulated in epoxy to provide additional protection. After encapsulating the bottom part, the wires were interconnected, providing one connection point to the working electrode. On the top part, a dam like structure was built to introduce into the system the repair gout, the reference electrode and the auxiliary electrode. The reference electrode was a 1 in. length and 1/8 in. diameter activated titanium rod, the auxiliary electrode was a 6 in. diameter activated titanium disc mesh and both were installed with approximately 1/4 in. separation within each other and 1/4 in. above the top surface of the section. The top section of the tendon was filled with a 0.45 water-cement ratio cement paste (neat grout). A schematic drawing is shown in Figure 3.1. This group was defined as Test Setup FS-SM. Triplicate samples were built, and identified as Test Setup FS-SM. Condition of the pre-existing grout will be discussed later.

Open Circuit Potential was monitored in this samples by placing a saturated calomel electrode, SCE, on top the hardened cement paste and voltage was measured with a handheld voltmeter. Potentiodynamic polarizations scans were performed from -200 mV below OCP (cathodically) to 400 mV above OCP (anodically) at a scan rate of 0.5 mV/s.

To be able to measure macrocell current on these samples, Test Setup FS-LG was built. These samples were built using similar procedure as Test Setup FS-SM but two sections were cast together, one in top of the other. A schematic drawing is shown in Figure 3.2. In this case, in both sections of the sample, wires were connected to each strand and sections interconnected together.

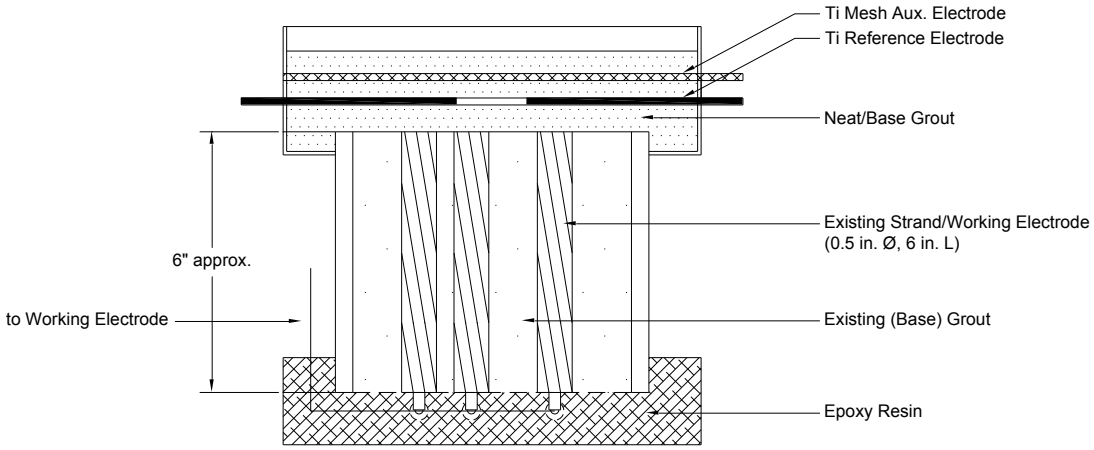

Figure 3.1 Schematic of corrosion test cell (Test Setup FS-SM).

Test Setup	Base Grout	Repair Grout	Sample Name
FS-SM	Existing	Neat Grout	FS-SM-1
			FS-SM-2
			FS-SM-3

Table 3.1 Test Setup FS-SM.

After the samples were cast together, a small switch was installed to connect the top and bottom working electrodes. Once built, the interconnecting switch was turned on and samples were left to polarize for a period of approximately twenty-four hours before taking initial macrocell measurements. In this setup, segments containing hardened grout, obtained from sections away from the failure where used on top, and segments containing segregated grout where corrosion was observed were installed in the bottom. Three samples were built in this test setup. See Table 3.2.

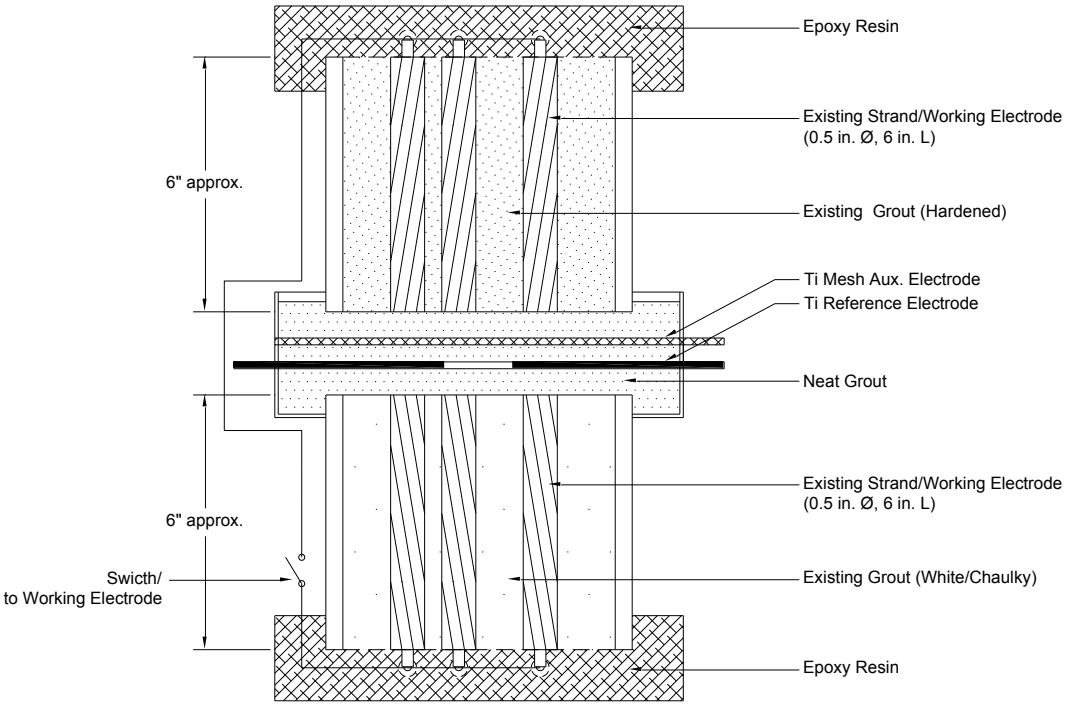

Figure 3.2 Schematic of corrosion test cell (Test Setup FS-LG).

Test Setup	Base Grout	Repair Grout	Sample Name
FS-LG	Existing	Neat Grout	FS-LG-1
			FS-LG-2
			FS-LG-3

Table 3.2 Test Setup FS-LG.

Open Circuit Potential, Macrocell current, Linear Polarization Resistance, and Electrochemical Impedance Spectroscopy tests were performed on these samples.

Open Circuit Potential was monitored in these samples by placing a saturated calomel electrode, SCE, on top the hardened cement paste and voltage was measured with a handheld voltmeter. Macrocell current was measured with a multimeter by momentarily turning the switch to the off position. Linear Polarization Resistance, LPR, was made by polarizing the steel cathodically 25 mV from the OCP at a scan rate of 0.025 mV/s. Electrochemical Impedance Spectroscopy, EIS, was made with a

frequency range of 100 kHz > f >1 mHz with an amplitude 10 mV. Data was acquired at 3 pts/decade. For both of these tests a Gamry potentiostat and impedance analyzer was used.

3.1.2 REPAIR OF VOIDS WITH DISSIMILAR GROUT (FS / FSR)

To simulate the repair of tendons with dissimilar grouts, samples were built using retrieved section from a failed tendon. For this purpose, two initial samples were built using 14 in. length sections. The tendons were 4 in. diameter with eighteen, 1/2 in. diameter wire strands. These samples had a void along its side of approximately 1-1/4 in. by 3-1/2 in. in its original condition. A cross sectional cut showing the void is shown in Figure 3.3a. Originally, the sample contained twenty-two strands but due to the lack of encapsulation of the strands near the void, four strands were removed. After cutting the sections to the desired length, the top face was encapsulated in an epoxy resin. On the bottom side of the sample, #18 wires were attached to the king wire of each strand (all eighteen strands will work as one working electrode). Each connection between the king wire and the wire was encapsulated in epoxy resin to provide extra protection for the connection. After each connection was individually protected, the complete bottom part was encapsulated in epoxy to provide additional protection. After encapsulating the bottom part, the eighteen wires were interconnected, providing one connection point to the working electrode. On the HDPE duct, along the void, a 5 in. by 2in. opening was made to introduce the reference and auxiliary electrode as shown in Figure 3.3.b. All loose material (grout) inside the section was carefully removed.

A 6 x 3 x 2 in. electrical box was attached and sealed around the opening to introduce the reference and auxiliary electrodes. The reference electrode was a 1 in. length and 1/8 in. diameter activated titanium rod, the auxiliary electrode was a 6 x 3 in. activated titanium mesh. The reference and auxiliary electrodes were installed with approximately 1/4 in. separation within each other and 1/4 in. above the top surface of the HDPE duct. Openings made at the top and bottom edge of the HDPE duct along the void permitted the inflow and outflow of the repair grout during the repair process. Openings were approximately 1/2 in. in diameter with 1/2 in. clear pvc tube extensions attached using a fitting. In the void space, two king wire strands were installed and interconnected together to allow measurement of macrocell current. A second electrical box was installed on the side of the sample to install the switches

used to interconnect the working electrodes. A schematic drawing is shown in Figure 3.4. The void was repaired using a pre-bagged grout mixed following manufacturer recommendations (repair grout 1). This test setup was identified as Test Setup FS. After construction of the samples was finished, the installed switch was turned to the on position to allow polarization of the steel for approximately twenty-four hours before taking initial macrocell measurements. These samples were built with one pre-bagged repair grout, and two identical samples were built as shown in Table 3.3.

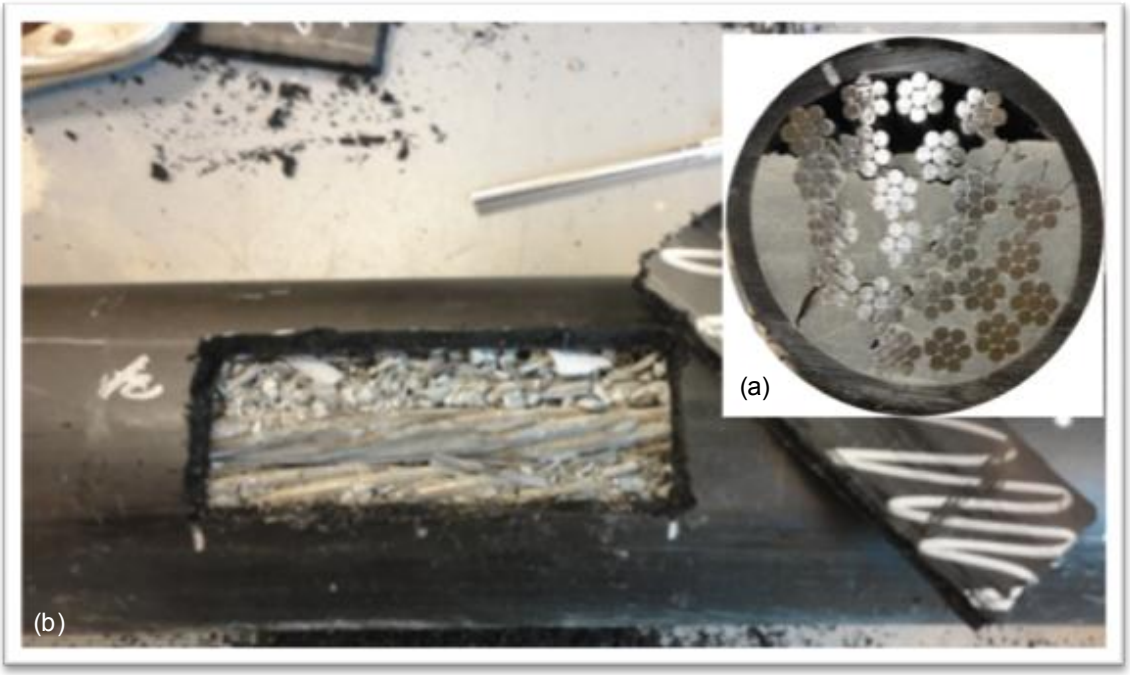

Figure 3.3 Field Tendon. a) Cross section of retrieved field tendon with void, b) Side opening for introduction of reference and auxiliary electrodes.

Open Circuit Potential, Macrocell current, Linear Polarization Resistance, and Electrochemical Impedance Spectroscopy tests were performed in these samples.

OCP was measured by placing a saturated calomel electrode, SCE, on the inflow opening and voltage was measured with a handheld voltmeter. Macrocell current was measured using a multimeter by momentarily turning the switch to the off position. Linear Polarization Resistance, LPR, was made by polarizing the steel 25 mV cathodically from the OCP at s scan rate of 0.025 mV/s. Electrochemical Impedance Spectroscopy, EIS, was made with a frequency range of 100 kHz > f >1 mHz with an

amplitude 10 mV. Data was acquired at 3 pts/decade. For both of these tests a Gamry potentiostat and impedance analyzer was used.

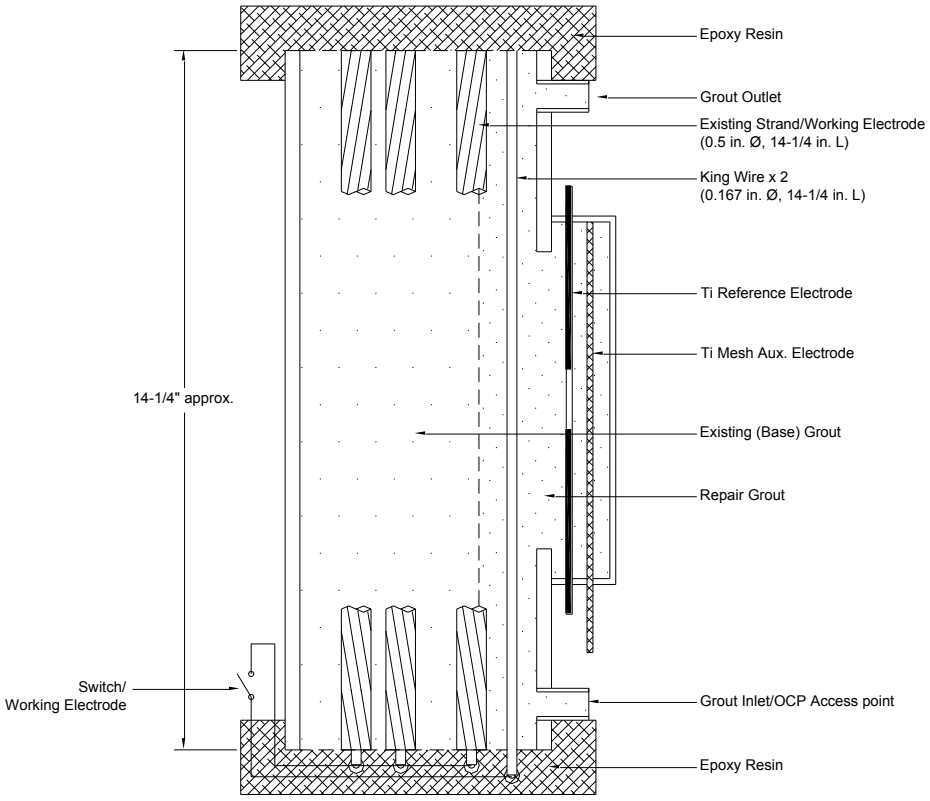

Figure 3.4 Schematic of corrosion test cell (Test Setup FS).

Test Setup	Base Grout	Repair Grout	Sample Name
FS	Existing	Repair Grout 1	FS-1
			FS-2

Table 3.3 Test Setup FS.

The second set of samples was built to simulate a repaired tendon using the retrieved tendon sections, and was designate as Test Setup FSR. The samples in this set were built using 18 in. length sections. Tendons were 4 in. diameter with twenty-two, 1/2 in. wire strands. These samples had a void along its side of approximately 1-1/4 in. by 3-1/2 in. in its original condition, as shown in Figure 3.3a. After cutting the sections to the desired length, the top face was encapsulated in an epoxy resin. On the bottom side of the sample, a #18 wire was attached to the king wire of each strand (all twenty-two strands

will work as one working electrode). Each connection between the king wire and the wire cable was encapsulated in epoxy resin to protect the connection. After each connection was individually protected, the complete bottom face was encapsulated in epoxy to provide additional protection. After encapsulating the bottom part, the twenty-two wires were interconnected, providing one connection point to the working electrode. On the HDPE duct, along the void, a 5 in. by 2in. opening was made to introduce the reference and auxiliary electrode as shown in Figure 3.3b. A 6 x 3 x 2 in. electrical box was attached and sealed around the opening. The electrical box was used to introduce the reference and auxiliary electrodes. The reference electrode was a 1 in. length and 1/8 in. diameter activated titanium rod, the auxiliary electrode was a 6 x 3 in. activated titanium mesh. The reference and auxiliary electrodes were installed with approximately 1/4 in. separation within each other and 1/4 in. above the top surface of the HDPE duct. Openings were made at the top and bottom edge of the HDPE duct along the void to allow the inflow and outflow of the repair grout during the repair of the void. Openings were approximately 1/2 in. in diameter with 1/2 in. clear pvc tube extensions attached using a fitting. A schematic drawing is shown in Figure 3.5. The void spaces were repaired using two pre-bagged grouts commercially available and listed in the FDOT Qualified Product List. Of the six samples, three were repaired with repair grout 1 and three were repaired with repair grout 2, as shown in Table 3.4. Pre-bagged grouts were mixed using recommendations by the manufacturer. The test setup of consisted of 6 samples, two setups built in triplicates.

Open Circuit Potential, Linear Polarization Resistance, and Electrochemical Impedance Spectroscopy tests were performed in these samples.

OCP was measured by placing a saturated calomel electrode, SCE, on the inflow opening and voltage was measured with a handheld voltmeter. Linear Polarization Resistance, LPR, was made by polarizing the steel 25 mV cathodically from the OCP at s scan rate of 0.025 mV/s. Electrochemical Impedance Spectroscopy, EIS, was made with a frequency range of 100 kHz > f >1 mHz with an amplitude 10 mV. Data was acquired at 3 pts/decade. For both of these tests a Gamry potentiostat and impedance analyzer was used.

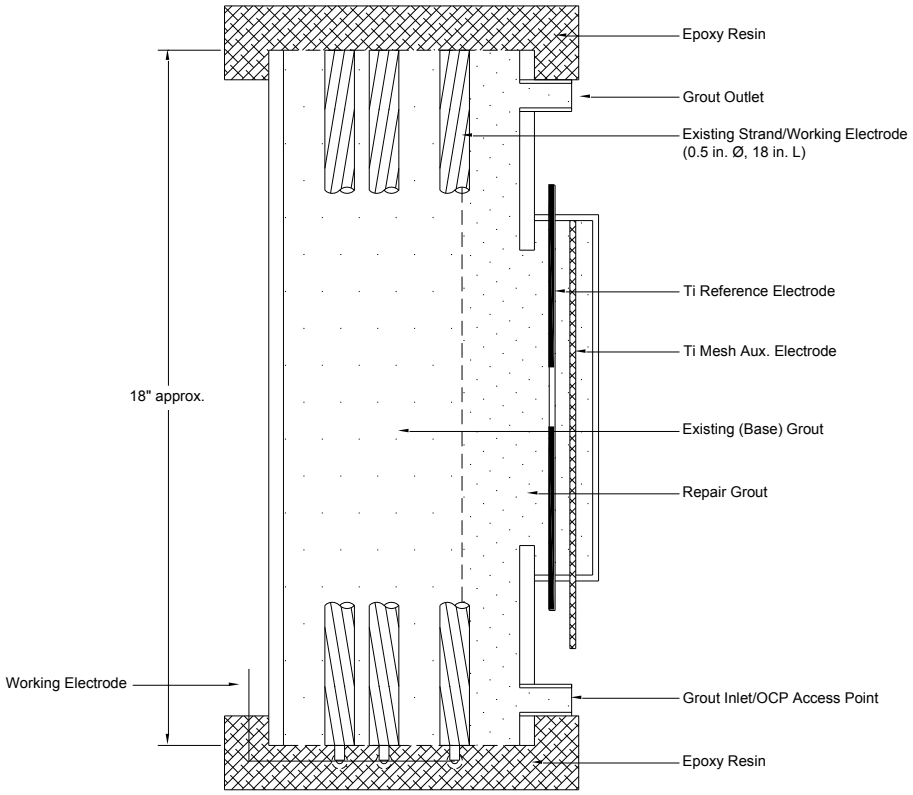

Figure 3.5 Schematic of corrosion test cell (Test Setup FSR).

Test Setup	Base Grout	Repair Grout	Sample Name
FSR	Existing	Repair Grout 1	FSR-R1-1
			FSR-R1-2
			FSR-R1-3
	Existing	Repair Grout 2	FSR-R2-1
			FSR-R2-2
			FSR-R2-3

Table 3.4 Test Setup FSR.

3.2 LABORATORY SAMPLES

3.2.1 REPAIR

3.2.1.1 Repair Materials (S)

To monitor the behavior of the repair materials independently, samples in a supplemental test setup was fabricated and identified as Test Setup S. This test setup simulated strands cast in a no repair, no void environment in new (clean surface) and pre-rusted wires.

To build the samples, king wires were extracted from strand sections cut to approximately 10 in. length. A #18 wire was attached to one end, and both ends were later covered in an epoxy resin to protect the connection and the end of the king wire. The total exposed king wire length was 8-1/4 inches. One of the king wire assemblies was stored in a 100% relative humidity environment for approximately thirty days, for rust to develop in its surface. The strand assemblies were inserted into a caped pvc pipe 2 in. diameter and 12-1/2 in. length. In these samples, a titanium reference electrode and a auxiliary referenced electrode were introduced. The reference electrode was a 2 in. length and 1/8 in. diameter activated titanium rod, the auxiliary electrode was a 1 in. by 2 in. activated titanium mesh installed on the inner sides of the pvc pipe, opposed to each other. Samples were filled with a base grout (0.45 water-cement ratio paste) and two pre-bagged grouts. After casting, a layer of approximately 1/2 in. of epoxy resin was cast on top of the sample to encapsulate the sample. On the side of the sample, 1/2 in. diameter openings were made using a drill bit to provide access to the grout to take OCP measurements. A schematic drawing is shown on Figure 3.6. Openings were kept sealed at all times except when taking measurements.

Open Circuit Potential, Solution Resistance, Linear Polarization Resistance, Electrochemical Impedance Spectroscopy, and Potentiodynamic Scan were performed in these samples.

OCP was measured by placing a saturated calomel electrode, SCE, on side opening and voltage was measured with a handheld voltmeter. Solution resistance was measured using three-pin resistance meter and measurements were taken through the clean and pre-rusted wires. Linear Polarization Resistance, LPR, was made by polarizing the steel 25 mV cathodically from the OCP at a scan rate of 0.025 mV/s. Electrochemical Impedance Spectroscopy, EIS, was made with a frequency range of 100

kHz > f >1 mHz with an amplitude 10 mV. The potentiodynamic scans were made from -750 mV below OCP (cathodically) to 750 mV above OCP (anodically) at a scan rate of 0.2 mV/s. For the Linear Polarization resistance, Electrochemical Impedance Spectroscopy and Potentiodynamic Scans a Gamry potentiostat and impedance analyzer was used.

These samples were built with three grouts, and triplicates of each, as shown on Table 3.5.

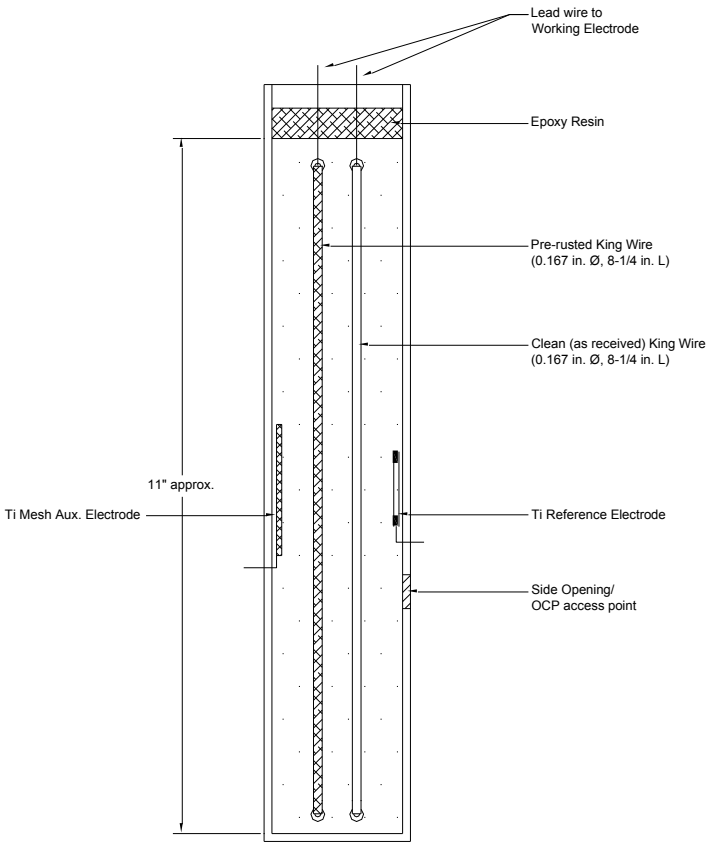

Figure 3.6 Schematic of corrosion test cell (Test Setup S).

Test Setup	Strand Condition	Grout	Sample Name
S	Clean/ Pre-rusted	Neat Grout	S-CP-B1-1
			S-CP-B1-2
			S-CP-B1-3
		Repair Grout 1	S-CP-R1-1
			S-CP-R1-2
			S-CP-R1-3
		Repair Grout 2	S-CP-R2-1
			S-CP-R2-2
			S-CP-R2-3

Table 3.5 Test Setup S.

3.2.1.2 Repair of Voids With Dissimilar Grouts (A / B)

To simulate repaired voids with dissimilar grouts, laboratory samples were fabricated in two different setups.

The first setup, Test Setup A, simulated a strand that extended into a void space and had developed surface rust and was repaired with a dissimilar (new, pre bagged) grout. To build the samples, king wires were extracted from strand sections cut to approximately 11 in. length. A # 18 wire was attached to one end, and both ends were later covered in epoxy resin to protect the connection and the end of the king wire. The total exposed king wire length was 9 inches. The strand assembly was inserted into a caped pvc pipe 2 in. diameter and 5-1/2 in. length. In this section of the pipe, a titanium reference electrode and an auxiliary referenced electrode were introduced. The reference electrode was a 2 in. length and 1/8 in. diameter activated titanium rod, the auxiliary electrode was a 1 in. by 2 in. activated titanium mesh installed on the inner sides of the pipe, opposed to each other. See schematic shown in Figure 3.7. This first section was filled with a 0.45 water-cement ratio cement paste (neat grout) to simulate the original tendon grout prior to the repair. After casting, the samples were placed in a 100% humidity room for approximately thirty days.

After the thirty day period, a second pipe section was installed on top of the previous section, making the overall length of the sample approximately 12 inches. Also in this section, a reference electrode and auxiliary reference electrode were introduced with similar setup as the bottom section.

These sections were filled with the repair grouts. After casting the second section with the repair grouts, a layer of approximately 1/2 in. of epoxy resin was cast on top of the sample to encapsulate the sample. On the side of the top and bottom sections, 1/2 in. diameter openings were made using a drill bit to provide access to the grout to take OCP measurements. Openings were kept sealed at all times except when taking measurements.

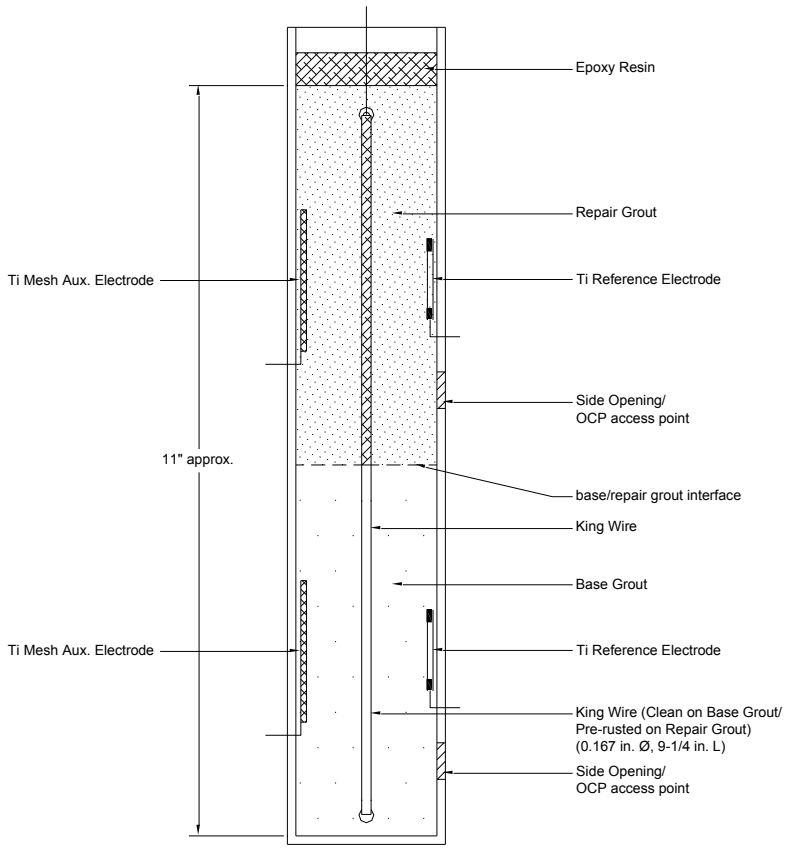

Figure 3.7 Schematic of corrosion test cell (Test Setup A).

Open Circuit Potential, Solution Resistance, and Linear Polarization Resistance tests were performed in these samples. OCP was measured by placing a saturated calomel electrode, SCE, on the side openings and voltage was measured with a handheld voltmeter in both the repair grout and base grout. Solution Resistance measurements were taken using a three-pin resistance meter and were taken through the repair and base grouts independently. Linear Polarization Resistance, LPR, was made by

polarizing the steel 25 mV cathodically from the OCP at s scan rate of 0.025 mV/s using a Gamry potentiostat.

These samples were built in three base-to-repair grout combinations, and triplicates of each combination, as shown on table 3.6.

Test Setup	Base Grout	Repair Grout	Sample Name
A	Neat Grout	Repair Grout 1	A-B1-R1-1
			A-B1-R1-2
			A-B1-R1-3
		Repair Grout 1	A-B1-R2-1
			A-B1-R2-2
			A-B1-R2-3
	Repair Grout 1	Repair Grout 2	A-B2-R2-1
			A-B2-R2-2
			A-B2-R2-3

Table 3.6 Test Setup A

The second setup, Test Setup B, simulated a strand that extended into a void space (with no rust development) and was repaired with a dissimilar (new, pre-bagged grout). This setup was modified from Test Setup A to allow for macrocell measurements. To built the samples, two king wires were extracted from strand sections cut to approximately 6 inches in length. A #18 wire was attached to one end, and both ends were later covered with an epoxy resin to protect the connection and the end of the king wire. The total exposed king wire length was 4 inches. One strand assembly was inserted into a capped pvc pipe 2 in. diameter and 5-1/2 in. length. In this section of the pipe, a titanium reference electrode and an auxiliary referenced electrode were introduced. The reference electrode was a 2 in. length and 1/8 in. diameter activated titanium rod, the auxiliary electrode was a 1 in. by 2 in. activated titanium mesh installed on the inner sides of the pvc pipe, opposed to each other. This first section was filled with a 0.45 water-cement ratio cement paste (neat grout) to simulate the original tendon grout. After casting, the samples were left hydrating for approximately thirty days. After the thirty day period, a second pipe section was installed on top of the previous, making the overall length of the sample approximately 12 inches. In this top section, the second king wire assembly was installed along with a reference electrode

and auxiliary reference electrode, similar to the bottom section. This section was filled with the repair grout. After casting the second section, a layer of approximately 1/2 in. of epoxy resin was cast on top of the sample to encapsulate the tendon. On the side of the top and bottom sections, 1/2 in. diameter openings were made using a drill bit to provide access to the grout to allow for OCP measurements. These openings were kept sealed at all times except when taking measurements. A schematic drawing is shown if Figure 3.8. After fabrication, a small on/off switch was installed to provide connection between the top and bottom king wires. This switch was used to measure macrocell current between the wire in the base and repair grouts.

Open Circuit Potential and Macrocell Current tests were performed in these samples. OCP was measured by placing a saturated calomel electrode, SCE, on the side openings and voltage was measured with a handheld voltmeter in both the repair and base grouts. Macrocell current was measured using a multimeter by momentarily turning the switch to the off position. These samples were built in three base-to-repair grout combinations, and triplicates of each combination as shown on table 3.7.

Test Setup	Base Grout	Repair Grout	Sample Name
B	Neat Grout	Repair Grout 1	B-B1-R1-1
			B-B1-R1-2
			B-B1-R1-3
		Repair Grout 2	B-B1-R2-1
			B-B1-R2-2
			B-B1-R2-3
	Repair Grout 1	Repair Grout 2	B-B2-R2-1
			B-B2-R2-2
			B-B2-R2-3

Table 3.7 Test Setup B

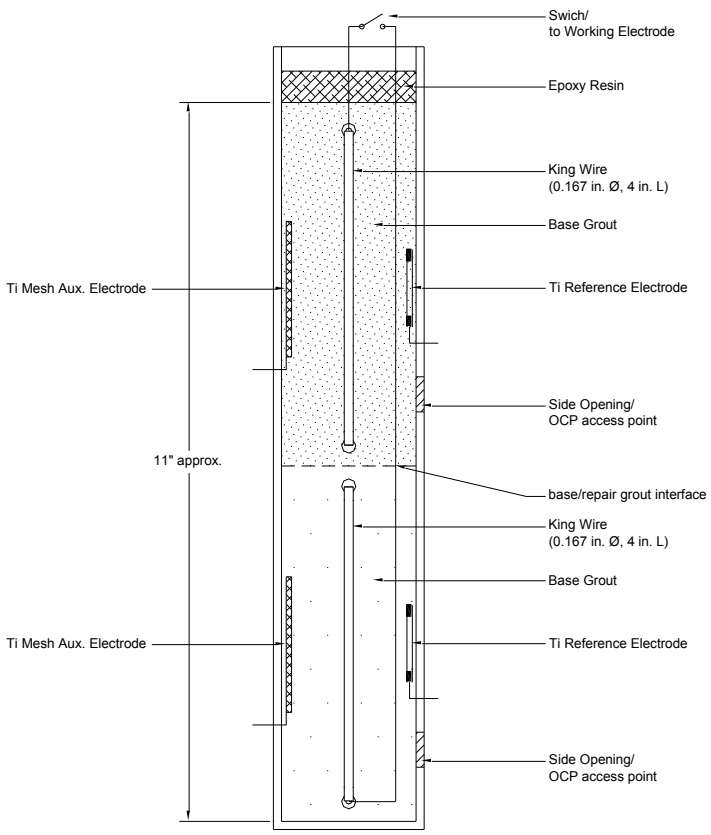

Figure 3.8 Schematic of corrosion test cell (Test Setup B).

3.2.1.3 Deficient Repair/Aggressive Environment (C)

To simulate deficient repairs of voids and/or aggressive environment on exposed strand in a void, Test Setup C was created.

To build the samples, two king wires were extracted from strand sections cut to approximately 5-1/2 in. length. A #18 wire was attached to one end, and both ends were covered with an epoxy resin to protect the connection and the exposed end of the king wire. The total exposed king wire length was 4-1/4 inches. One strand assembly was inserted into a capped pvc pipe 2 in. diameter and 7 in. length. In this section, a titanium reference electrode and an auxiliary referenced electrode were introduced. The reference electrode was a 2 in. length and 1/8 in. diameter activated titanium rod, the auxiliary electrode was a 1 in. by 2 in. activated titanium mesh installed on the inner sides of the pipe, opposed to each

other. This first section was filled with a pre-bagged grout (repair grout). After curing for approximately thirty days, a second pipe section, 3-1/4 in. length, was installed on top of the previous section, making the overall length of the sample approximately 11 inches. In this top section, the second king wire assembly was installed along with a reference electrode and auxiliary reference electrode, similar to the bottom section. This section was filled with a 0.45 water-cement ratio cement paste (neat grout), leaving approximately 2-1/4 in. length of the king wire exposed. Over this exposed section of the king wire, a third section of capped clear plastic pvc pipe was installed to provide the area of deficient repair/aggressive environment exposure. See schematic shown in Figure 3.9.

The deficient/aggressive environments were be provided by the use of simulated pore solutions (SPS) with varying pH, sulfate, and chloride concentration as stated in Table 3.8 and 3.9. In addition, a high humidity environment was tested. An opening was made on top of the clear pvc pipe section to provide an inflow point for the simulated pore solutions and OCP measurements. On the side of the bottom section, a 1/2 in. diameter opening was made using a drill bit to provide access to the grout to take OCP measurements. Openings were kept sealed at all times except while taking measurements. After fabrication, a small on/off switch was installed to provide connection between the top and bottom king wires. The switch was used to measure macrocell current between the wire in the base and repair grout. The switch was turned to the on position and the steel polarized for approximately twenty-four hours before taking initial macrocell measurements.

Open Circuit Potential, Macrocell Current, and Linear Polarization Resistance tests were performed in these samples. OCP was measured by placing a saturated calomel electrode, SCE, on the side and top openings. Voltage was measured with a handheld voltmeter in both the repair grout and the deficient/aggressive environment solution. Macrocell current was measured using a multimeter and turning the switch to the off position momentarily. Linear Polarization Resistance, LPR, was made by polarizing the steel 25 mV cathodically from the OCP at s scan rate of 0.025 mV/s using a Gamry potentiostat.

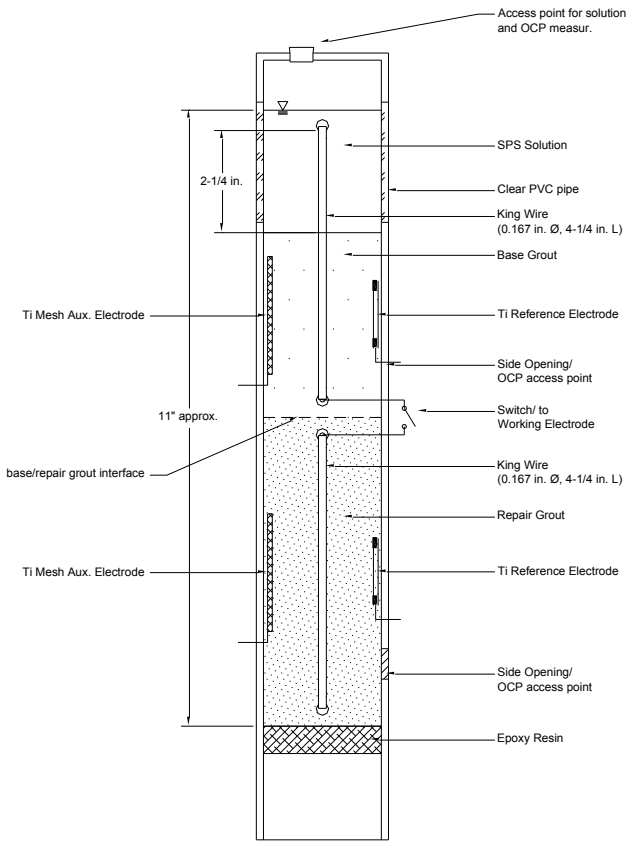

Figure 3.9 Schematic of corrosion test cell (Test Setup C: samples C-G1-V1-1, C-G1-V1-2, C-G1-V2-1, C-G1-V2-2, C-G1-V3m-1, and C-G1-V3m-2).

These samples were built in one base-to-repair grout combination, and duplicate of each combination as shown on table 3.8. Four deficient/aggressive environment were tested, 1) high humidity, 2) simulated pore water solution with pH 13.3 and varying concentration of sulfate and chloride (chloride concentration below corrosion threshold), 3) simulated pore water solution with pH 13.3, varying concentrations of sulfate and no chloride, and 4) simulated pore water solution with pH 12.6 and 2,000-ppm concentration of sulfates. Solution concentrations are shown in Table 3.8.

To test the low pH pore solution, samples C-G1-V3-1 and C-G1-V3-2, were modified from its original setup (Figure 3.9) and named C-G1-V3m-1 and C-G1-V3m-2 as shown in the schematic drawing in Figure 3.10. The constituents of the simulated pore solution for shown in Table 3.9.

Test Setup	Base/Repair Grout	SPS	pH	Added Ion/Concentration	Sample Name
C	Neat/ Repair Grout 1	SPS B	13.3	$0 < Cl^- < 2{,}000$-ppm $0 < SO_4^{-2} < 85{,}000$-ppm	C-G1-V1-1
					C-G1-V1-2
		SPS B	13.3	$0 < SO_4^{-2} < 85{,}000$-ppm	C-G1-V2-1
					C-G1-V2-2
		High RH	--	--	C-G1-V3-1
					C-G1-V3-2
		SPS A	12.6	$S0_4^{-2}$ - 2,000-ppm	C-G1-V3m-1
					C-G1-V3m-2

Table 3.8 Test Setup S.

Solution	$Ca(OH)_2$	NaOH	KOH	pH
SPS A	2.1 g/L†	-	-	12.6
SPS B	2.1 g/L†	3.6 g/L	10.5 g/L	13.3

† not fully dissolved in solution

Table 3.9 Constituents of simulated pore solutions.

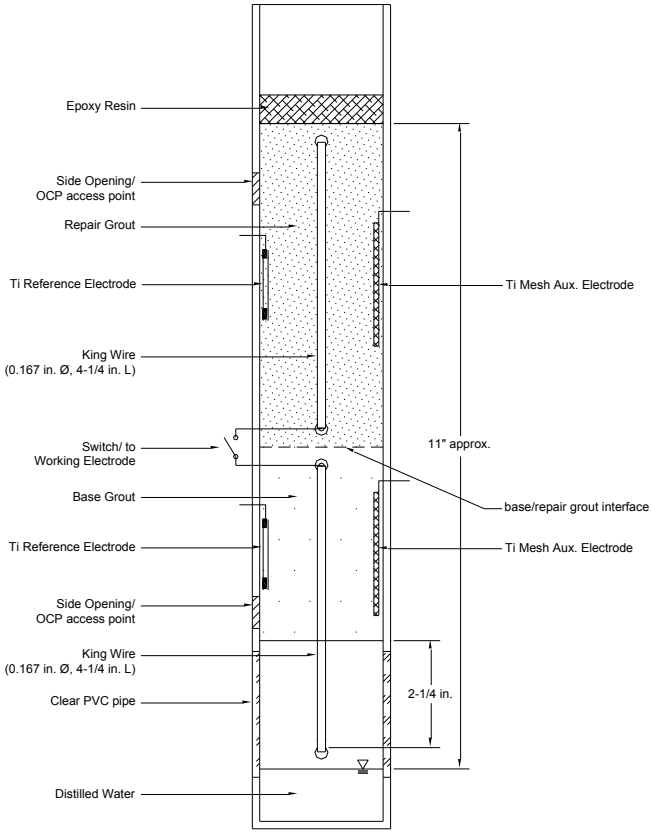

Figure 3.10 Schematic of corrosion test cell (Test Setup C: samples C-G1-V3-1 and C-G1-V3-2).

3.2.2 SIMULATED PORE WATER SOLUTION (SPS-KW / SPS-CS)

To better describe and characterize the significance of the presence of sulfates in high pH solution, additional laboratory samples with simulated pore solution were built.

To build the samples on Test Setup SPS-KW, king wires were extracted from strand sections that were cut to a length of approximately 2-1/2 inches. A #18 wire was attached to one end of the wire and protected with epoxy resin. The other was clean cut and left exposed. Samples were submerged in a partially de-aerated simulated pore solution with varying sulfate concentration. See schematic drawing in Figure 3.11.

For sample on Test Setup-CS, similar setup was used as described above for sample in Test Setup-KW but only the cross sectional area of the wire was exposed to the tested solutions. In this case, the strand wires were encapsulated in an epoxy resin. In this test setup, the samples were protected from changes in pH due to carbonation by sealing the test from the atmospheric carbon dioxide. See schematic in Figure 3.12.

Simulated pore solutions were prepared as shown on table 3.10. Steel surface conditions were tested in as-received (cleaned with methanol before submersing in solution) and pre-rusted conditions. Pre rusted samples were kept in a 100% humidity room for one week before submersing in solution. Samples in this test setup were polished to 0.3-micron finish. A saturated calomel electrode, SCE, was used as a reference electrode and an activated titanium mesh disc was used as the auxiliary electrode.

To de-aerate the solution, nitrogen was continuously added to the simulated pore solution to replace the dissolved oxygen.

Linear Polarization Resistance, LPR, was made by polarizing the steel 25 mV cathodically from the OCP at s scan rate of 0.025 mV/s using a Gamry potentiostat. Anodic Polarization scans were made from -100 mV below OCP (cathodically) to 100 mV above OCP (anodically) at a scan rate of 0.5 mV/s. OCP was measured by placing a saturated calomel electrode on the solution and voltage was measured with a handheld voltmeter.

Sample Setup	$Ca(OH)_2$	NaOH	KOH	Na_2SO_4	pH
SPS-KW-1	2.1 g/L†	-	-	0 mg/L	12.6
				2,000 mg/L	12.4
				20,000 mg/L	12.4
SPS-KW-2	2.1 g/L†	3.6 g/L	10.5 g/L	0 mg/L	13.2
				2,000 mg/L	13.1
				20,000 mg/L	13.1

† Not fully dissolved in solution

Table 3.10 Constituents of simulated pore water solutions with varying ion sulfate concentration.

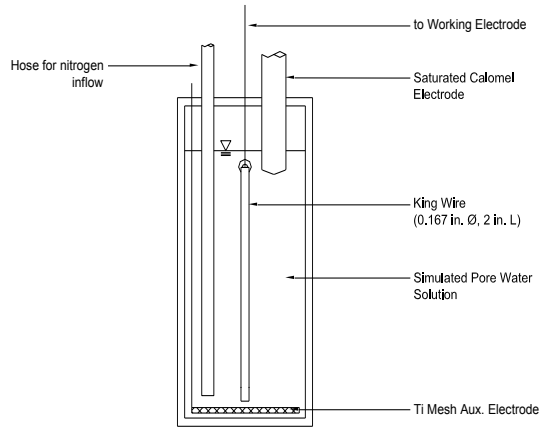

Figure 3.11 Schematic of corrosion test cell (Test Setup SPS-KW).

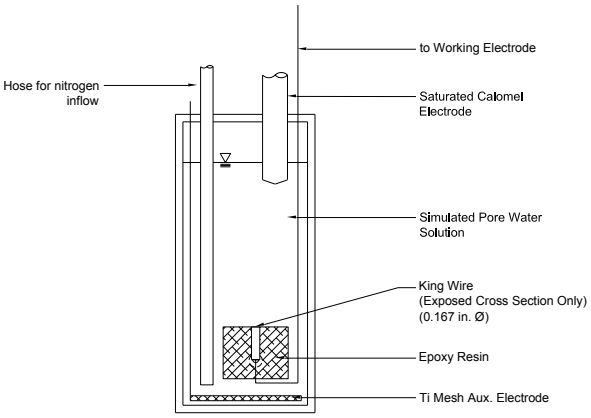

Figure 3.12 Schematic of corrosion test cell (Test Setup SPS-CS).

3.3 GROUT CHARACTERIZATION

Grout from the failed tendon section was characterized by x-ray fluorescence (XRF), x-ray diffraction (XRD) and comparisons were made between the 0.45 water-cement ratio neat grout and the pre-bagged grouts. Grout samples of the neat and repair grouts were obtained from the autopsy of Test Setup S after testing for approximately 4 months. Grout obtained from samples of Test Setup FS-SM was obtained after the autopsy of those samples.

Laboratory tests to determine chloride content in accordance with FM 5-516 were also performed in the extracted grouts.

CHAPTER 4 - RESULTS AND DISCUSSION

4.1 FIELD SAMPLES

4.1.1 DEFICIENT GROUT CONDITION (FS-SM / FS-LG)

The corrosion test cells used for electrochemical testing on Test Setup FS-SM and FS-LG had unique features not present typically in tendon sections. First, a layer of fresh cement paste was cast over the cross sectional section of the tendon in order to introduce a reference and auxiliary electrodes and second, the grout in the tendon may have aged in the time between failure and testing. During that period, the tendon was left intact and prior to testing and after cutting to the desired length, the samples were sealed in airtight plastic bags during sample fabrication. However, the samples with white/chalky and segregated grout, which showed to have very high initial water content, showed changes in the material during this period. A distinct color change was observed in the grout of sample FS-SM-1 and corrosion was observed at the surface of the cross section. Grouts obtained from wet/plastic unhardened locations along the failed tendon tend to become dry and incoherent after exposure to air. Sample FS-SM-2 showed significant wet corrosion product accumulation in the surface of the embedded strand. Sample FS-SM-3 showed significant surface rusting. Samples built for Test Setup FS-LG were built using sections with wet/plastic grout as the bottom part and grey hardened grout on the top part. In addition, sections with the wet/plastic grout showed higher moisture content than the grey hardened grout. The values of moisture content, grout characteristics, and observed corrosion on Test Setup FS-SM and FS-LG are shown in Table 4.1.

Due to the presence of two grouts in the samples, fresh paste and existing grout, an idealized equivalent analog circuit, as shown in Figure 4.1 and described in Equation 4.1, was used as an initial approach to measure the material properties and corrosion rate. The capacitive components were treated as constant phase elements (CPE). The total impedance, Z_T, of the cell is shown in Equation 4.1. The equation related to the proposed circuit analog is composed of: 1) ω (angular frequency), 2) R_s

(solution resistance mainly of the fresh paste), 3) R_C (solution resistance of the pore and interstitial spaces of the existing grout), 4) R_P (polarization resistance of the strand assembly), 5) Y_{oM} and n_M (CPE components of the metal solution interface) and, 6) Y_{oC} and n_C (CPE components relevant to the electrochemical behavior of the existing grout).

Test Setup	Sample		Moisture Content (%)	Grout Characteristic	Corrosion Observed
FS-SM	FS-SM-1		41	White/Chalky	Yes
	FS-SM-2		19	Grey/Hardened	Yes
	FS-SM-3		19	Grey/Hardened	Yes
FS-LG	FS-LG-1	TOP	--	Grey/Hardened	No
		BOTT.	40	Mixed w/ wet-plastic	Yes
	FS-LG-2	TOP	--	Grey/Hardened	No
		BOTT.	40	Mixed w/ wet-plastic	Yes
	FS-LG-3	TOP	--	Grey/Hardened	No
		BOTT.	> 40	Mixed w/ wet-plastic	Yes

Table 4.1 Field samples grout characteristics (Test Setup FS-SM and FS-LG).

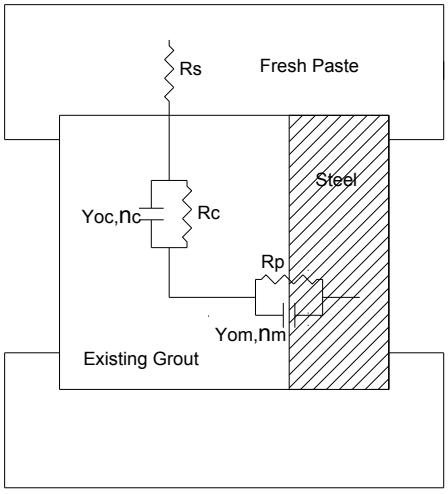

Figure 4.1 Idealized equivalent analog circuit.

$$Z_t[\Omega] = R_s + \frac{1}{R_c + Y_{oC}(j\omega)^{nC}} + \frac{1}{R_p + Y_{oM}(j\omega)^{nM}} \quad \text{Eq. 4.1}$$

Results from approximately one week after initial casting of the fresh paste are shown in Figures 4.2 to 4.10 (Lines represents best fit as per Equation 4.1). The response of the system at high and

intermediate frequencies was considered to correspond to the dielectric and interface properties of the cement paste and grout. The low frequency was considered to correspond to the faradic and metal-solution interface properties of the system.

Manifested in the impedance spectra of all samples were two distinct loops. The high frequency limit of the high frequency loop was attributed to the solution resistance (R_s) of the freshly cast paste. Figure 4.11 shows similar trends for R_s in all samples. Samples on Test Setup FS-LG showed some difference between the top and bottom tendon segments. The difference is attributed to the fact that the reference electrode was located approximately 2/3 closer to the bottom face than the top face of the segments. After one week, the values for R_s were approximately 20 ohms, consistent with values expected for a 0.45 water-cement ratio paste. R_s values compared with measurements taken with a Nilsson three point resistance meter showed strong correlation.

The transition between the high and low frequency loops was consistently observed at $1 < f < 100$ Hz. Unlike R_s, the low limit of the high frequency loop (R_c), attributed to the electrical resistance of the existing grout, did not greatly increase and apparent terminal values were observed within a few days of testing. This phenomenon is thought to be associated with the hydration of introduced cement paste into the tendon pore, voids and interstitial spaces of the strands. As shown in Figure 4.12, R_c for samples with grout white/chalky or segregated grout was significantly lower than of samples with grey/hardened grout. This is consistent with the high moisture content measured on samples with the white/chalky or segregated grout.

The capacitive behavior associated with the high frequency loop, as a first approximation, was thought to be associated with the dielectric behavior of the grout solid phase (Cabeza, Keddam, Nóvoa, Sánchez, & Takenouti, 2006; Cabeza, Merino, P. Miranda, & Sánchez, 2002; Keddam, Takenouti, Nóvoa, Andrade, & Alonso, 1997; Lau & Sagües, 2007).

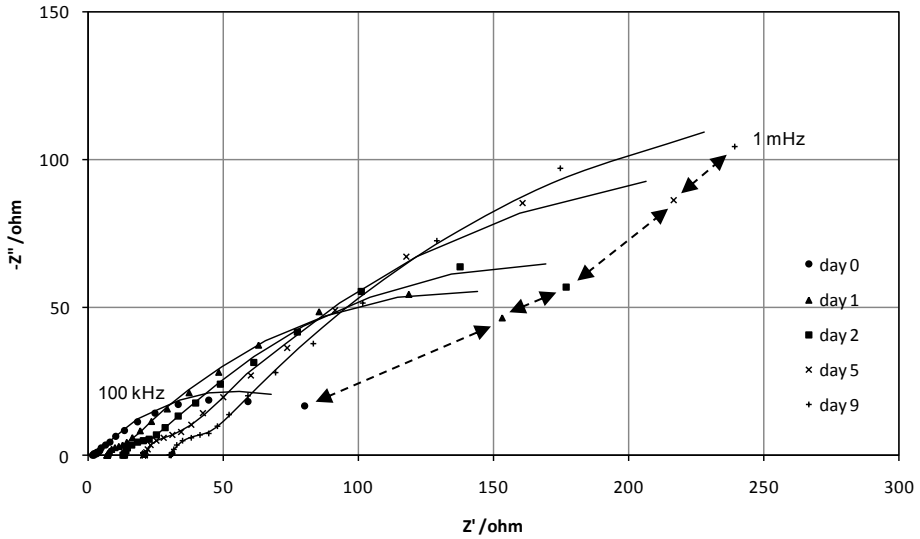

Figure 4.2 EIS results (Sample FS-SM-1).

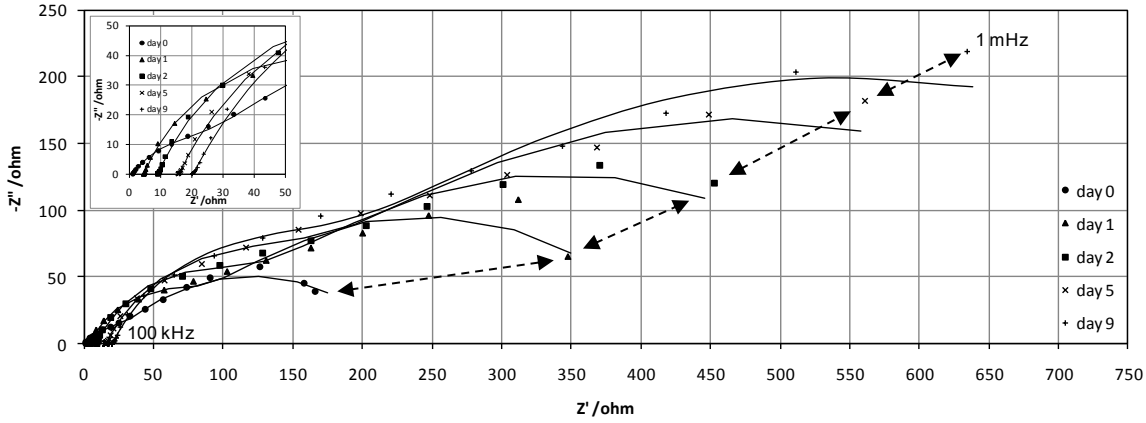

Figure 4.3 EIS results (Sample FS-SM-2).

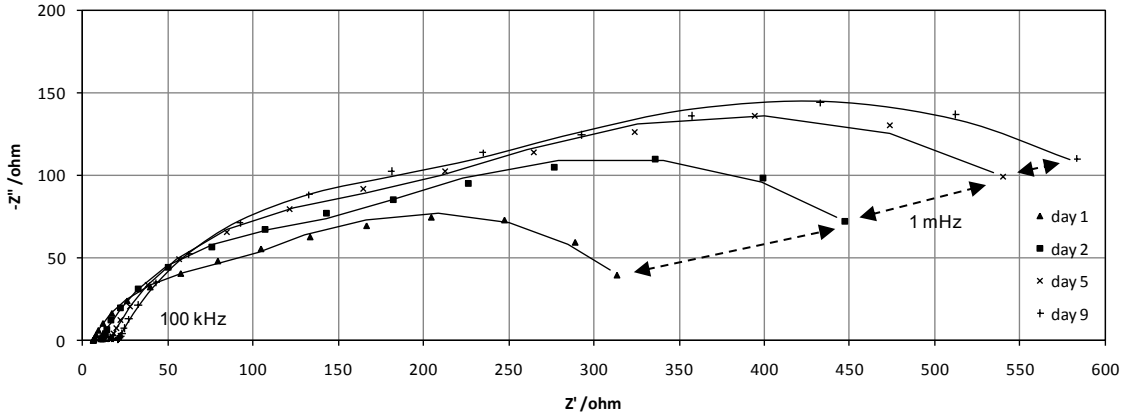

Figure 4.4 EIS results (Sample FS-SM-3).

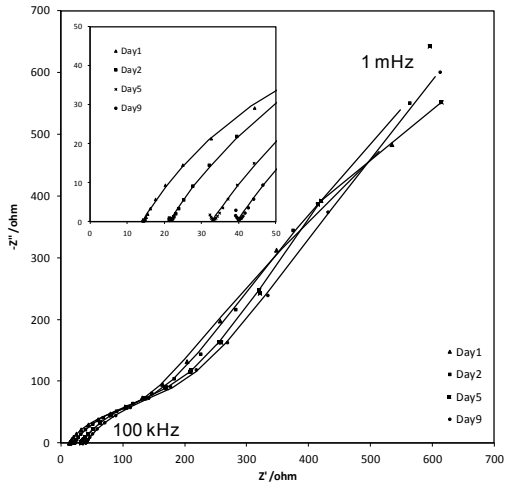

Figure 4.5 EIS results (Sample FS-LG-1-TOP).

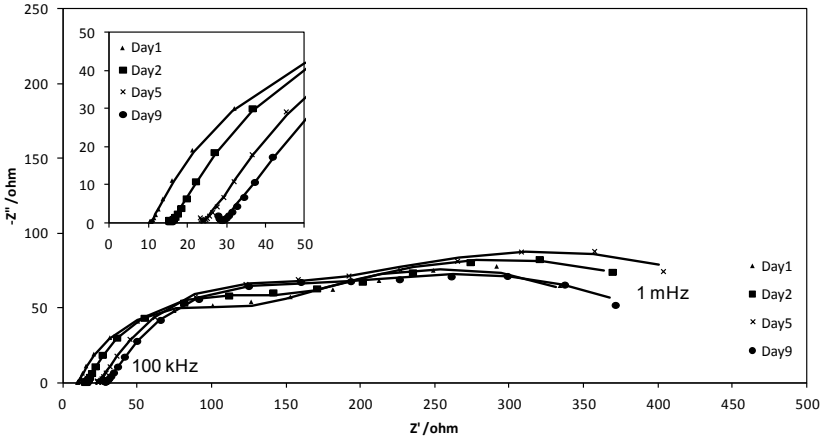

Figure 4.6 EIS results (Sample FS-LG-2-TOP).

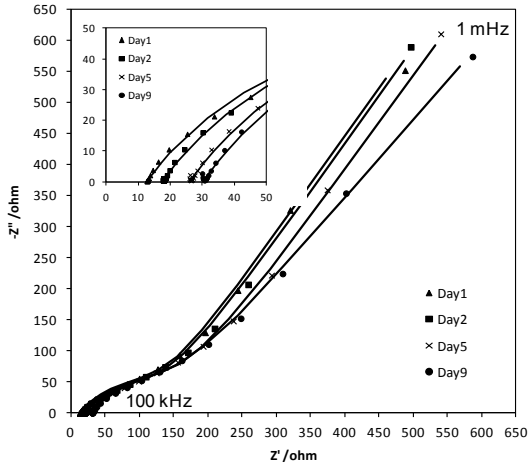

Figure 4.7 EIS results (Sample FS-LG-3-TOP).

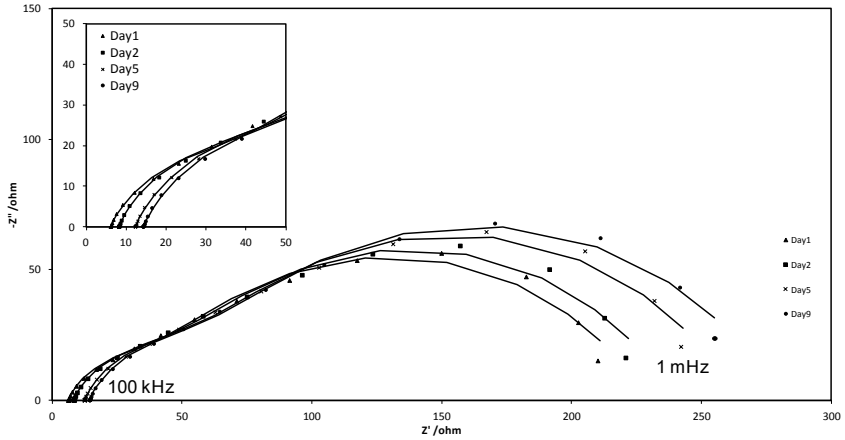

Figure 4.8 EIS results (Sample FS-LG-1-BOTTOM).

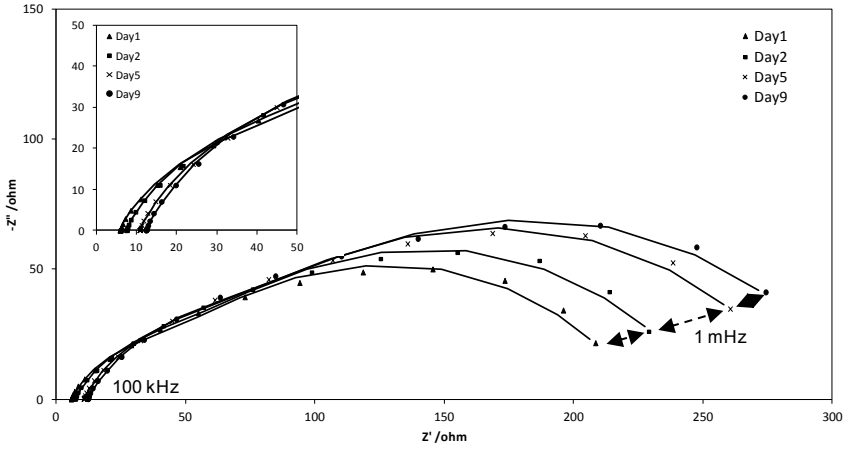

Figure 4.9 EIS results (Sample FS-LG-3-BOTTOM).

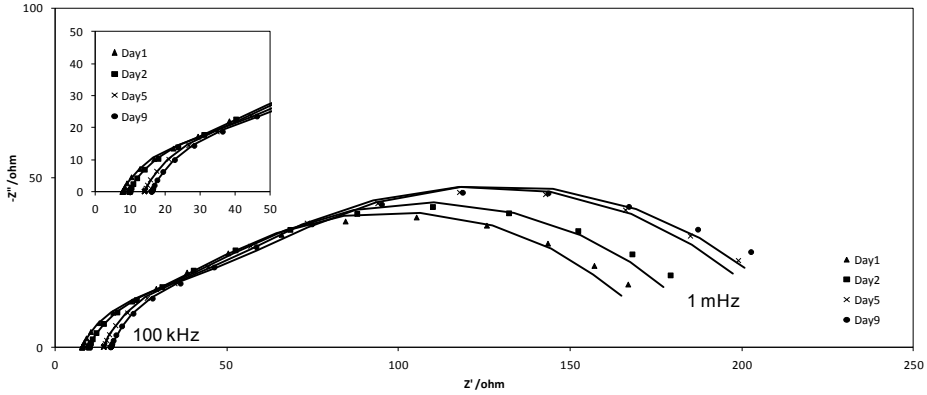

Figure 4.10 EIS results (Sample FS-LG-3-BOTTOM).

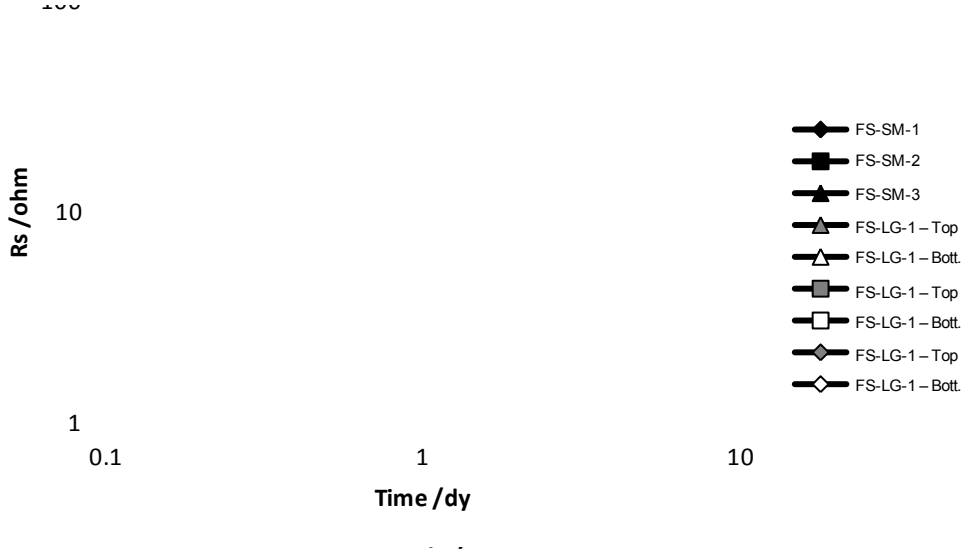

Figure 4.11 Solution Resistance (R_s) of the fresh paste.

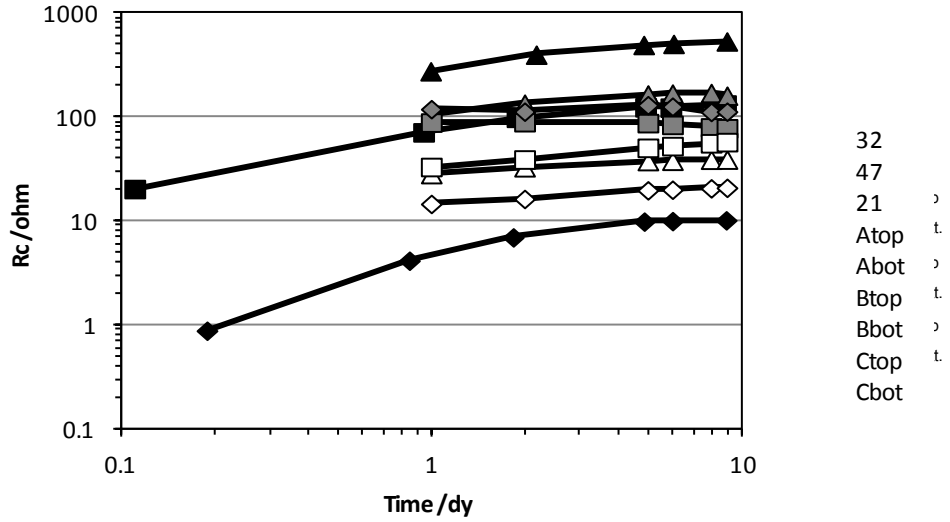

Figure 4.12 Solution Resistance (R_c) of existing grout.

The capacitance of the solid phase can be expressed as Equation 4.2, where ε is the solid phase dielectric constant, ε_0= 8.85x10^{-14} F/cm, and d is the thickness of the medium. Similar to findings by Lau and Sagüés, 2007 (Lau & Sagües, 2007), a general correlation between the pre-exponential CPE term, Y_{oc} (normalized to the lower bound of the estimated steel area in the sample, see Table 4.2) and n_c was observed, as shown in Figure 4.13.

$$C\left[\frac{F}{cm^2}\right] = \frac{\varepsilon\,\varepsilon_0}{d} \qquad \text{Eq. 4.2}$$

Extrapolation of Y_{oc} to an ideal case with n=1 (pure capacitance) yielded higher values for sample FS-SM-1 than for FS-SM-2. If a constant value is assumed for the thickness of the medium, ε for sample FS-SM-1 yields a value approximately two times greater than the ε obtained for sample FS-SM-2, consistent with the moisture content difference between the samples. The actual value of d was unknown but expected to be less than a fraction of a millimeter if the strand interstitial spaces and grout void was considered. Although general trends were observed, unique extrapolation for the other samples could not be made.

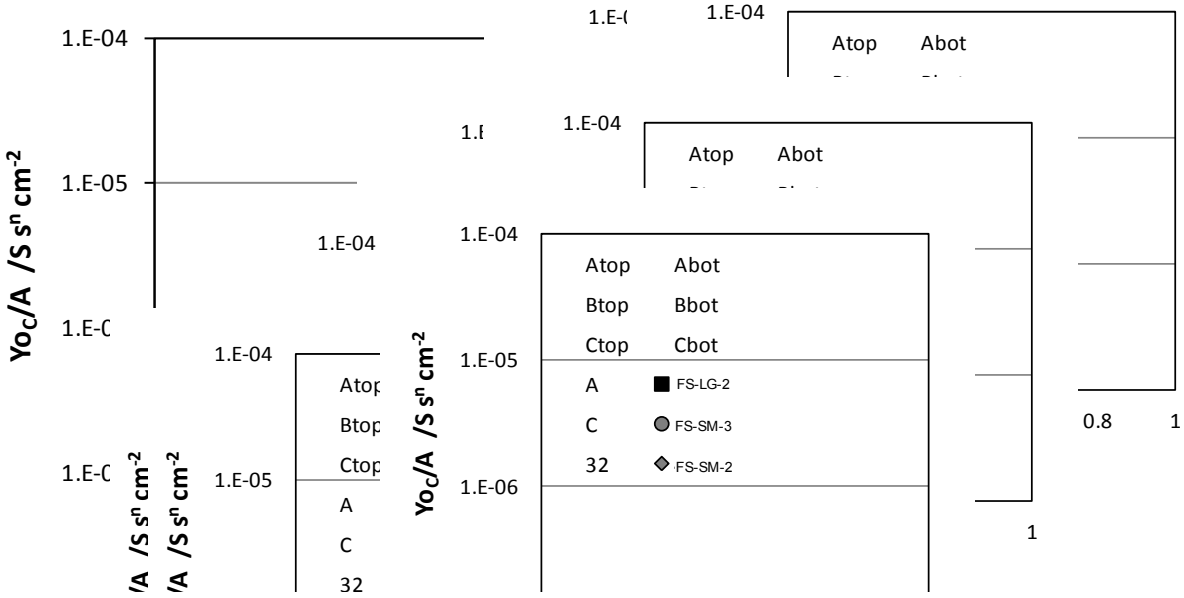

Figure 4.13 Correlation of Y_{oc} and n_c.

The low frequency limit of the impedance spectra was attributed to the faradaic processes at the metal-solution interface. Figure 4.14 and 4.15 shows the apparent corrosion current density, i_{corr}, defined by equation 4.3.

$$i_{corr}\left[\frac{A}{cm^2}\right] = \frac{B}{Rp} \qquad \text{Eq. 4.3}$$

The polarization resistance calculated by LPR end EIS for Test Setup FS-SM and FS-LG were generally consistent. See Figures 4.14 and 4.15. Because an exact area of the strand in contact with the grout was unknown and could vary depending on the amount of filling in the interstitial spaces within the strands and the introduced cracks in the grout due to the stress release during the failure, upper and lower bound areas were calculated. See Table 4.2. Upper bound areas are based on total surface area of the strands and the lower bound are based on a bar with a diameter of 1.5 cm. The exposed surface area of the cross sectional was accounted for.

Test Setup	Sample		Length (cm)	Area (upper Bound) (cm^2)	Area (upper Bound) (cm^2)
FS-SM	FS-SM-1		7.6	1874	833
	FS-SM-2		10.2	2488	1000
	FS-SM-3		10.2	2488	1000
FS-LG	FS-LG-1	TOP	10.2	2488	1000
		BOTT.	10.2	2488	1000
	FS-LG-2	TOP	10.2	2488	1000
		BOTT.	10.2	2488	1000
	FS-LG-3	TOP	10.2	2488	1000
		BOTT.	10.2	2488	1000

Table 4.2 Corrosion test cell areas.

The corrosion rate measured by electrochemical methods here cannot be used quantitatively as the area of steel in contact with the grout and the area with active corrosion are not precisely known. The case can be made that even if the tendon grout did not completely filled the strand interstitial spaces, moisture from the cast cement paste may have filled a significant portion of the voids, and the apparent corrosion current density would be closer to values calculated with the lower bound area. Of notice, the i_{corr}, calculated by LPR, in samples with white/chalky grout was greater than for samples with the hardened grout. At first, apparent corrosion rates calculated for samples in Test Setup FS-LG may be indicative that no significant corrosion rates were present at the time of the experiments. However, corrosion at these locations would not be expected to be uniform, and i_{corr} values would not necessarily be representative of corrosion at anodic spots. This would prove particularly true for tendons where only portions of the cross section containing deficient grout material had strand with active corrosion.

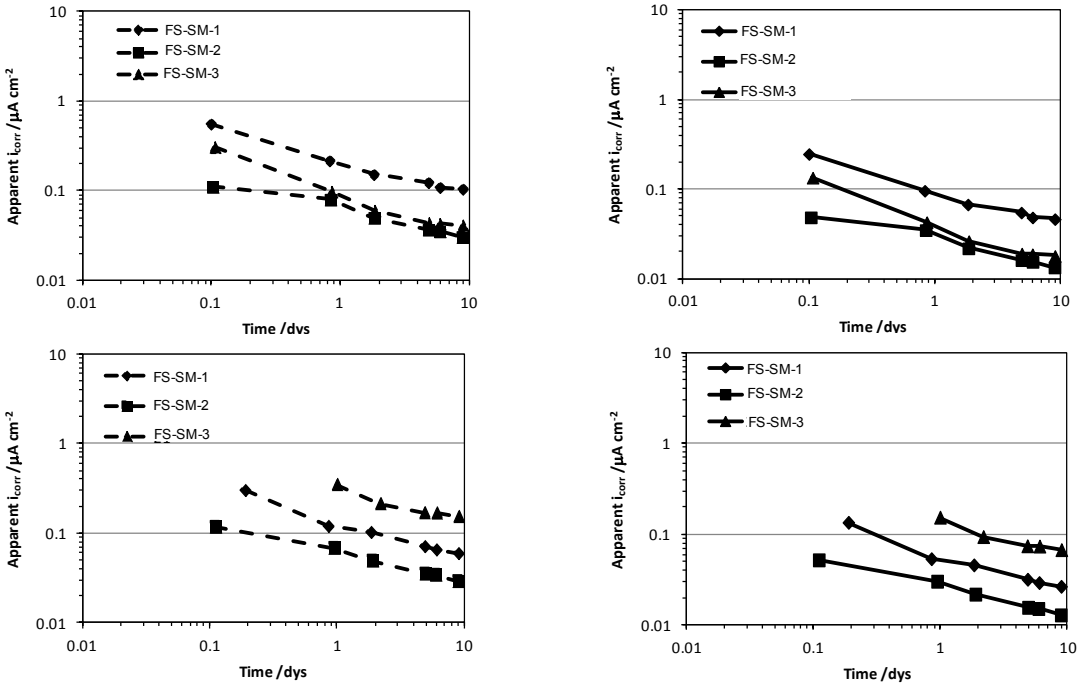

Figure 4.14 Apparent i_{corr} for Test Setup FS-SM. (a) determined by LPR and upper bound area, (b) determined by LPR and lower bound area, (c) determined by EIS and upper bound area, (d) determined by EIS and lower bound area.

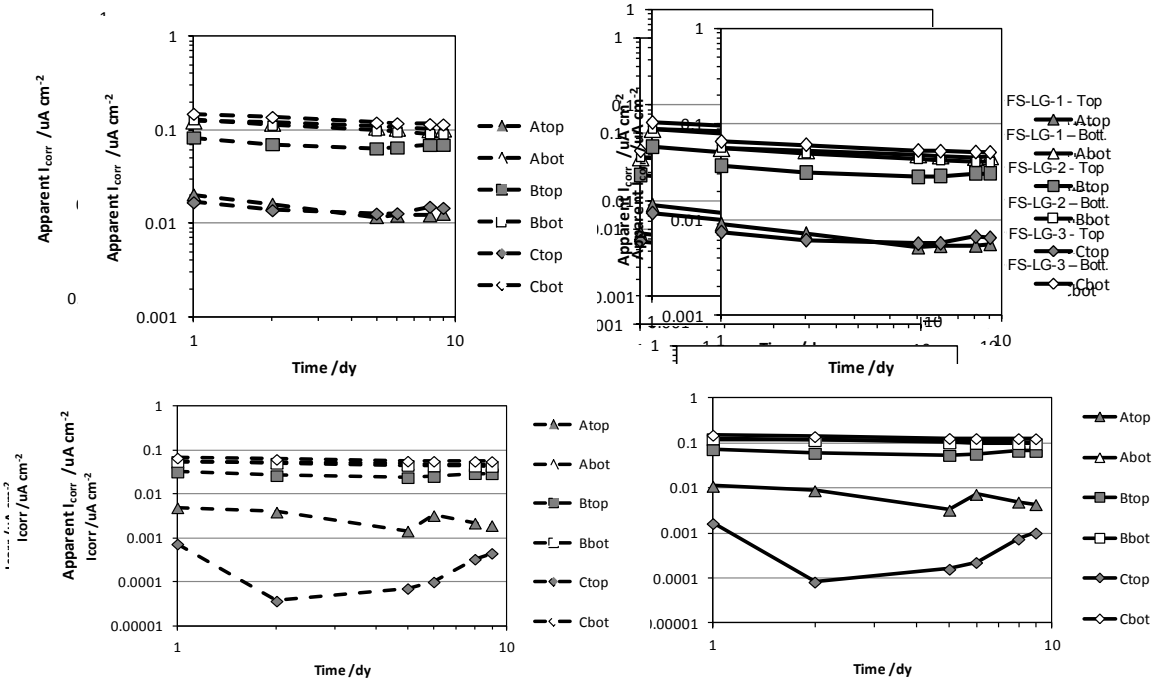

Figure 4.15 Apparent i_{corr} for Test Setup FS-LG. (a) determined by LPR and lower bound area, (b) determined by LPR and upper bound area, (c) determined by EIS and upper bound area, (d) determined by EIS and lower bound area.

As shown in Figure 4.16, autopsy examination of the samples in Test Setup FS-SM after testing did show surface rust on the strands on all three samples. However, in sample FS-SM-1 (Figure 4.16a), in which the white/chalky grout was present, greater corrosion product was appreciated. In this sample, corrosion product was concentrated near the interstitial spaces and the center wire. The observed corrosion may have in part been present prior to laboratory testing as corrosion was evident in nearby autopsied tendon sections reported elsewhere. However, the amount of corrosion present on sample FS-SM-1 after the autopsy was more extensive than previously examined, and is thought to be associated with the rewetting process of the sample interstitial spaces from the newly introduced cement paste. This observation may raise concerns of possible corrosion concern for repair procedures where new repair grout is introduced in the tendon.

From result from Test Setup FS-LG, generally active corrosion was measured in the strand or sections of the tendon with the white/chalky grout (bottom section of the sample). The steel strand generally remained passive in the hardened grout, except for the top section of sample FS-LG-2. This section gave indication of more active corrosion even thought replicate sample from the same section of the failed tendon showed passive conditions. Steel surface condition after testing is shown in Figure 4.16.

(a) (b) (c)

Figure 4.16 Autopsy of Test Setup SF-SM: (a) FS-SM-1, (b) FS-SM-2, (c) FS-SM-3.

Apparent corrosion rates in the presence of the white/chalky and wet plastic state was significantly higher than the strands embedded in the hardened grout, which generally showed passive corrosion condition. In comparison, the bottom sections of the Test Setup FS-LG (with white/chalky or wet/plastic grout) showed corrosion rates comparable to the rates obtained from samples in Test Setup FS-SM.

It was also appreciated that for the bottom sections of Test Setup FS-LG, OCP showed potentials more negative than -350 mV_{SCE}. This is consistent with the active corrosion observed and measured by LPR and EIS. The OCP potentials for the top sections of this test group were constantly in the range of -250 < E < -200 $mV_{SCE,}$ giving the appearance less active corrosion conditions.

Supplemental potentiodynamic polarization measurements were made for samples in Test Setup FS-SM from -200 mV to 400 mV with respect to OCP, and results are shown in Figure 4.17. Current density was calculated using the lower bound steel area as shown on Table 4.2. The anodic portion of the curves showed an incremental increase in anodic current with an increase in applied anodic overvoltage. The applied anodic Tafel slope appears to be > 600 mV/decade. This response is indicative of near passive behavior of the strand at the time of testing.

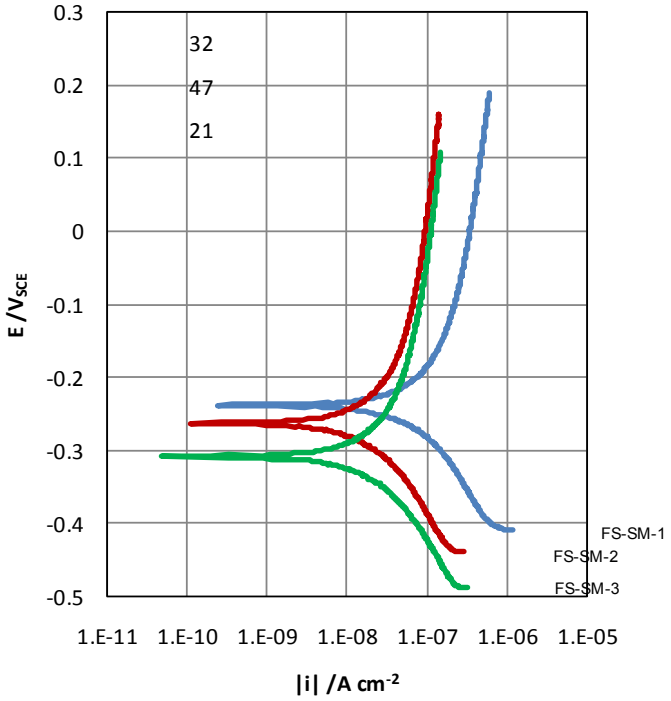

Figure 4.17 Potentiodynamic Polarization (Test Setup FS-SM).

It can be observed that the apparent near passive current density for sample FS-SM-1 (with segregated grout) was approximately three times higher than for sample FS-SM-2 and FS-SM-3. This may be indicative of weaker passivation conditions in the segregated grout but care must be taken as this

difference may be within the limits of uncertainty introduce by the unknown area of the strand in contact with the grout. If galvanic coupling is possible, such as that implicated by the variation in OCP within the same tendon, anodic polarization of 100 mV could more than double the corrosion rate. The cathodic performance of the strand was not evaluated.

For the samples in Test Setup FS-LG, tendency to macrocell corrosion was evaluated by coupling sections with white/chalky or wet/plastic with sections with hardened grout as describe in Chapter 3 - Methodology. After approximately ten days of casting the samples, sections were coupled and OCP, corrosion rate, and macrocell current were monitored. Figures 4.18 through 4.21 show the results. Prior to coupling, OCP for top and bottom sections were monitored as independent sections. As expected, the galvanic coupling of the sections created a mixed potential intermediate to the independent sections OCP. Results are shown in Figure 4.18. This potential was stable through the first month of testing. This provided anodic polarization of the bottom section that already had active corrosion and thus enhanced the steel dissolution rate. Two of the test samples showed large corrosion macrocell current corresponding to the bottom section acting as the anode.

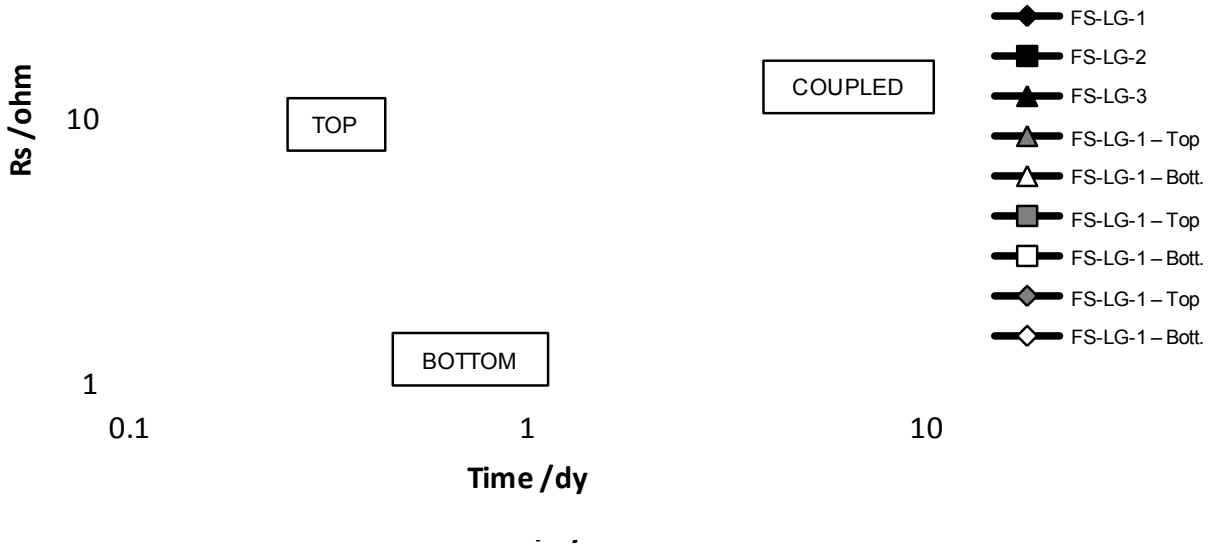

Figure 4.18 OCP before and after coupling (Test Setup FS-LG).

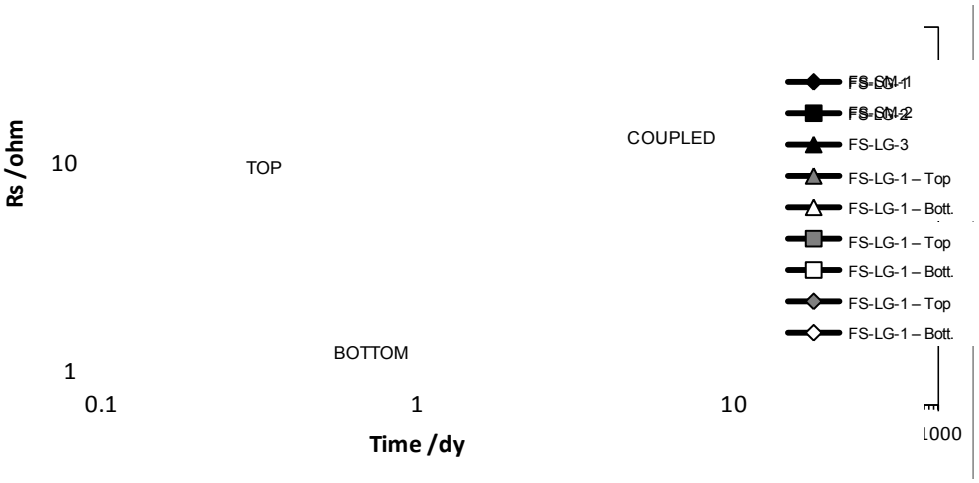

Figure 4.19 Macrocell current after coupling (Test Setup FS-LG).

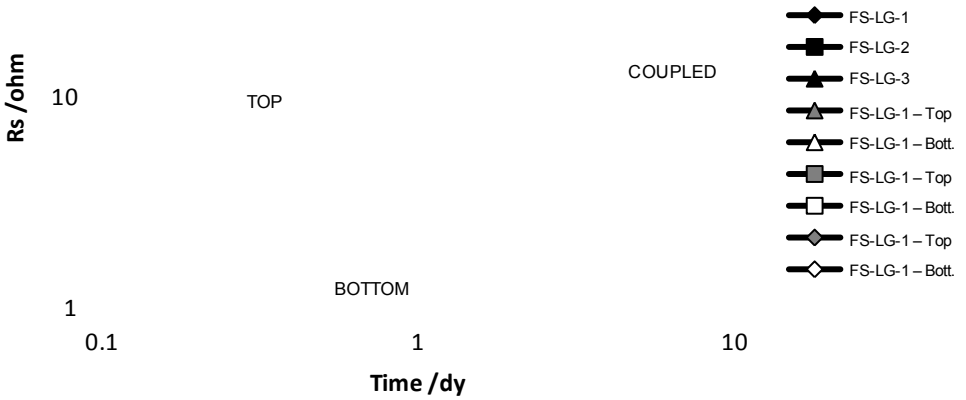

Figure 4.20 Developed corrosion rate after galvanic coupling calculated by LPR.

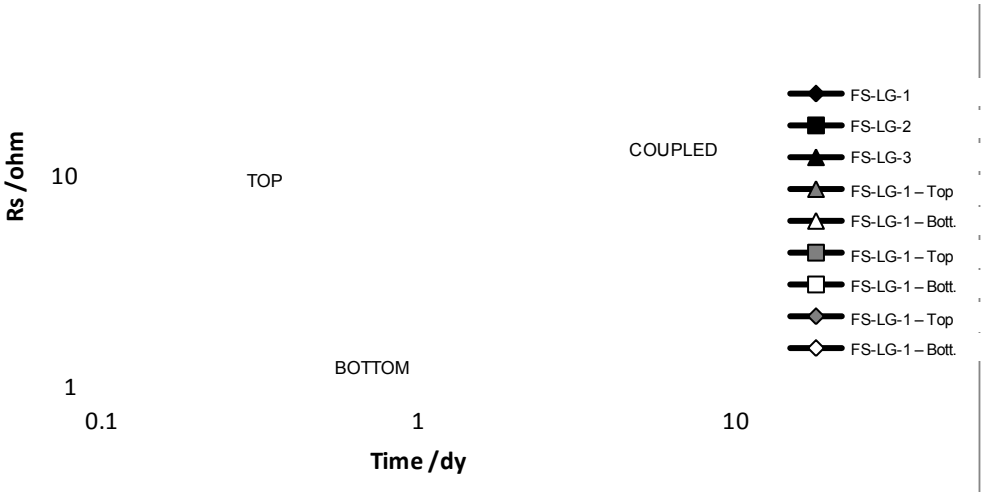

Figure 4.21 Developed Corrosion rate after galvanic coupling calculated by EIS.

As shown in Figure 4.19, one of the samples showed the top section acting as an anode for the first two months. The macrocell current after approximately 1 day of testing was between 60 to 120 μA and decreased to about 40 μA after approximately 4 months. This decrease is in part attributed to the increase in resistance of the fresh paste due to associated hydration. The macrocell at the time of coupling was generally in agreement with the measured potentials difference between the top and bottom sections.

As a general estimation, macrocell current can be estimated as the quotient of the potential difference and solution resistance as given by Equation 4.4, but generally yields values six to seven times greater than those actually measured.

$$i_{macrocell,est} = \frac{E}{R_s + R_c} \qquad \text{Eq. 4.4}$$

Of notice, the surface of the fresh paste (Figure 3.1) was not sealed and oxygen diffusion was not impaired through the sample. This may provide different oxygen availability to the anodic and cathodic areas, providing larger macrocell polarization and possibly greater degree of enhanced corrosion. This can be the case in actual field tendons, if differences in oxygen availability exist due to the presence of cracks in the ducts, poorly sealed connections or poorly sealed grout inlets or outlets.

The apparent corrosion rate as calculated by LPR and EIS showed increase after coupling of the sections. In Figures 4.20 and 4.21, the apparent corrosion rate has not been normalized by area, since the areas corresponding to the anodic and cathodic sites are unknown. As expected, the macrocell current was less than the apparent corrosion current due to the macrocell being a measure of the net behavior between local and extended anodic and cathodic regions in the top and bottom sections. Figure 4.22 shows a correlation graph between apparent corrosion current and macrocell corrosion.

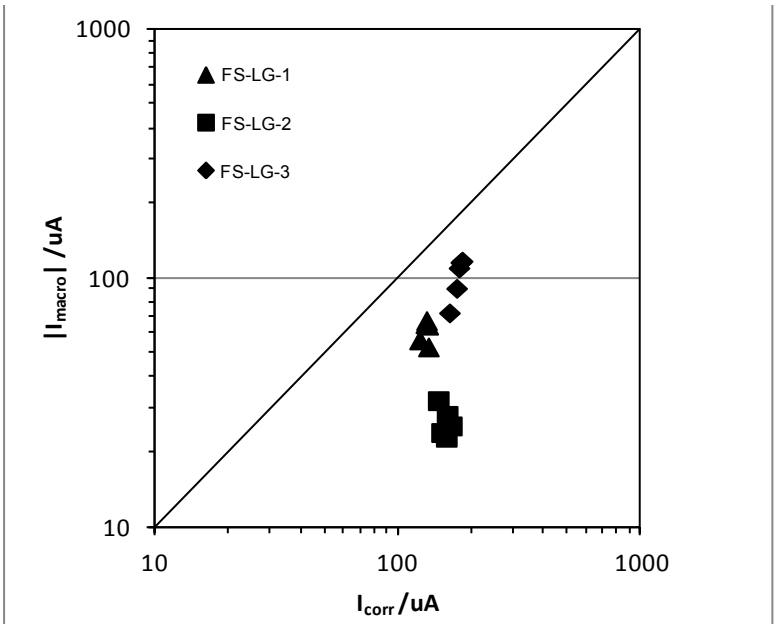

Figure 4.22 Comparison of apparent corrosion current (I_{corr}) and macrocell corrosion

4.1.2 REPAIR OF VOIDS WITH DISSIMILAR GROUT (FS / FSR)

As shown in Table 4.3, samples in Test Setup FS showed what appear to be grey/hardened grouts with low moisture content and no corrosion was evident when samples were built.

Test Setup	Sample	Moisture Content (%)	Grout Characteristic	Corrosion Observed
FS	FS-1	10	Grey/Hardened	No
	FS-2	15	Grey/Hardened	No

Table 4.3 Field samples grout characteristics (Test Setup FS).

From analysis of the EIS testing data displayed on Figures 4.23 and 4.24, manifestation of the two distinct loops was also evident, although less obvious on sample FS1. The high frequency limit of the high frequency loop, R_s, that has been attributed to the solution resistance of the freshly cast paste, showed similar trend as previous samples and as discussed for Test Setup FS-SM (see insert on figures 4.23 and 4.24). After approximately 300 days of testing, values for R_s were approximately between 375 to 425 ohms. The solution resistance attributed to the existing grout, R_c, can be obtained from the high limit of the low frequency loop. From the values obtained for the polarization resistance, R_p, the apparent

corrosion current density can be calculated by using equation 4.3. Complete results from EIS for Test Setup FS and FSR are presented in Appendix B.

In Test Setup FS, the embedded strands in the sample showed typical passive like behavior with OCP values more positive than approximately -200 mV_{SCE}. The overall apparent corrosion rates were lower than 0.001$\mu A*cm^{-2}$, also indicative of passive like behavior, as shown in Figure 4.25 and 4.26. Also noted, sample FS1 showed greater corrosion density and more negative potentials than sample FS2. For approximately the first fifty days, sample FS1 showed an enhanced corrosion activity of the steel embedded in the existing grout, as shown in Figure 4.27.

From the analysis of macrocell corrosion development, the cumulative anodic charge for the steel in the existing grout was calculated for the period that the anodic behavior was manifested, (approximately the fifty days from begin of testing), and is shown in Figure 4.28.

It is important to note that the ratio of steel area in the repair grout to the steel in the existing rout was <0.02. This low ratio was due to limitations of the geometry of the field extracted specimen. If active corrosion were to be present in the existing grout, the macrocell current would be expected to be significantly higher if there was more steel in the repair grout (introduced strand wires as describe in Chapter 3 - Methodology).

As shown in Figure 4.27, corrosion dissipated to negligible currents after aprroximately fifty days which can associated to the increase in the solution resistance of the existing grout. As discussed earlier, the component of solution resistance, R_c, was thought to be associated with the grout solution resistance in the interspaces of the existing grout. The increase in R_c, shown in Figure 4.29, is in part attributed to continued hydration after introduction of water and later reabsorbtion in the cracks of the grout.

Both samples on Test Setup FS (after day fifty) showed relatively low macrocell currents with net anodic current for steel embedded in the repair grout in the order of approximately 0.5 μA. Although not insignificant here for the geometry of the test specimen, anodic behavior in the repair grout is expected to be mitigated in bridge tendons in time as the grout continues to hydrate (assuming prevention of external moisture, aggressive chemical species contamination and proper repair grout setting).

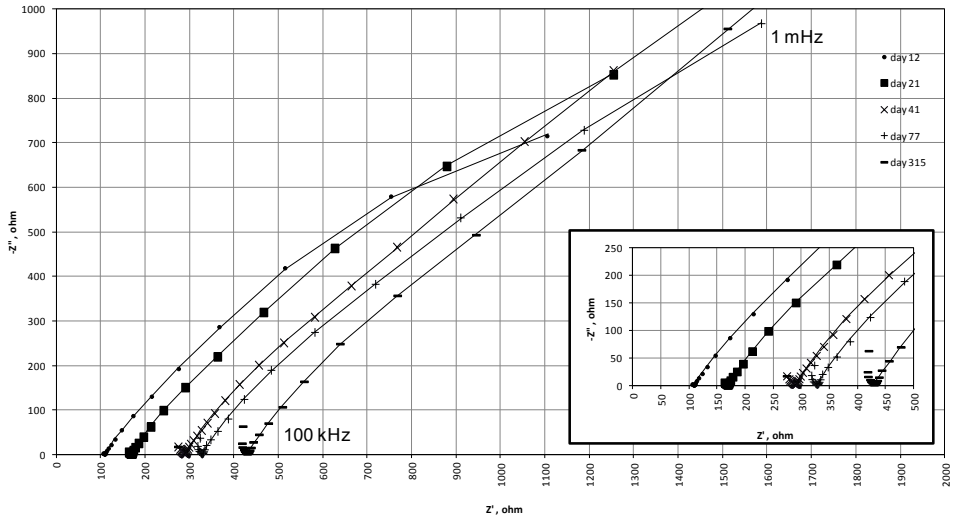

Figure 4.23 Nyquist Plot for impedance spectrum data and best fit by Eq. 3.1 (Test Sample FS1).

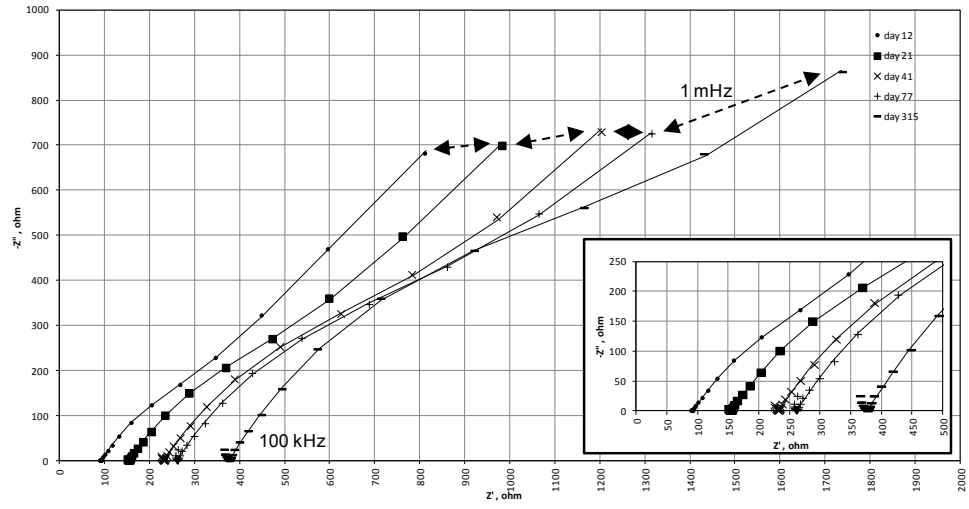

Figure 4.24 Nyquist Plot for impedance spectrum data and best fit by Eq. 3.1 (Test Sample FS2).

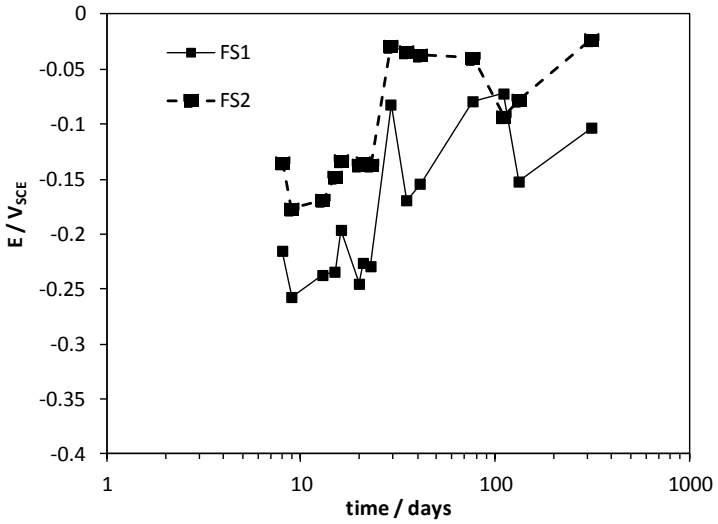

Figure 4.25 OCP measurements (Test Setup FS).

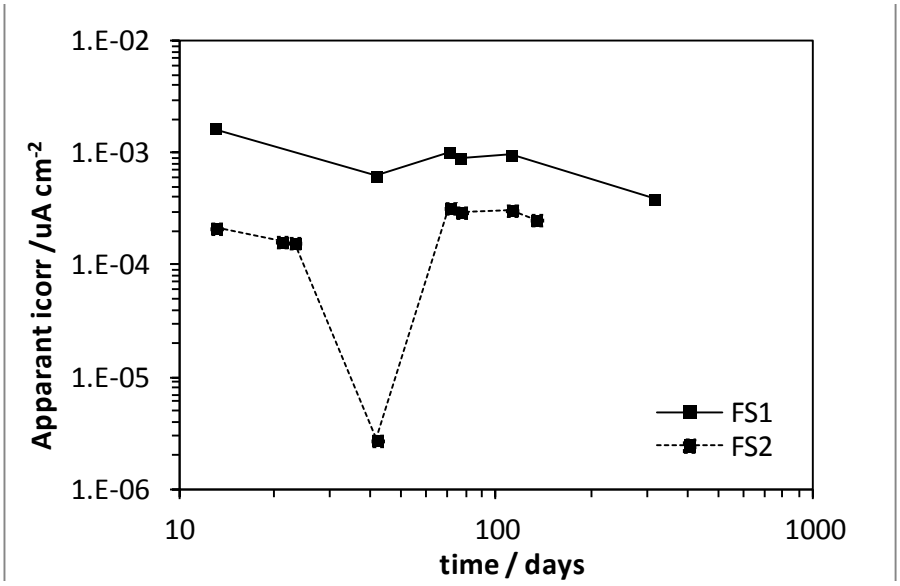

Figure 4.26 Apparent corrosion density calculated by LPR (Test Setup FS).

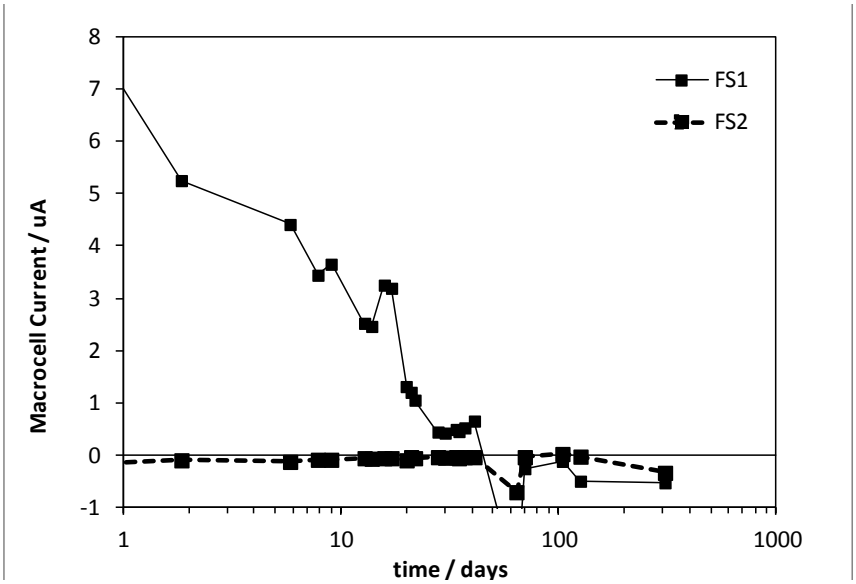

Figure 4.27 Macrocell current development (Test Setup FS).
(Positive current indicates steel in existing grout is the net anode).

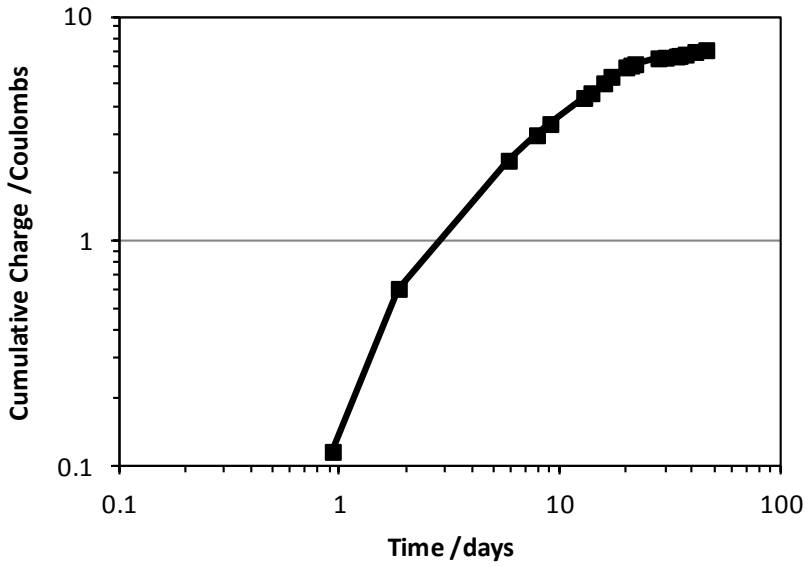

Figure 4.28 Cumulative charge of anodic behavior (Sample FS1).

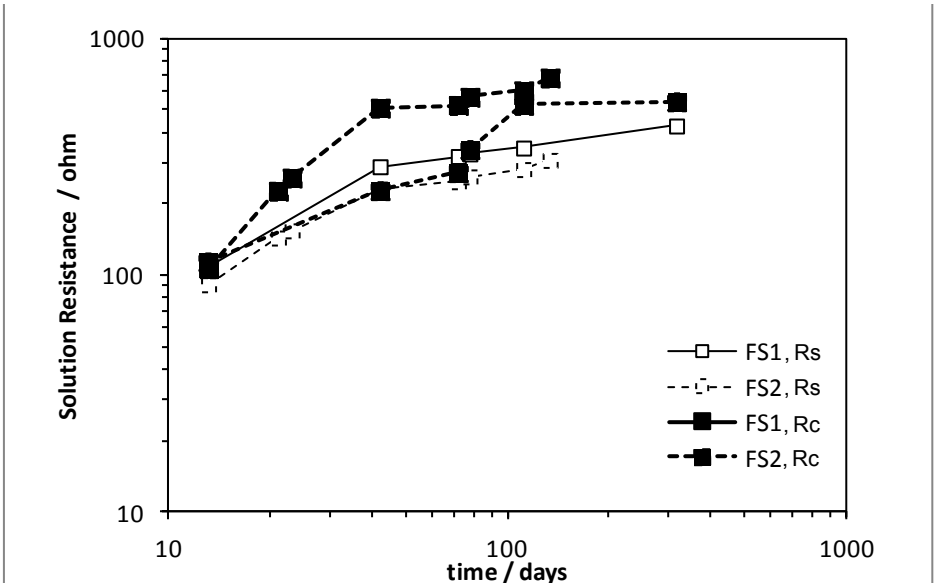

Figure 4.29 Development of solution resistance (Test Setup FS).

Although there were major cracks in the existing grout, the overall integrity of the repair did not appear to contain significant deficiencies in grout setting, incongruities of physical appearance, and electrical properties at the cold joint. The effect and assesment of surface contamination by either dust or excess moisture was not considerd.

After performing an autopsy of the samples on Test Setup FS, the manifested corrosion was associated to a localized pocket of white/chalky grout located at the edge of the pre-existing void, and shown in Figure 4.30. The corrosion was thought to begin after introduction of excess moisture from the repair grout into the crevice area formed by the cracks in the existing grout. The surface of the steel wire embedded in the repair grout did not show any appearance of corrosion after autopsy and final examination of the samples, as evident in Figure 4.31a and 4.31b.

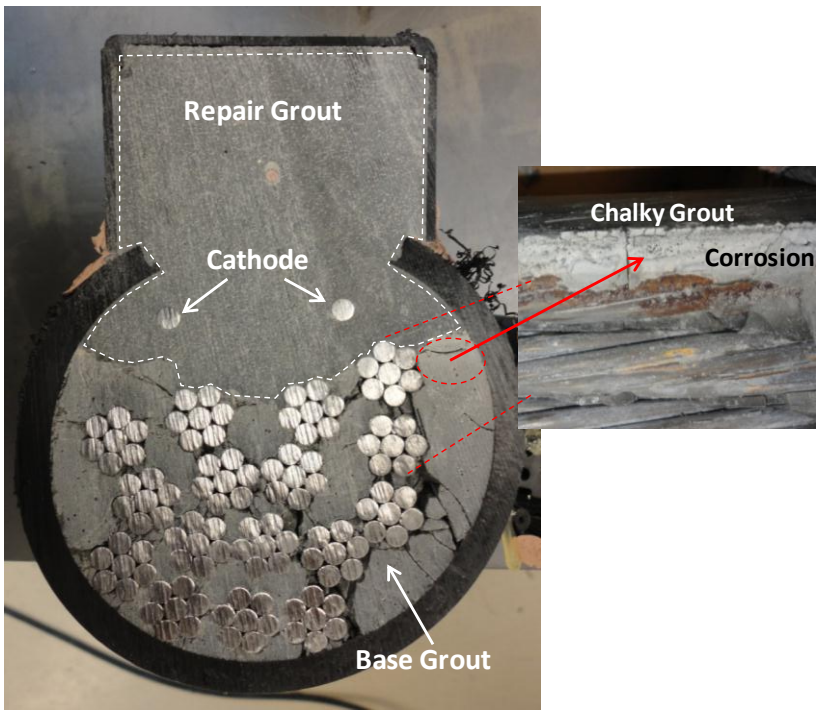

Figure 4.30 Cross section of sample FS1 after autopsy.

Figure 4.31 Strand embedded in existing grout after testing. (a) Sample FS1 with corrosion manifestation, (b) Sample FS2.

. Similar to previous samples, in Test Setup FSR, the high frequency limit of the high frequency loop, R_s (attributed to the solution resistance of the freshly cast paste) showed similar trend reaching values of approximately from 500 to 600 ohms after approximately 160 days of testing (see insert on figures 4.32 and 4.33). The solution resistance attributed to the existing grout, R_c, can be obtained from the high limit of the low frequency loop. From the values obtained for the polarization resistance, R_p, the apparent corrosion current density can be calculated using Eq. 4.1. Figure 4.32 and 4.33 show typical EIS Results for this test setup. Appendix B presents complete results for all samples in Test Setup FS and FSR.

For these samples, the embedded strands in the sample showed typical passive like behavior with OCP values more positive than approximately -200 mV_{SCE} after 20 days of casting, as shown in Figure 4.34. Also noted, the initial OCP for samples cast with repair grout 1 did show potentials that were more negative during initial testing. The initial difference in potential observed between repair grouts could be attributed to different water cement content ratio at time of mixture. Grouts were mixed according to manufacturer specifications with the minimum recommended amount of water. However, water cement ratio could not be determined, since the specific content of cement of the grouts was not available.

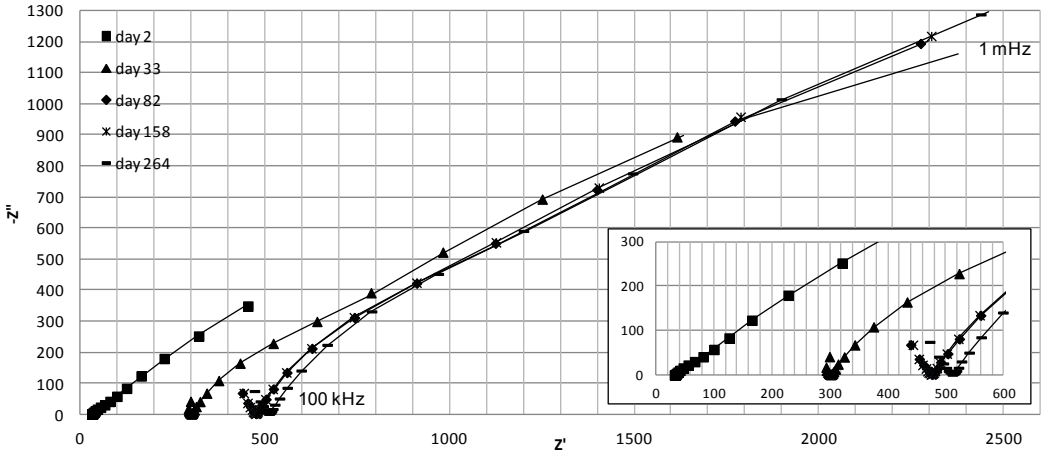

Figure 4.32 Nyquist Plot for impedance spectrum data and best fit by Equation 3.1 (Test Sample FSR-R1-1).

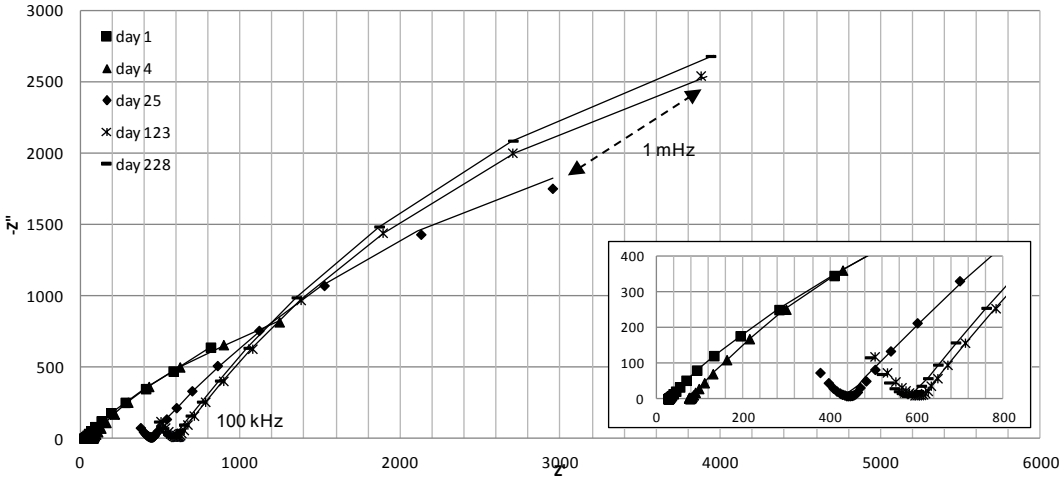

Figure 4.33 Nyquist Plot for impedance spectrum data and best fit by Equation 3.1 (Test Sample FSR-R2-1).

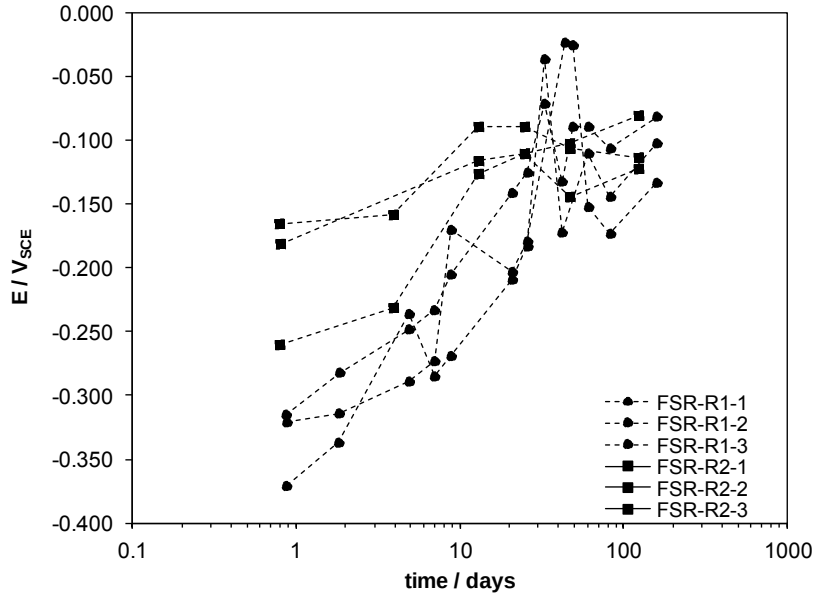

Figure 4.34 Developed OCP (Test Setup FSR).

Similar passive like behavior was observed for the samples in corrosion densities calculated by LPR and EIS, as the overall apparent corrosion rates, shown in Figure 4.35, were lower than 0.01 $\mu A*cm^{-2}$. Also noted, the apparent corrosion density obtained for samples repaired with repair grout 1, when calculated by EIS, showed higher values than rates obtained by LPR. Still, the values obtained by EIS were below $0.1\mu A*cm^{-2}$, suggestive of passive behavior.

Also in this test setup, the component of solution resistance was thought to be associated with the grout solution resistance in the interspaces of the existing grout. The increase in R_s in time was in part attributed to continued hydration after introduction of water along the repair grout, and later reabsorbtion of into the cracks of the grout, as shown in Figure 4.36.

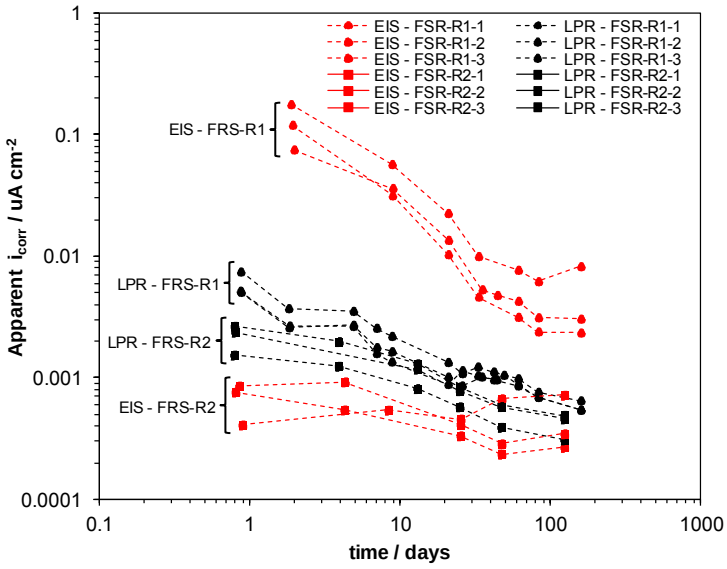

Figure 4.35 Corrosion current density calculated by LPR and EIS (Test Setup FSR).

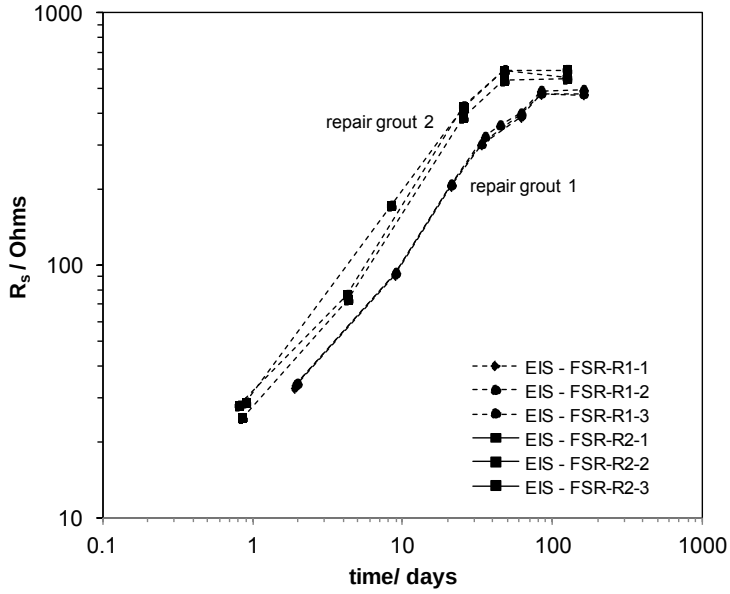

Figure 4.36 Development of solution resistance (Test Setup FSR).

4.2 LABORATORY SAMPLES

4.2.1 REPAIR

4.2.1.1 Repair Materials (S)

From analysis of results from Test Setup S, a baseline of corrosion conditions of clean and pre-rusted wires was assessed. After approximately two months of testing, OCP in all grouts were similar with values ranging from -100 > E > -200 mV_{SCE}, and a corrosion current density below 0.1 $\mu A*cm^{-2}$. These results are consistent with near passive conditions, as shown in Figures 4.37 and 4.38.

At early stages of testing, the steel in the repair grouts showed more negative potentials than the wires embedded in the neat grout, showing differences of several hundred mV. In general, steel with pre-rusted surface showed more negative potentials and higher apparent corrosion density through the test period than the as received wires.

Measurements of solution resistance showed significantly lower values for the neat grout than for the pre-bagged grouts, as shown in Figure 4.39. Results were consistent for measurement made with the three-point resistance meter and values obtained from EIS. The low solution resistance values in the neat grout may be due to the lack of pozzolans on the cement paste. This may be indicative that the porosity of the neat grout could be higher and thus, capable of accommodating more pore solution.

Differentiation between grouts was also apparent in anodic and cathodic polarization behavior. The apparent passive corrosion current densities of the steel in the base grout were greater than in the repair grouts. In addition, the apparent current density in each grout was higher for the pre-rusted wires than for the as-received wires. In the presence of surface rust, lower cathodic currents were measured, possibly indicating decreased oxygen reduction efficiency in the pre-rusted surfaces. The larger anodic currents in the pre-rusted condition suggest conditions not favorable for early steel passivation in the cementitious material consistent with observations by González, Ramírez, Bautista, & Feliu, 1995. Novak, Mala, & L.Joska, 2001 suggested that unacceptable corrosion rates might even occur at low chloride concentrations for steel with pre-rusted surfaces.

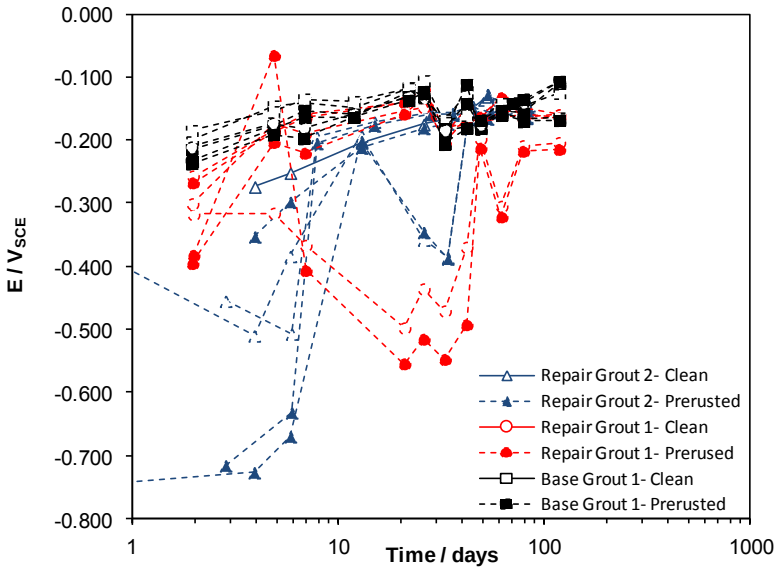

Figure 4.37 Developed OCP (Test Setup S).

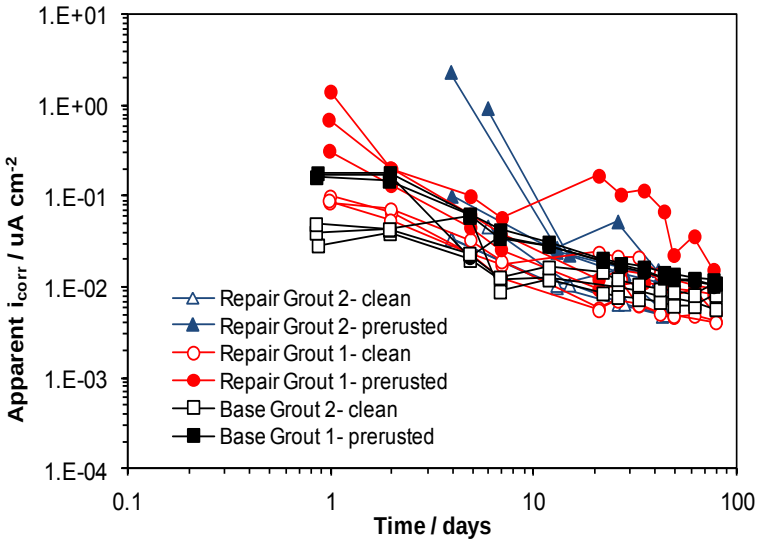

Figure 4.38 Apparent corrosion densities calculated by LPR (Test Setup S).

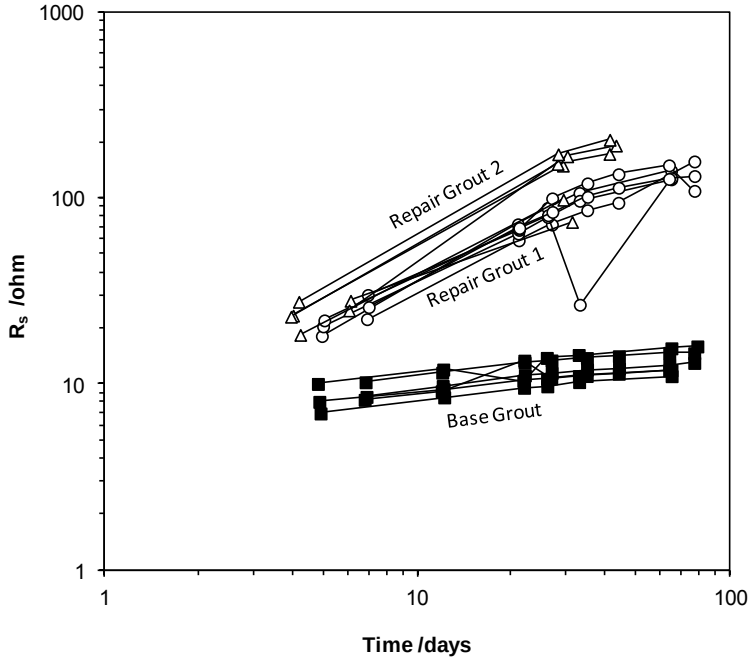

Figure 4.39 Solution resistance of base (neat) and repair grouts.

The rates of the cathodic processes of the steel at negative potentials are dependant of the oxygen availability at the steel surface (Luca Bertolini, 2004). For a given potential, rates decreases are associated with increase in moisture content (less oxygen) in the concrete. However, as the as-received and pre-rusted wires were cast in the same sample, and thus, moisture content variation should be negligible, data suggest that the oxygen reduction reaction would be less efficient in the pre-rusted wires for a given grout.

Differences in the corrosion behavior of steel in the base grout and repair grouts as well as the extent of surface rust present may be a parameter for corrosion development in repaired tendon conditions. Coupling of steel embedded in the pre-existing grout and in repair grout that have similar corrosion characteristics described above, may lead to somewhat enhanced corrosion of steel in the pre-existing grout if cathodic oxygen reduction is significantly more efficient in the repair grout. This effect would be detrimental for the steel in the base grout where anodic polarization may lead to a greater anodic current, particularly with the presence of surface rust.

It is noted, that the open circuit potentials and corrosion currents were generally similar in the different grout materials, as shown in Figures 4.37 and 4.38. As such, for conditions present during laboratory testing, the extent of macrocell polarization between the base grout and repair grout would not seem to be adverse.

However, the local relative proportion of steel area in the repair grout and base grout would be of significance. To further elaborate on the scenario presented above, a case with a larger, more efficient cathode would represent a condition where the tendon would have a large void space (with minimally rusted strand) filled with repair grout. The oxygen availability would depend on the amount of moisture in the grout and access outside of the duct. As seen in Figure 4.39, the higher measured R_S for the repair grout than base grout would suggest less moisture in the repair grout and thus greater oxygen availability within the grout.

The difference in anodic and cathodic behavior is in part, related to differences in the grout chemistry and steel surface conditions. The larger anodic currents measured for steel embedded in the base grout are likely, attributed to the lower solution resistance in the grout. But as seen in laboratory tests in solution, larger anodic currents can also be attributed to increases in the anodic current exchange density due to increase in pH and presence of aggressive chemical species. Presence of surface rust would cause similar behavior. Lower moisture presence in the repair grout may in part account for greater oxygen presence and higher cathodic currents at potentials less negative than -400 mV_{SCE}. At more negative cathodic potentials, the cathodic reaction would become limited by diffusion of oxygen in the bulk pore solution at the steel surface. See Figures 4.40, 4.41 and 4.42.

After performing an autopsy of the samples, the clean and pre-rusted steel surfaces appeared as expected. Shown in Figure 4.43 are representative samples of the strand wires after testing for Test Setup S. Compatible with presented results, no evidence of surface rust was observed in either the clean or the pre-rusted wires.

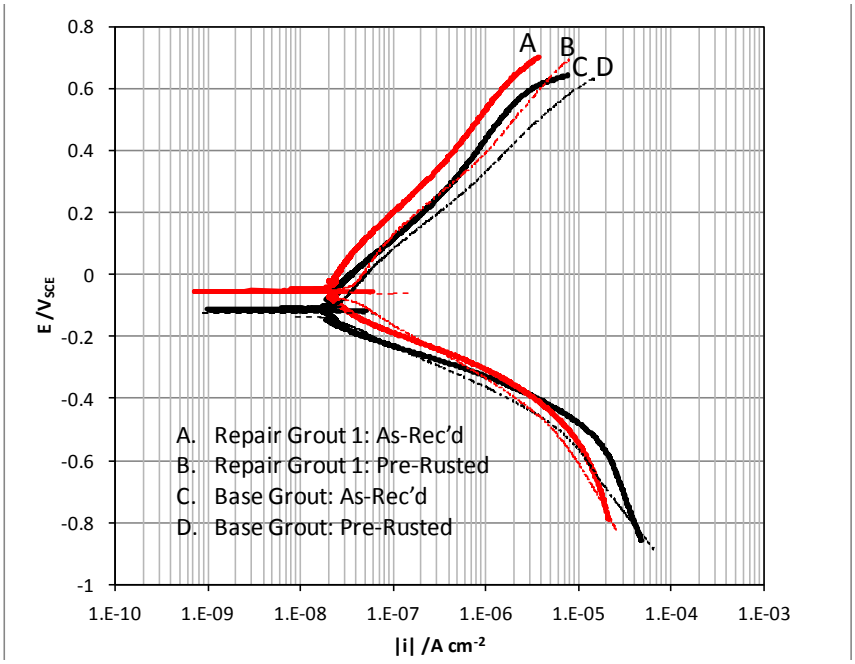

Figure 4.40 Anodic and cathodic polarization of steel in base and repair grouts.

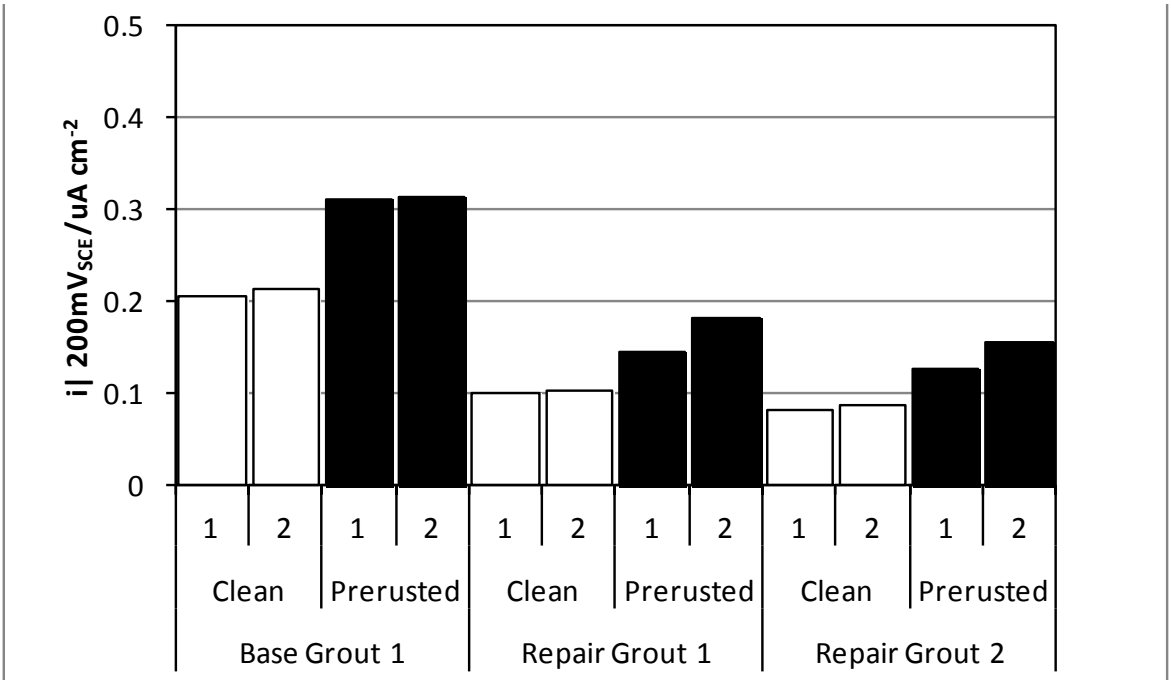

Figure 4.41 Anodic current at potentiodynamic polarization, |i| at 200 mV$_{SCE}$.

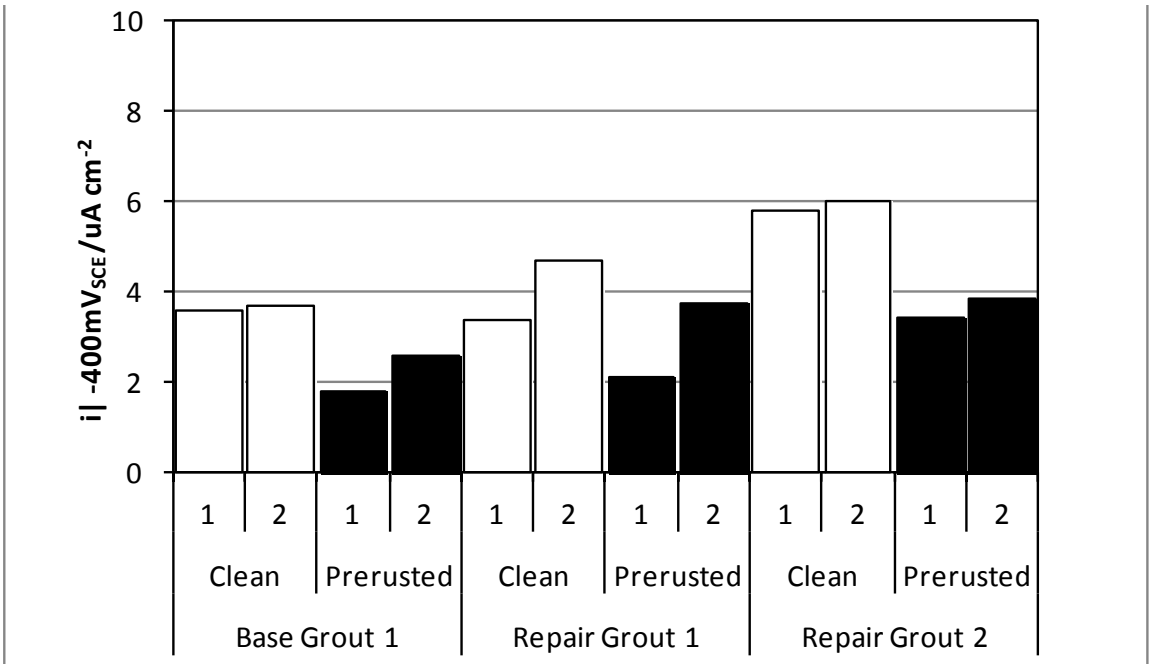

Figure 4.42 Cathodic current at potentiodynamic polarization, |i| at -400 mV$_{SCE}$.

Figure 4.43 Autopsy of Test Setup S.

4.2.1.2 Repair of Voids With Dissimilar Grouts (A / B)

The OCP of the steel wire embedded in the neat and repair grouts after one month of testing was generally indicative of passive conditions. During this period, the open circuit potential were constantly between -200 < E < -100 mV_{SCE}. This was also manifested in the low corrosion current density measured by LPR, which after approximately thirty days were below 0.1 $\mu A*cm^{-2}$. The measured corrosion densities showed a decrease in time that is indicative of the increase in solution resistance due to the hydration processes, as shown in Figures 4.44 and 4.45.

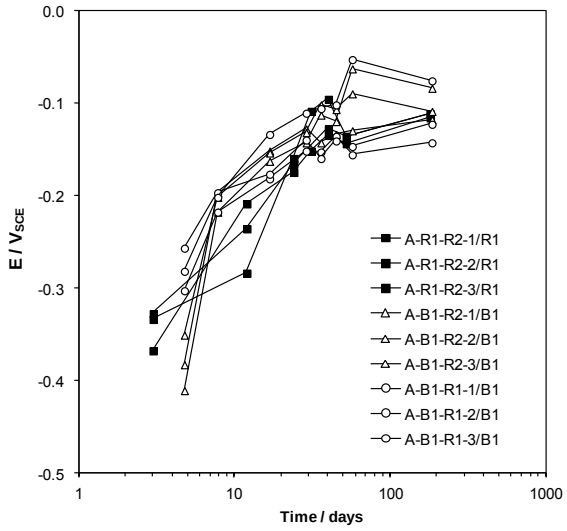

Figure 4.44 OCP of steel in dissimilar grout (Test Setup A).

Early macrocell current measurements showed indications of higher anodic current of the steel in the repair grout, as shown in Figure 4.46. This was in part due to the initial placement of the repair grout where the solution resistance was relatively low due to the early hydration process. This noted, with more mature grout hydration, measured macrocell current dropped significantly after approximately fourteen days. In all test samples the macrocell current dropped to low levels and eventually stabilized at values <0.02 μA. This is indicative of no corrosion activity due to the placement of steel in dissimilar grouts in conditions as tested.

The clean and pre-rusted steel surface appeared as expected after sample autopsy. Shown in Figure 4.47 and 4.48 are representative samples of the strand wires after testing for Test Setup A and

Test Setup B, respectively. The surface condition of the steel wire embedded in the grout with 0.45 w/c paste did not show any indication of corrosion in either test setup.

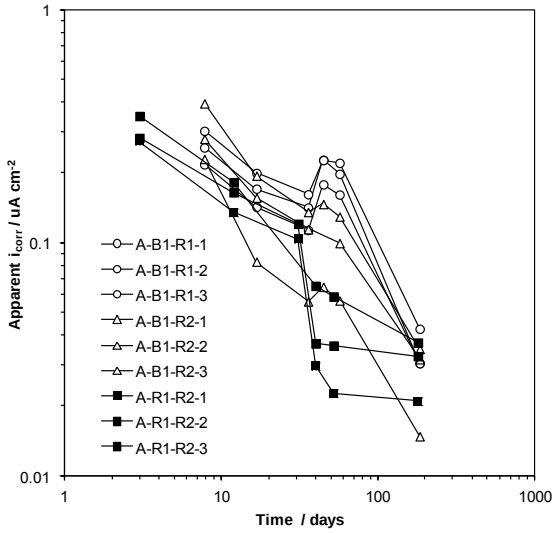

Figure 4.45 Apparent corrosion densities of steel in dissimilar grout (Test Setup A).

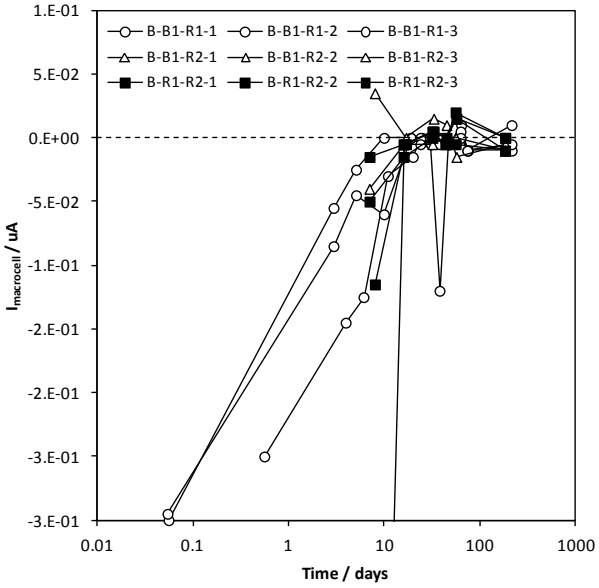

Figure 4.46 Macrocell current between base and repair grouts (Test Setup B).

In Test Setup B, at the steel interface between the base grout and repair grout, corrosion appeared to increase and in some instances and some loss in cross-section was measured. For one sample, losses greater than 50 μm in diameter were measured. In this case, corrosion was thought to

have occurred prior to casting of the repair grout when the sample was exposed to 100% relative humidity conditions and moisture accumulated at the base grout Interface, as shown in Figure 4.49.

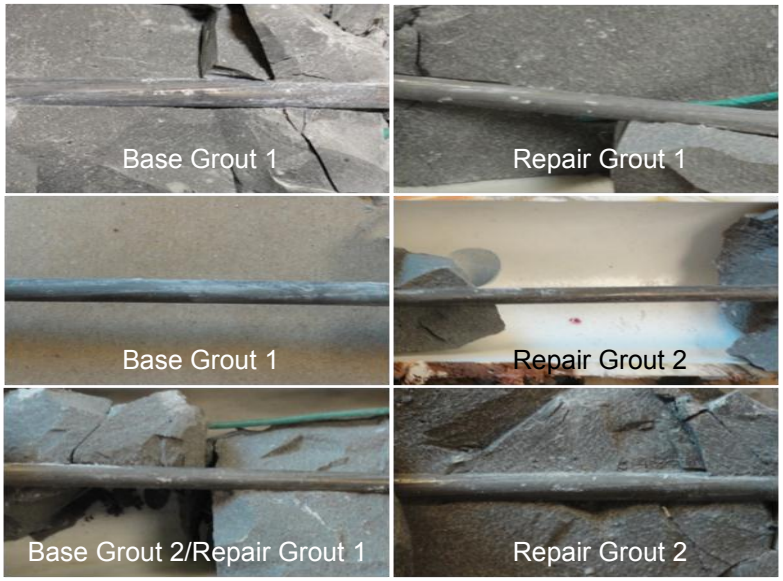

Figure 4.47 Individual steel wire surface condition after testing. Steel in repair grout was pre-rusted. (Test Setup A).

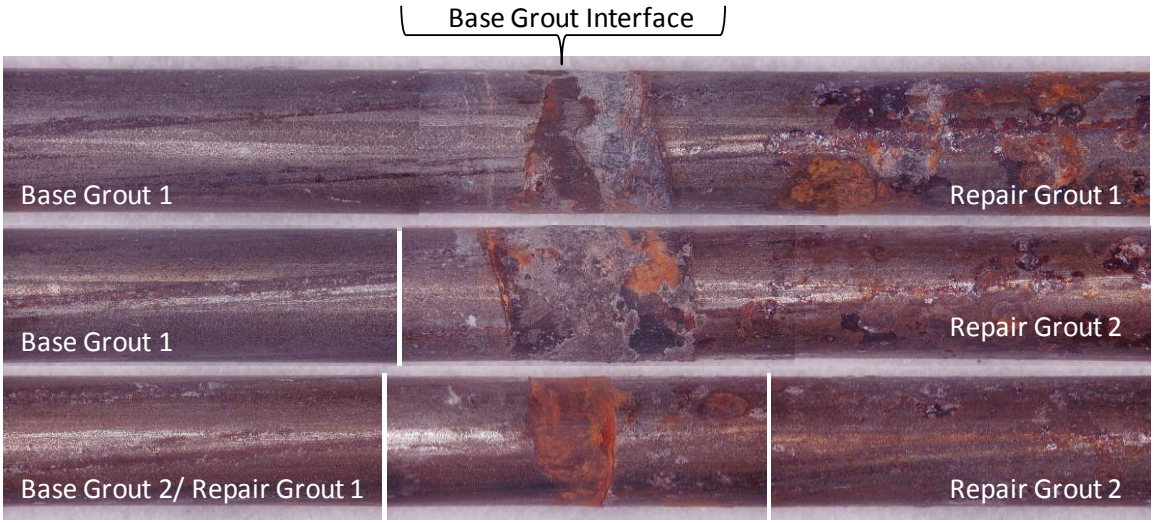

Figure 4.48 Continuous steel wire surface condition after testing (Test Setup B).

Figure 4.49 Accumulation of rust at base grout interface after exposure to 100% humidity for a period of 30 days (Test Setup B).

4.2.1.3 Deficient Repair/Aggressive Environment (C)

As described in Chapter 3 of Methodology, SPS B was introduced in the void space of samples C-G1-V1-1 and C-G1-V1-2. A base condition with no added chlorides or sulfate ions was tested for approximately sixty days. In that period, the steel likely developed adequate passivity as indicated by the negligible corrosion current and passive like open circuit potentials measured showed in Figure 4.50. Addition of sodium sulfate (Na_2SO_4) was done incrementally during a period of approximately 150 days and up to a concentration of 85,000-ppm. This achieved sodium sulfate concentration at 85,000-ppm is equivalent to approximately 0.14 M SO_4^{-2} (1.3% SO_4^{-2}) and in the order of concentration observed in grout from the failed tendon (reported elsewhere).

Similarly, SPS B was introduced in samples C-G1-V2-1 and C-G1-V2-2. In this case, additions of sodium sulfate (Na_2SO_4) and sodium chloride (NaCl) had the purpose of determining their combined effect on corrosion development. The final concentration of NaCl was 2,000-ppm, which corresponds to approximately 0.03 M Cl^-. For SPS B, with pH level 13.2, the [Cl-]/[OH-] was below 0.3. This ratio is below the reported critical chloride threshold level as discussed in section 2.4.2.3. Like the previous

samples, the final Na_2SO_4 concentration was 85,000-ppm. In addition, no indication of corrosion activity beyond the first month was observed, as seen in Figure 4.50 and 4.51 for this test setup. As observed earlier, the initial anodic activity of the steel in the base grout/void was attributed to the early passive behavior of the steel in the solution. The net anodic current quickly declined to very low levels representative of a stable passive film.

Samples C-G1-V3-1 and C-G1-V3-2 were tested by keeping the void space at 100% relative humidity for approximately 150 days. In this period, minor surface corrosion was observed in the exposed steel but no visual indication of significant activity was apparent. Open circuit potentials indicative of passive conditions were measured, as shown in Figure 4.52 and 4.53. Of notice, the initial net anodic behavior of the steel on the base grout/void in these samples was greater than that measured in previous samples. This is attributed to the greater availability of oxygen in the void space in this configuration.

After approximately 150 days and no significant development of corrosion (indicated in Figure 4.52 and 4.53 by the vertical line)[2], the void space was filled with SPS A. This solution had pH 12.6 and 2,000-ppm Na_2SO_4 (0.014M SO_4^{2-}, 0.13% SO_4^{2-}), as describe in Chapter 3. Corrosion activity developed shortly after introduction of the sulfate solution, causing a drop in the open circuit potential approximately from -200 to -500 mV_{SCE}. This is indicative of active corrosion. The anodic macrocell current from the steel in the base grout/void increased from approximately from 0.01 μA to current in excess of 10 μA. Furthermore, significant amounts of solid corrosion products developed on the steel and could be visually identified, as shown in Figure 4.54.

The corrosion development in samples C-G1-V3-1m and C-G1-V3-2m, where 0.13% sulfates were added to pH 12.6 solution, contrasts with the passive corrosion behavior described earlier for samples of Test Setup C where up to 0.12% Cl^- and 1.3% SO_4^{2-} was added to the pH13.2 solution. The higher pH solution there may have promoted stability of the steel passive film even with the enhanced chloride and sulfate concentrations, and corrosion initiation was not evident. Significant corrosion

[2] it is reminded that samples C-G1-V3-1 and C-G1-V3-2 where relabeled as C-G1-V3-1m and C-G1-V3-2m after introduction of SPS A as described in Chapter 3 - Methodology.

developed when the $[SO_4^{2-}]/[OH^-]$ was 0.35 (Setup C) but the steel remained passive when $[SO_4^{2-}]/[OH^-]$ was 0.70.

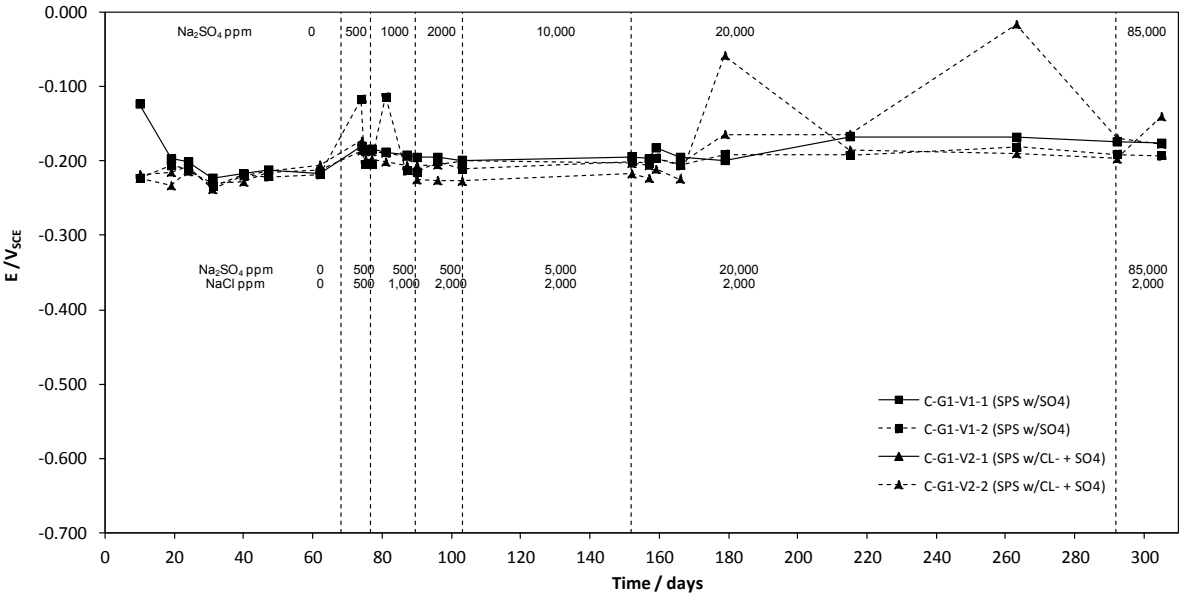

Figure 4.50 Open circuit potentials (Test Setup C).

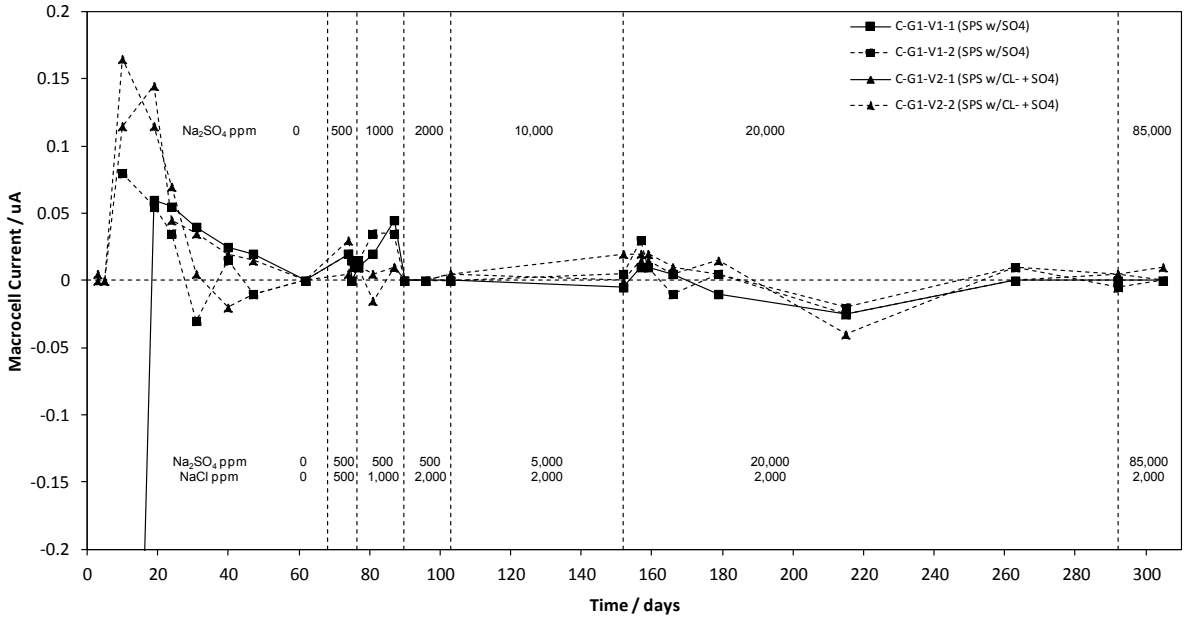

Figure 4.51 Macrocell corrosion currents (Test Setup C).

From these findings, it may be apparent that corrosion in the presence of Na_2SO_4 occurs if the steel stable passive layer is prevented from forming by the early introduction of sulfates at concentrations as low as 0.13% in pH 12.6 environments. If the stable passive layer is initially allowed to form in non-aggressive alkaline solutions (taking as long as approximately seventy days), added sulfate concentrations as high as 1.3% or in addition to chloride concentrations as high as 0.12% did not readily initiated steel corrosion in pH 13.2 environments.

Additional LPR measurements were made for samples in this sub group of Test Setup C (C-G1-V3-1, C-G1-V3-2, C-G1-V3-1m, and C-G1-V3-2m) to establish self-corrosion rates and determine if enhanced macrocell corrosion may occur in deficient tendon and partial repair conditions. When the void space was maintained at 100% RH condition, the steel in the base grout/void location had a more negative OCP and slightly higher corrosion rate than steel in the repair grout although the values and extent of corrosion was negligible. Coupling of the electrodes did create macrocell conditions between the net anode in the base grout/void and the net cathode in the repair grout as evidenced by the mixed potential showing minor anodic polarization of the steel in the base grout/void. The effect was minor and the corrosion rate was in the order of 0.1 $\mu A*cm^{-2}$.

The effect was more significant after corrosion initiation occurred when sulfate solution, as described earlier, was added into the void space. An intermediate mixed system OCP developed where the steel in the repair grout/void location, that already had initiated corrosion, was anodically polarized as much as 30 to 90 mV, as seen in Figure 4.55 and 4.56. The steel in the repair grout remained passive with corrosion currents in the order of 0.1 µA. The corrosion rate of the steel in the grout/void location more than doubled from approximately 20 µA to 40 µA, as shown in Figure 4.56.

The presence of an extended net cathode, such as steel in properly mixed repair grout in conjunction to steel in deficient grout, where corrosion is active does enhance the rate of metal dissolution. The presence of high humidity did not create significant corrosion rates during the time of the experiment. However, the presence of excess moisture that may have accumulated and came in contact with the steel, may had formed a significantly more aggressive situation regardless of pH of the moisture. This has been described in case studies where steel corrosion in PT systems occurred due to

accumulation of grout bleed water and grout void formation. Significant enhancement of corrosion occurred with the addition of solution. The enhanced corrosion current is expected to be larger if the ratio of net cathode to net anode is larger, as would form if the presence of deficient grout is small, in relation to the total length of the tendon.

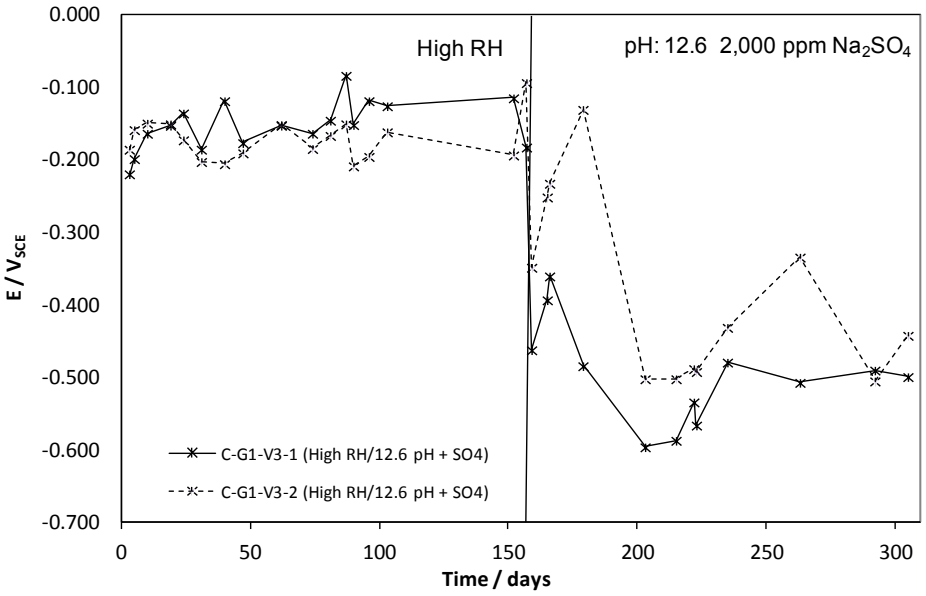

Figure 4.52 Developed OCP (Samples C-G1-V3-1/1m and C-G1-V3-2/2m).

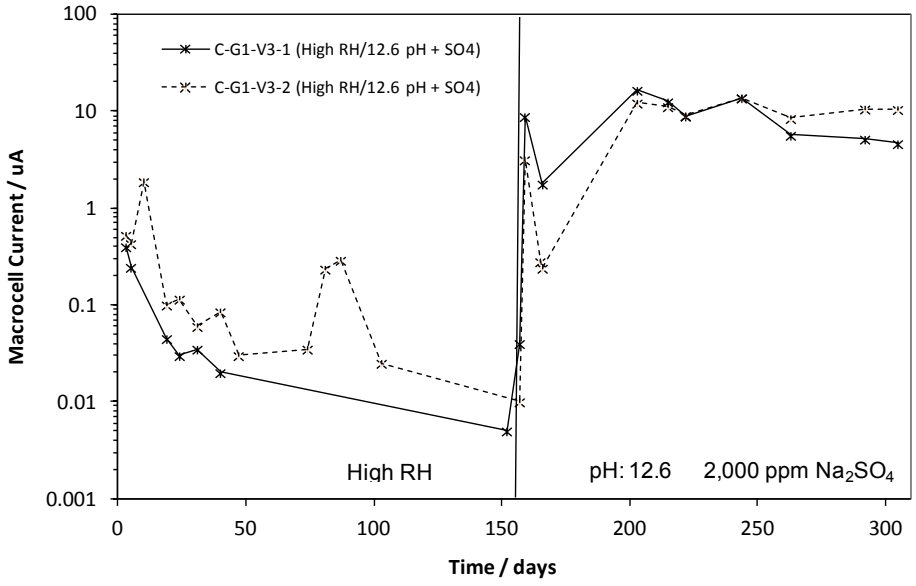

Figure 4.53 Macrocell currents development (Samples C-G1-V3-1/1m and C-G1-V3-2/2m).

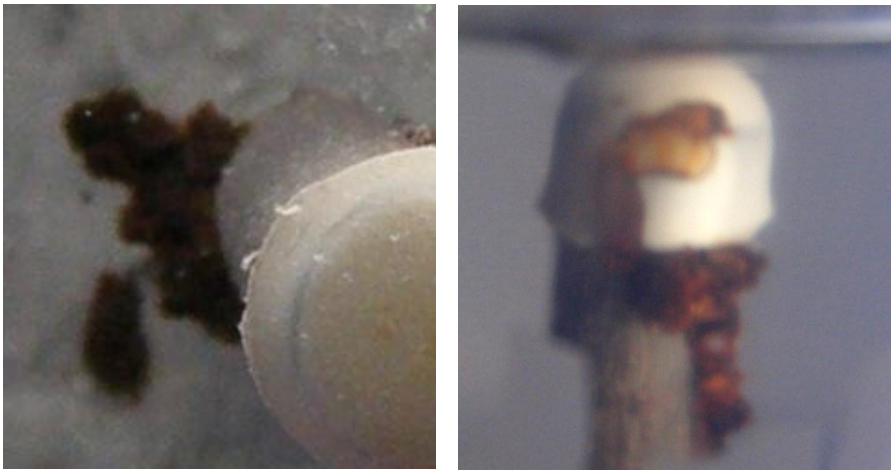

Figure 4.54 Accumulation of corrosion product (Samples C-G1-V3-1m and C-G1-V3-2m, after exposure to SPS A).

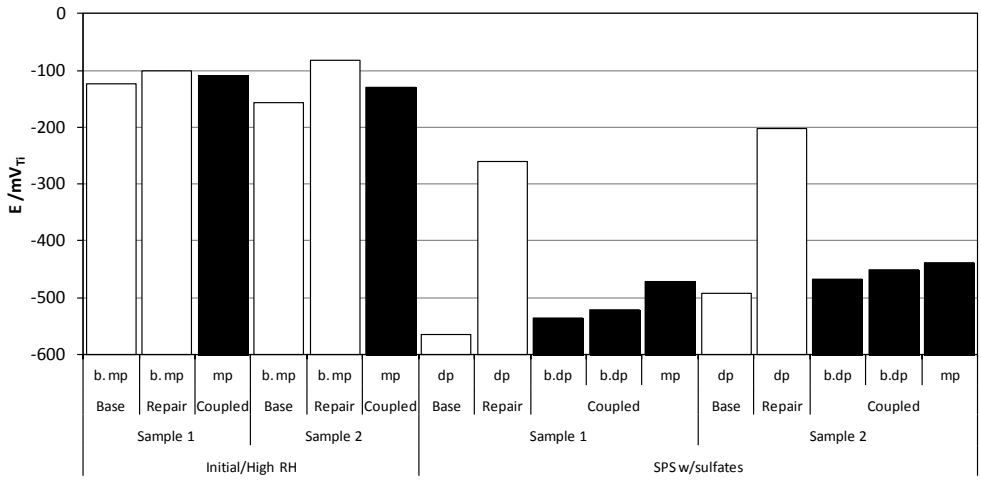

Figure 4.55 Measured OCP of coupled and un-coupled tendons (Samples C-G1-V3-1, C-G1-V3-2, C-G1-V3-1m, and C-G1-V3-2m).

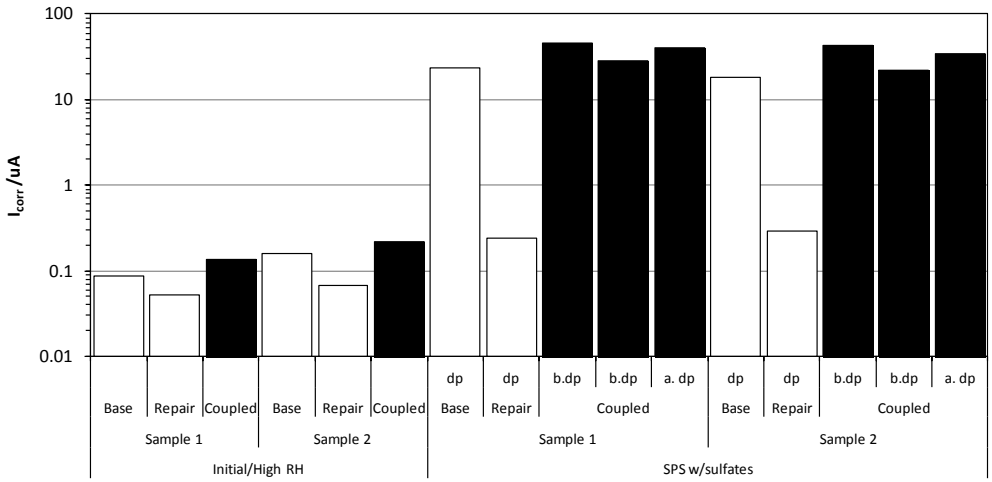

Figure 4.56 Measured I_{corr} of coupled and un-coupled tendons (Samples C-G1-V3-1, C-G1-V3-2, C-G1-V3-1m, and C-G1-V3-2m).

4.2.2 SIMULATED PORE SOLUTION

As describe in Chapter 3 - Methodology, samples were tested in as-received or pre-rusted conditions. Anodic Polarization results for Test Setup SPS-KW, are presented in Figures 4.57 and 4.58. In Figure 4.59, current at -100 mV_{SCE} from each test condition is presented. Data was extracted from results in Figures 4.57 and 4.58. Comparisons of current describe next refers to this metric.

The anodic behavior of steel in sulfate free SPS A and SPS B solution showed passive behavior (as expected for steel in high pH solutions) with small increases in anodic current with anodic polarization. Corrosion current was between three to seventy times greater in the pre-rusted wires than in the clean wires. The passive current for steel in SPS B was observed to be greater than SPS A.

Addition of 2,000-ppm of sodium sulfate to SPS B (pH 13.2) showed no strong measurable change in behavior from the free sulfate condition for either clean or pre rusted condition. Some indication of destabilization of passivity was manifested in some places in both clean and pre-rusted conditions in SPS A (pH 12.6). In these cases, the near passive current was larger (approximately seven to thirty times) than the free sulfate condition and was more strongly manifested in the pre-rusted wires. For the pre-rusted wires, small anodic current excursion in the polarization following recovery may be indicative of conditions not favorable for passivation or detection of small pitting events.

Anodic polarization behavior of the steel in presence of 20,000-ppm sodium sulfate did show increase in current from the ones measured in previous concentrations, but it was strongly manifested in SPS B. The polarization behavior for steel in as received condition in SPS B showed currents approximately seven to nine times larger than in the free sulfate solution.

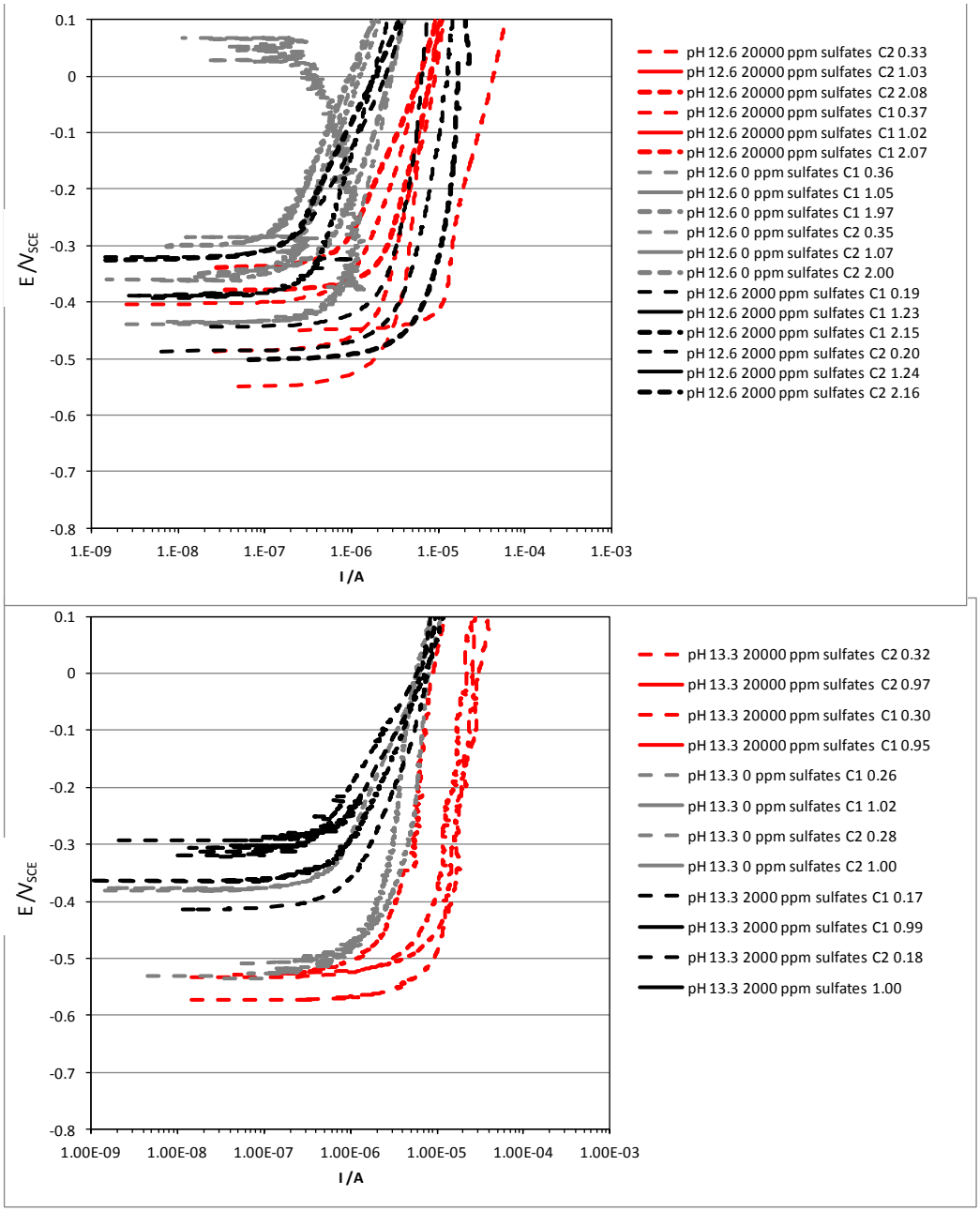

Figure 4.57 Anodic polarization scans for steel in as-received condition in SPS A (pH 12.6) (Top) and SPS B (pH 13.2) (Bottom). Day 0 - dashed lines, Day 1 - solid lines.

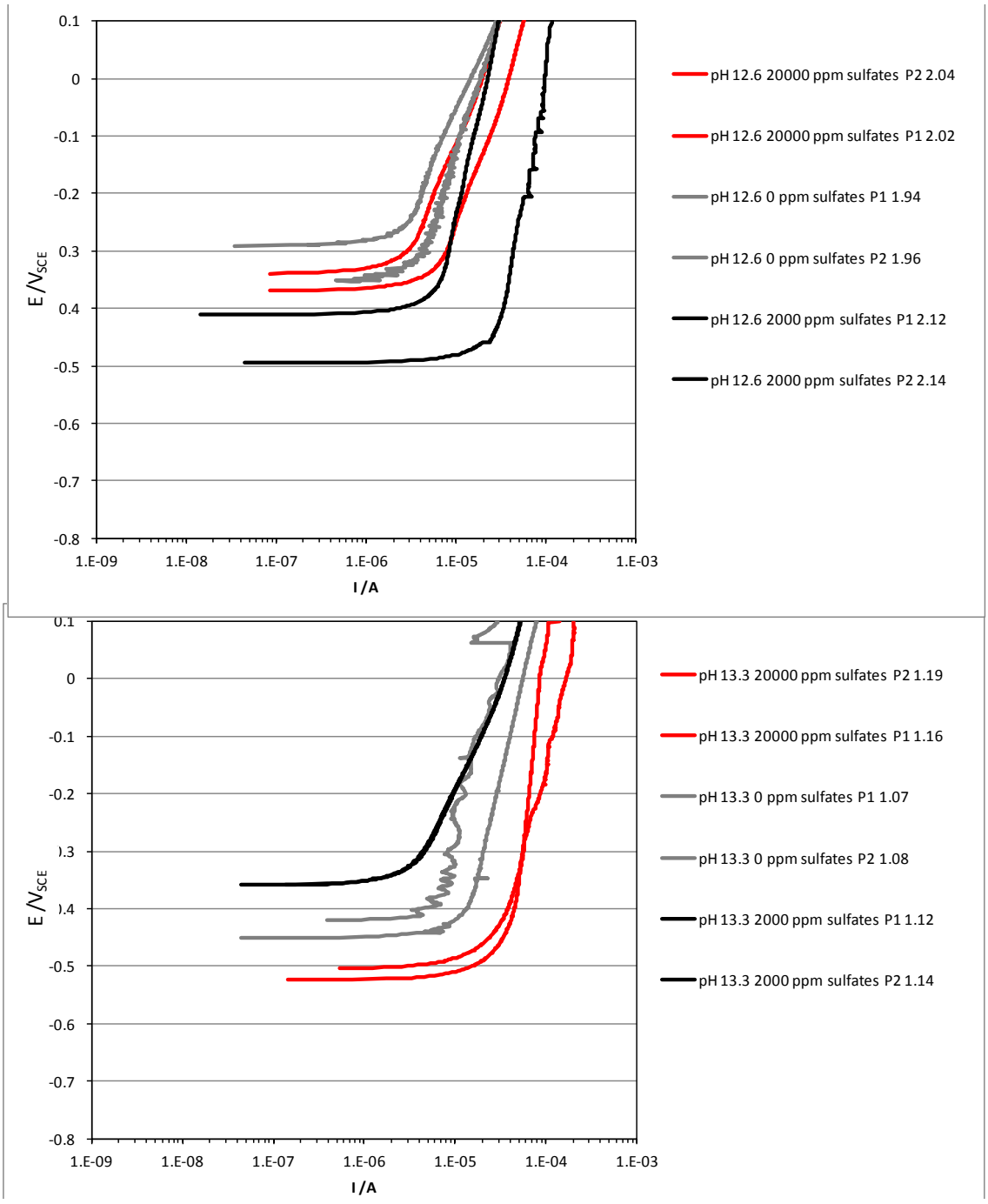

Figure 4.58 Anodic polarization scans for steel in pre-rusted condition in SPS A (pH 12.6) (Top, Day 2) and SPS B (pH 13.2) (Bottom, Day 1).

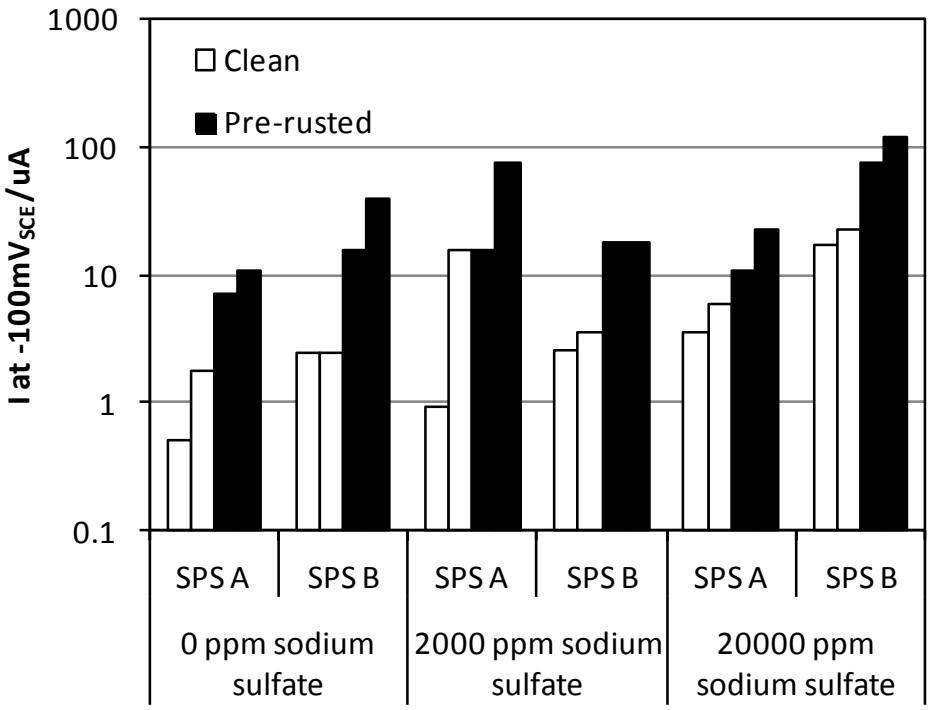

Figure 4.59 Anodic current at -100 mV$_{SCE}$.

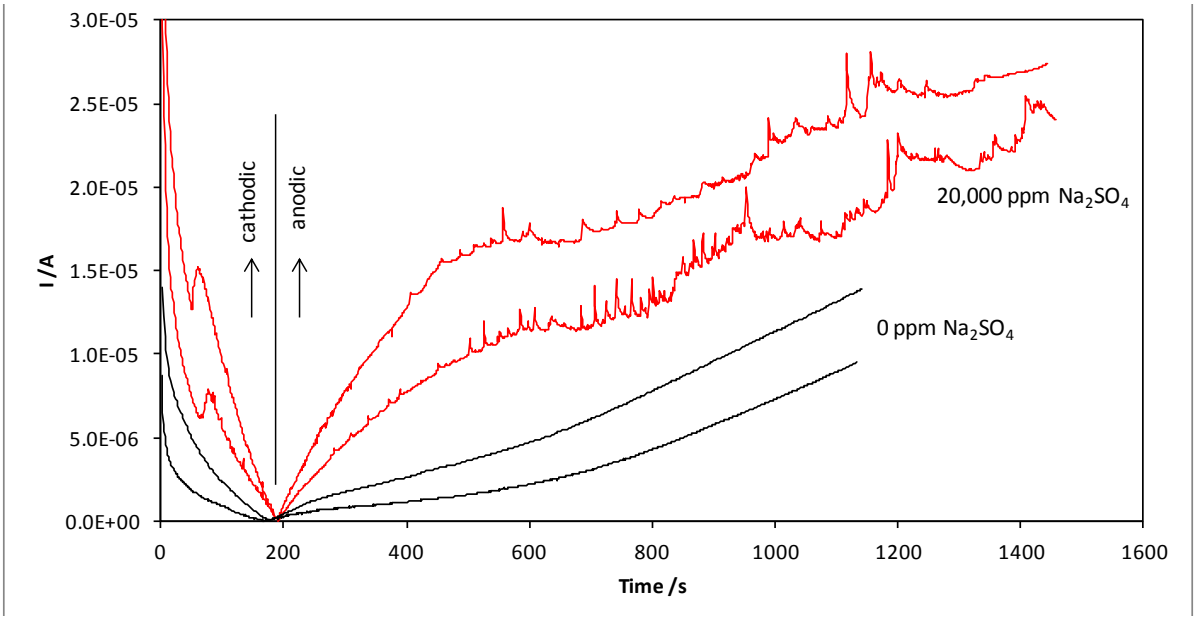

Figure 4.60 Current excursion events during anodic polarization for as-received wire in SPS B.

Results appear to indicate that the presence of sulfates did not cause total or uniform disruption of the steel passive layer during these short-term tests, but it may begin to cause depassivation of the steel as shown by the current excursion manifested in some cases as shown in Figure 4.60.

Also noticed, is that for a given amount of oxygen present, the corrosion current of the steel in presence of sulfates tend be greater than without sulfates and more negative open potential would develop. In addition to concentration polarization, the more negative potentials developed in the sulfate rich pore solution would lead to a greater extent of anodic polarization if the strand in the grout were to be coupled with a larger net cathode present along the length of the tendon. The role of chlorides and sulfate ions in the same solution, as measured in the segregated grout was not addressed in these experiments.

For Test Setup SPS-CS, the strands maintained open circuit potential of $-100 < E < -300$ mV_{SCE} for over a month and no strong correlation between the developed OCP and sulfate concentration was identified in SPS A (pH12.6), as shown in Figure 4.61. In addition, no visual sign of active corrosion was observed.

Differentiation in OCP was observed in SPS B (pH 13.2). For this case, OCP in high sulfate concentration was approximately 100 to 300 mV more negative when compared with those in SPS A and SPS B with low concentrations (Figure 4.61 and 4.62). Only one wire did show corrosion product accumulated at the edges of the cross section area and current density for this wire was in agreement with the visual indication of active corrosion. In agreement with this observation, the apparent corrosion density for the samples exposed to 20,000-ppm in SPS B (pH 13.2) was significantly higher than all other samples. No active corrosion was apparent in any of the samples in SPS A.

During the test period the pH of both SPS A and SPS B solutions were monitored and no significant variation was observed with time or due to sulfate concentrations, as shown in Figure 4.64.

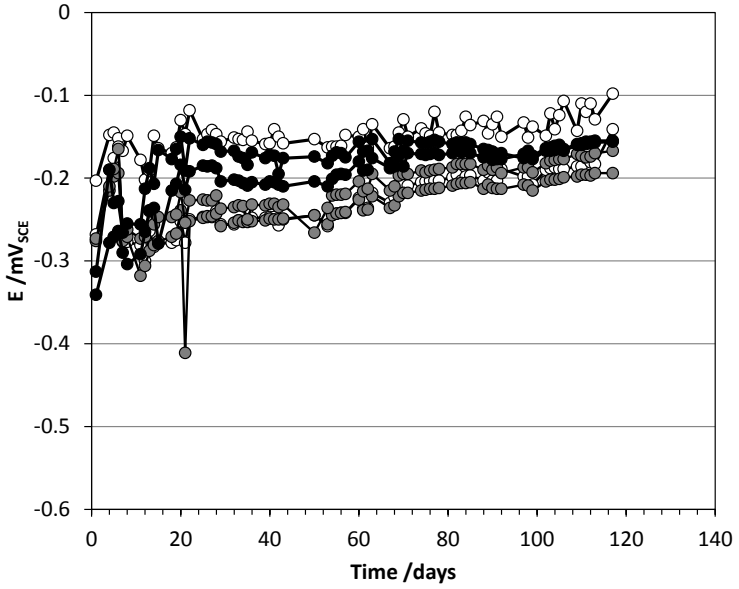

Figure 4.61 OCP Development (Test Setup A, pH 12.6):
White - no sulfates, Grey - 2,000-ppm, Black - 20,000-ppm.

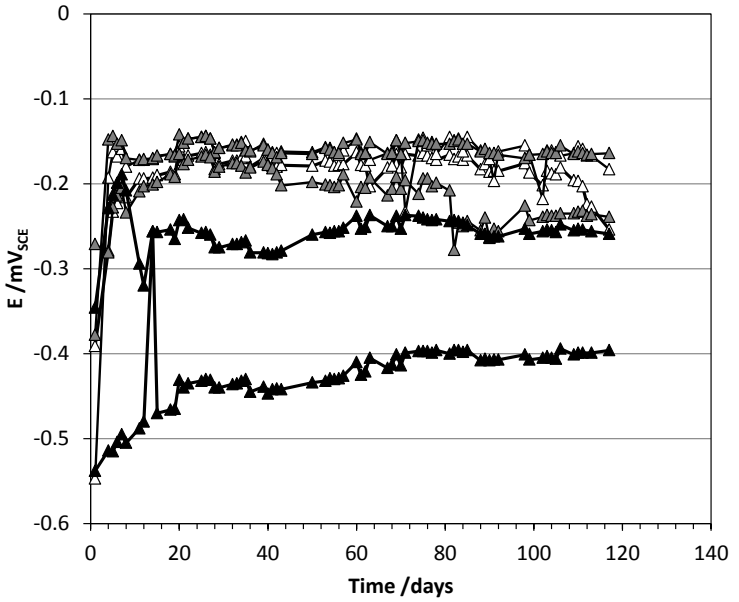

Figure 4.62 OCP Development (Test Setup B, pH 13.2):
White - no sulfates, Grey - 2,000-ppm, Black - 20,000-ppm.

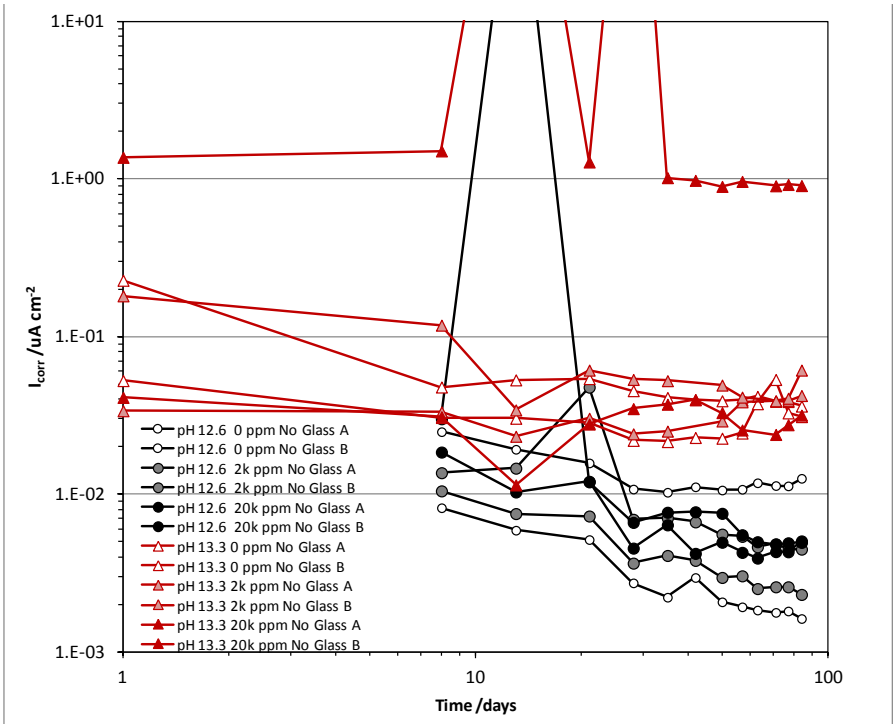

Figure 4.63 Apparent corrosion densities calculated by LPR (Test Setup SPS-CS).

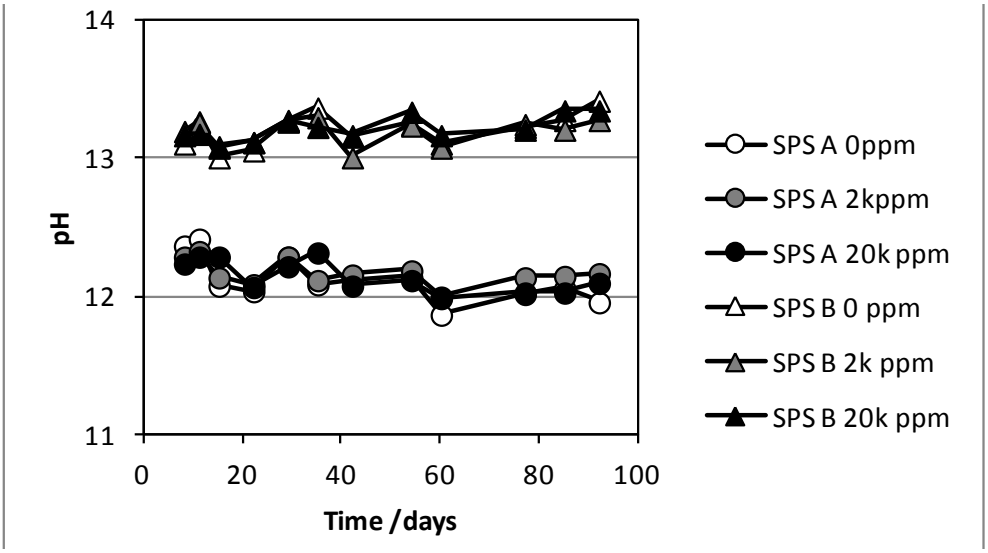

Figure 4.64 pH evolution.

4.3 GROUT CHARACTERIZATION

Results show higher concentrations of Na, K, S and Sr in the grout obtained from the field tendon (samples from Test Setup FS-SM) than in the neat (0.45 w/c ratio cement paste) and repair grouts (pre-bagged). Results are shown in Figure 4.65. XRD results, shown in Figure 4.66, from sample FS-SM-1 (white/chalky grout) indicate the presence of small traces Thaumasite. Thaumasite is a silicate mineral that can form along other calcium-silicate hydrates (CSH, small colloidal particles of hydrated calcium silicate product of the hydration process of Portland Cement (Bentur, Diamond, & Berke, 1997), especially when sulfate attack develops. The conversion of the CSH matrix into thaumasite results in a loss of binding material and integrity of the concrete or concrete based material. A loss of strength and softening of material also has been attributed to decalcification of the CSH matrix due to attack from Magnesium sulfates ($MgSO_4$ x H_2O, hydrate form) (Hooton & Thomas, 2002). In a more conventional type of sulfate attack, sodium sulfates can react with the hydrated aluminates (C3A) in the paste to form gypsum (identified in all samples), which may cause damage in itself or react with monosulfates to form ettringite, which has been identified in early measurements of similar samples reported elsewhere.

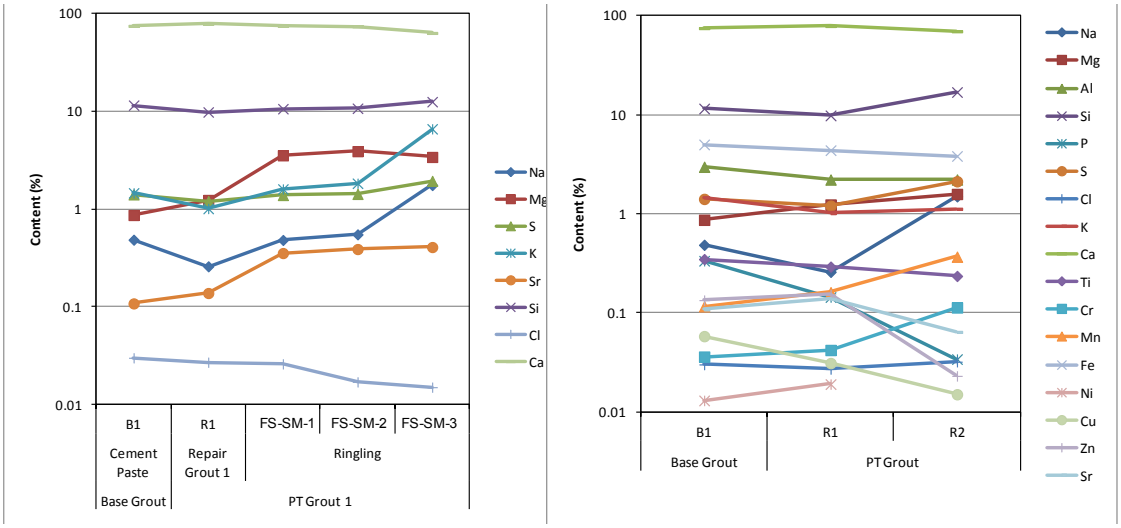

Figure 4.65 X-ray fluorescence of selected grouts (a) selected elements (b) complete list of elements.

Identification of ettringite and thaumasite formation in these samples may be suggestive of sulfate attack and because of durability concerns, should be further addressed.

Results from FM 5-516 performed on the grout samples yielded that for the base neat grout, repair grout 1 and repair grout 2, chloride content was compliant with current FDOT specifications (0.332, 0.334 and 0.170 lb/yd^3 respectively).

Complete results from FM 5-516 and X-ray diffraction are presented in Appendix C.

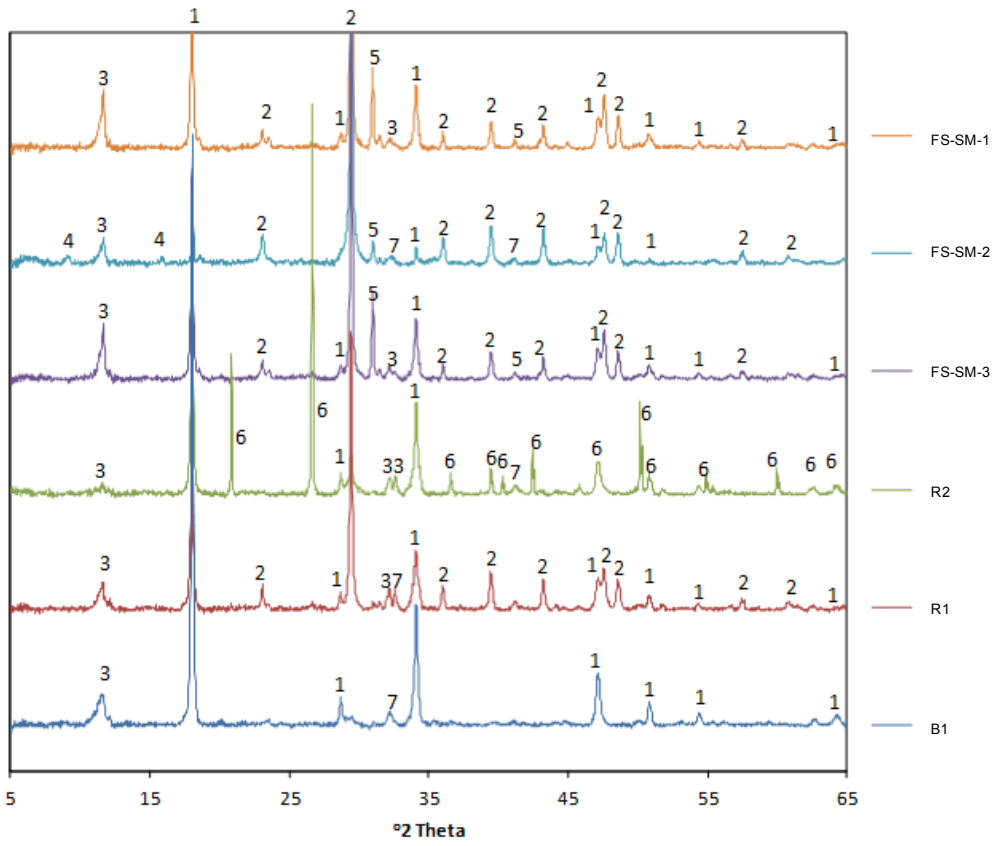

Figure 4.66 X-Ray diffraction of selected grouts:
1. Portlandite, 2. Calcite, 3. Gypsum, 4. Thaumasite, 5. Dolomite, 6. SiO_2, 7. Calcium Silicate.

4.4. GENERAL DISCUSSION AND RESULTS IMPLICATIONS

From the experiments presented earlier, there was no evidence of significant corrosion development in PT tendons with voids repaired with dissimilar grout when the base and repair grouts

were properly cast and conditions were free of material deficiencies. In the laboratory experiments, no indication of corrosion development was observed with steel embedded in a 0.45 w/c base neat grout and coupled with steel embedded in commercially available repair grouts. The conditions represented in those experiments showed open circuit potentials and corrosion rates typical for passive corrosion conditions. Macrocell development across steel in the base and repair grout appeared to be negligible. Furthermore, the condition of the steel after autopsy of the samples remained in similar condition as prior to casting and did not appear to show any indication of active corrosion.

The laboratory tests incorporating field extracted tendon segments with pre-existing voids and repaired with commercially available repair grouts also typically showed passive corrosion behavior as evident by passive open circuit potentials, low corrosion currents, and insignificant macrocell current development. Only in one case, some minor corrosion did develop. However, the active corrosion appeared to have diminished after approximately one month. That location had a localized region of deficient grout (white chalky grout) and significant cracking. The corrosion activity in this sample was associated to the moisture introduced from the repair grout.

The laboratory tests incorporating base neat grout and field-extracted tendon segments cast with commercially available repair grouts showed indication of corrosion mitigation. However, there was some marked differentiation of corrosion behavior of the samples between the two repair grouts. In test setup FSR, where the pre-existing voids were repaired with pre-bagged grouts, the samples repaired with repair grout 1 had apparent corrosion rates greater than tendons repaired with repair grout 2. Similar observations were made for test setup with the continuous steel wire placed in base neat grout and the repair grouts. In the mentioned samples, the apparent corrosion current density was slightly greater when repair grout 1 was used. It was noted that the near passive corrosion current density of steel embedded in repair grout 1 was also greater than that for repair grout 2. These differences were attributed to the marginally lower developed solution resistance of repair grout 1. In addition, the developed solution resistances for both repair grouts were about an order magnitude greater than that for the base neat grout. It should be noted that the differences were small and that corrosion mitigation was observed for both repair materials.

Of notice, is the behavior when the steel samples had surface rust prior to casting the repair grout. The laboratory tests of steel in pre-rusted surface condition showed greater corrosion currents and anodic current densities in anodic polarization tests, which may indicate possibility for greater corrosion damage. However, the pre-rusted surfaces showed to be poorer cathodes, which may mitigate enhanced macrocell corrosion. For steel samples partially cast in grout and exposed to 100% humidity prior to casting of the repair grout, corrosion developed on the surface of the steel wire at the surface of the base grout. In this area, bleed water and moisture condensation may have likely accumulated, and corrosion loss up to 50μm of the steel wire diameter was measured at the base grout interface. However, corrosion activity was significantly reduced after introduction of the repair material. Upon maturation of the repair grout, the apparent corrosion current density decreased to levels indicative of passive behavior. The possible corrosion mitigation after placement of the repair grout, should be further addressed as severe corrosion initiation of PT strand after corrosion repair had been documented elsewhere (Trejo, et al., 2009). If the accumulated moisture does not contain aggressive chemical species such as chloride ions, the moisture may likely combine with the repair grout without significant detrimental long-term effects.

In congruity with the tendon corrosion failure, significant corrosion activity was observed in field-extracted samples with deficient grout characterized as white/chalky and/or wet plastic consistency. As reported elsewhere, analysis of the deficient grout revealed high pH level, low chloride content, and enhanced concentrations of sulfates. When steel embedded in these deficient grout materials were coupled to steel in hardened grout, it was apparent that enhanced corrosion could occur by macrocell coupling. The steel in the deficient grout acts as the local anode and the rest of the strand assembly acts as an extended cathode.

The cause of lack of steel passivation (or loss thereof) that led to corrosion activity and enhanced macrocell corrosion was attributed to the presence of high free sulfate concentrations in the highly segregated grout. High moisture content was also evident in segregated grout. In field-extracted samples, severe corrosion was manifested in the presence of segregated grout. The segregated grout consistently showed high moisture content, high pH, low chloride concentrations, and enhanced sulfate concentrations as high as 10,000-ppm. In laboratory testing in solution, significant corrosion activity was

identified in samples initially exposed to pore solution with high concentrations of sulfates in very short periods after exposure (approximately one day).

In other laboratory tests, samples initially exposed to alkaline pore solution free of chlorides and sulfates for up to 60 days did not show significant corrosion activity despite subsequent addition of sodium chloride and sodium sulfate up to 2,000 and 85,000-ppm, respectively. It was thought that if steel was allowed to develop a stable passive layer, later exposure to sulfates at levels tested might not be sufficient in the high pH environment to cause local depassivation of the steel and corrosion development. The results suggest that if there is early exposure to sulfates in the deficient grout, development of a stable passive layer may be impaired.

The pH of the pore water solution greatly affects the corrosion behavior of steel in alkaline environments. Generally, higher pH levels help create stable passivation of the steel. It was noted however, that greater corrosion current densities were observed at higher pore water pH. The near passive current density was as much as an order of magnitude greater in pH 13.3 than pH 12.6 albeit at moderate to low currents.

Corrosion activity was appreciated in steel samples exposed to pH 13.3 and 20,000-ppm sodium sulfate. However, severe corrosion development also occurred in laboratory samples with pH 12.6 and 2,000-ppm sodium sulfate. A plot of the corrosion potential and corrosion rate developed at the various test conditions of sulfate to hydroxyl ion concentration ratio is shown in Figure 4.67. The minimum ratio for corrosion to develop can be considered with an upper bound value of 0.35 where corrosion initiation may occur at ratios above that value. It was assumed, in those cases where corrosion activated, that passivity was prevented from initially forming. When the steel was allowed to passivate, it is seen that $[SO_4^{2-}]/[OH^-]$ as low as three did not cause depassivation during the time of the experiment (approximately 13 days for the last dosage regime) even when up to 0.12% chloride was added.

The source of enhanced concentrations of free sulfate ions in the deficient grout in the samples obtained from the Ringling Bridge was not identified, but was thought to be associated with dissolution of phases in cement, particularly gypsum. Regardless, high moisture content was associated with the deficient grout. The high moisture may have contributed to the leaching of sulfates into solution. It was

noteworthy that there was a strong presence of ettringite crystals in the deficient grout yet the pore solution retained enhanced sulfate concentrations (up to 10,000-ppm SO_4^{2-}) after several years, indicative of an abundance of free sulfates.

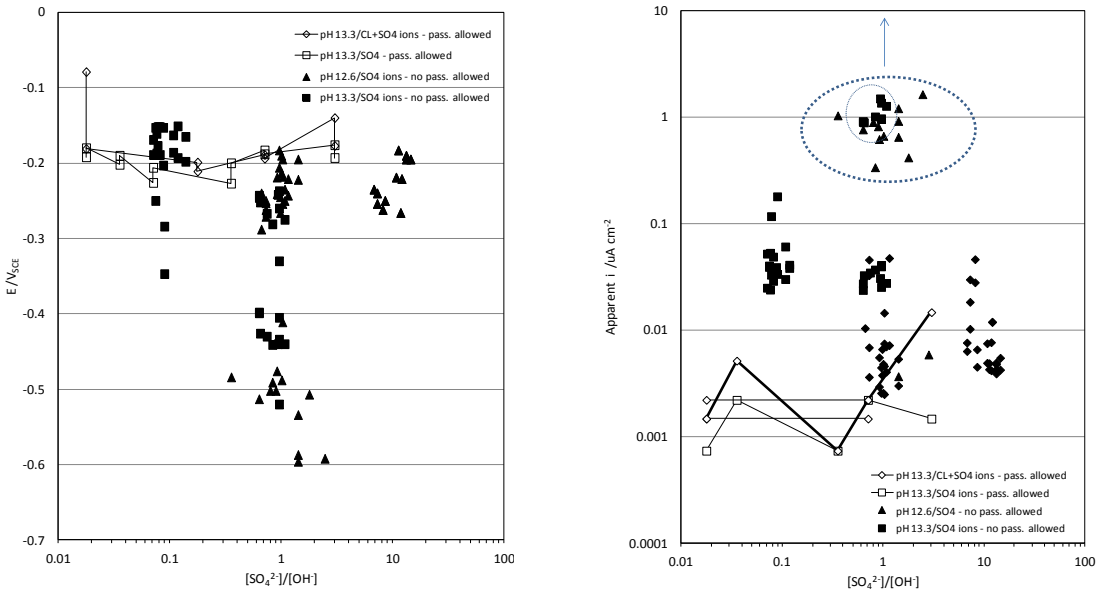

Figure 4.67 (a) Potential versus sulfate to hydroxyl ratio, (b) apparent corrosion current density versus sulfate to hydroxyl ratio.

The amount of sulfates in solution considered detrimental in terms of corrosion development has not been well established in the literature, and there is reluctance to prematurely ascribe a critical concentration that can be generally applied by practitioners. Work by Gouda and Halaka, 1970, (Gouda, 1970) showed that passivity of steel in concrete containing up to 8% sodium sulfate was not affected but corrosion occurred in steel immersed in alkaline solution with as little as 0.2% sulfate. The corrosion behavior in concrete was interpreted as being due to reaction of most of the sulfates with cement phases. Their results however do not necessarily disagree with observations of the deficient grout considered here. The deficient grout associated with corrosion as mentioned earlier was associated with water contents as high as 80% by mass and there was indication that the deficient grout does not contained high cement content. In such a condition, the sulfate ions would mostly be in the aqueous phase and indeed concentrations as high as 0.9-1% sulfate were measured.

Repair of tendons should include not only identification of grout filling deficiencies (as is conventionally done) but also grout material deficiencies. Moisture accumulation and corrosion development in tendon locations with voids should be assessed. In absence of abnormal grout and other tendon deficiencies, repair of void space with dissimilar repair grout materials should not affect or promote future corrosion development. Both grout materials should yield high pH environments and the steel should maintain passive corrosion behavior. Moderate levels of polarization in the anodic region due to coupling of steel in the dissimilar grout materials is not expected to cause significant enhanced corrosion rates if, the repair is made to prevent moisture accumulation and exposure from aggressive chemical species. It is important to have assurance that the void space is completely filled. Partial or incomplete repairs that result in part of the strand remaining exposed could be susceptible for corrosion development.

In the presence of deficient grout, extra consideration for repair should be made. The effect of the presence of accumulated external bleed water was not fully addressed in this research (and any structural/mechanical implications of strand corrosion are not considered here), but limited laboratory testing did show corrosion mitigation after placement of repair material. This issue should be addressed in the future. Deficient grout with manifestation of severe segregation, high moisture content, and enhanced concentrations of sulfate ions did experience significant corrosion activity. The size of the grout deficiency can vary, but filling of the tendon with repair material may likely enhance macrocell corrosion of steel in contact with the severely deficient base grout. The higher electrical resistance of the commercially available low bleed grouts, in comparison to a 0.45 w/c neat grout, is a benefit to reduce macrocell corrosion development. The geometric effects were not directly addressed in this study, but larger area ratios of steel in repair or hardened grout material to steel in deficient grout is likely to create greater macrocell corrosion currents. Complete removal of deficient grout is suggested.

CHAPTER 5 - CONCLUSIONS

- No evidence of significant corrosion development was apparent when the base and repair grout were properly cast and in absence of tendon material deficiencies.
- Significant corrosion was identified in the presence of non-homogeneous/segregated grout.
- Corrosion activity observed in deficient (segregated) grout was attributed to the presence of high free sulfate concentrations and high moisture conditions.
- Macrocell coupling of steel between deficient and hardened (or non-deficient/repair) grouts appeared to increase corrosion.
- Steel in pre-rusted surface conditions showed susceptibility for greater corrosion damage than non pre-rusted steel.
- The presence of either high sulfate concentrations or high pH leads to higher passive anodic currents.
- Corrosion activity at the steel interface of the base grout and void space, where moisture accumulation may form prior to casting of repair grout, can be significantly reduced after repairing of the void.
- Commercially available repair grouts showed differences in developed solution resistance. Measured values were up to 10 times greater than those in 0.45 w/c neat grout.
- Corrosion currents for steel in repair grouts were significantly lower than in 0.45 w/c neat grout. Cathodic reduction reactions capacity appeared lower for repair grouts than 0.45 w/c neat grout.
- Early exposure to sulfate concentrations as low as 0.13% may prevent steel passivation from forming and result in early high rates of corrosion. $[SO_4^{2-}]/[OH^-]$ ratio as high as 0.7 may not be sufficient to initiate corrosion after formation of stable passive layer in alkaline pore solution.

APPENDIX A - TEST SETUP SAMPLE PICTURES

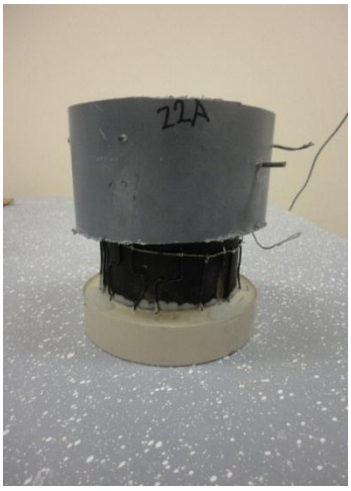

Test Setup FS-SM

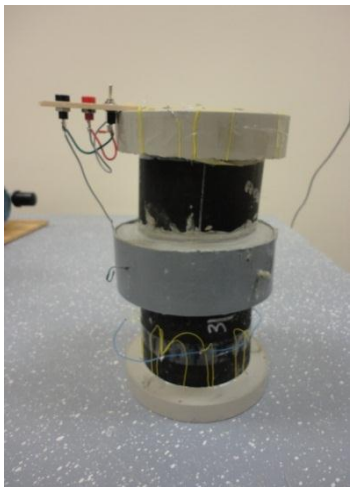

Test Setup FS-LG

Test Setup FS

Test Setup FSR

Test Setup A

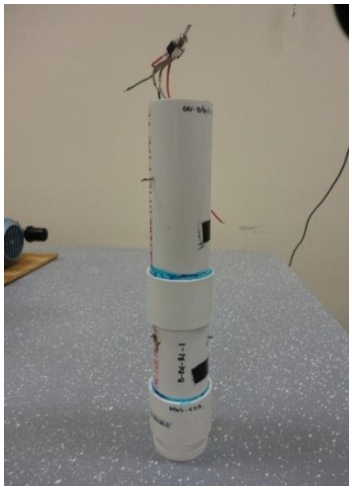

Test Setup B

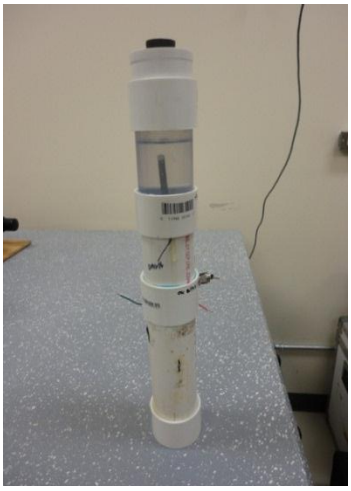

Test Setup C

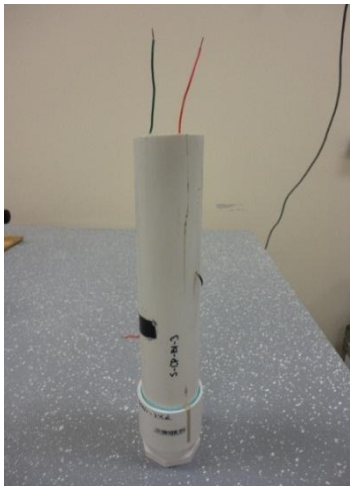

Test Setup S

Test Setup SPS

Figure A.1 Test Setup Pictures

APPENDIX B - EIS RESULTS (NYQUIST PLOT/BODE DIAGRAMS)

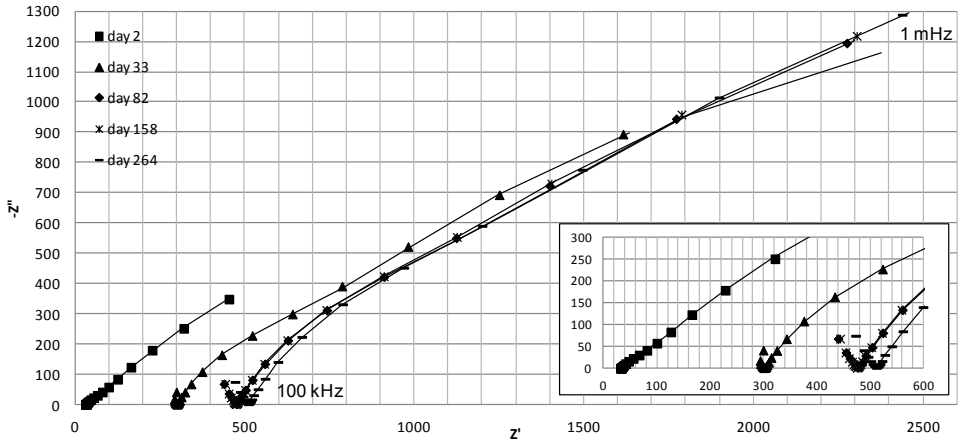

Figure B.1 EIS Nyquist Plot and best fit by Eq. 4.1. Test Sample FSR-R1-1.

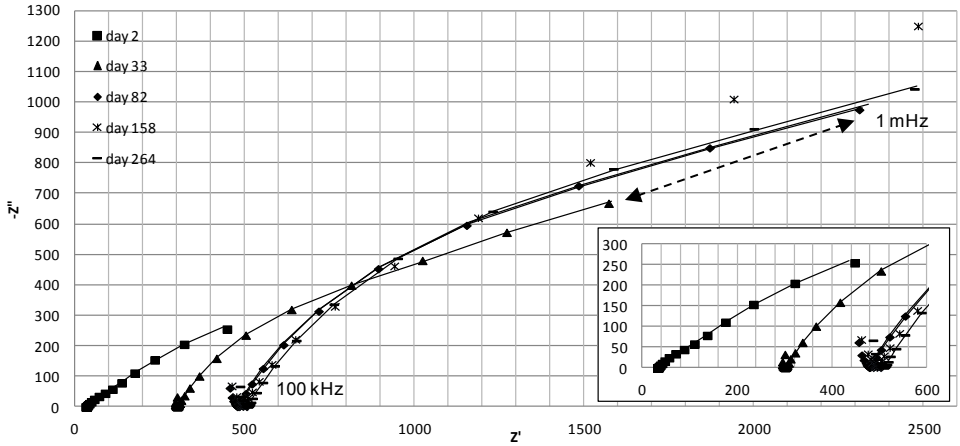

Figure B.2 EIS Nyquist Plot and best fit by Eq. 4.1. Test Sample FSR-R1-2.

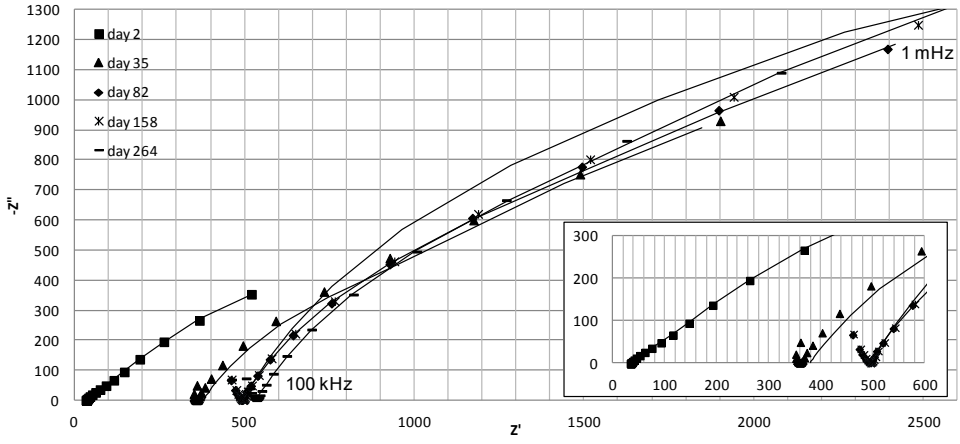

Figure B.3 EIS Nyquist Plot and best fit by Eq. 4.1. Test Sample FSR-R1-3.

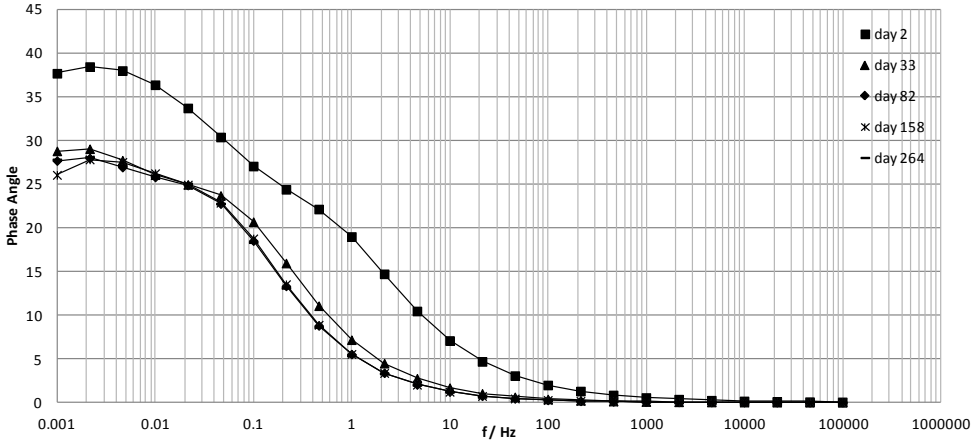

Figure B.4 EIS Phase Angle Bode Diagram. Test Sample FSR-R1-1.

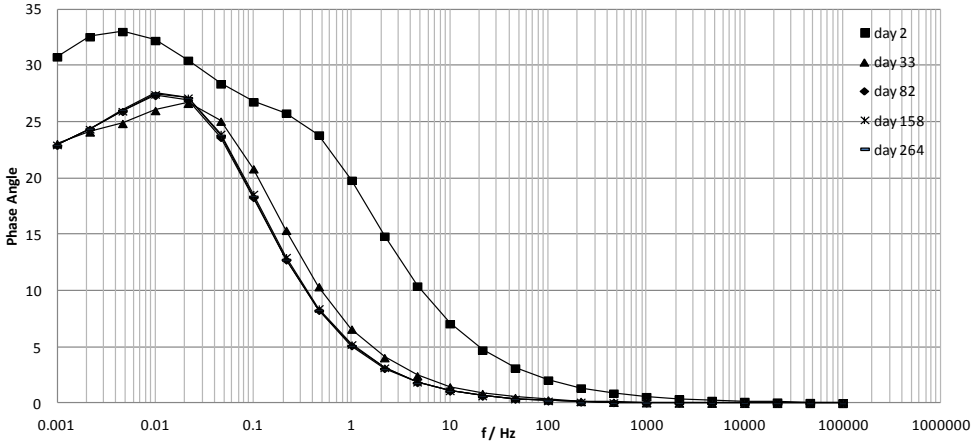

Figure B.5 EIS Phase Angle Bode Diagram. Test Sample FSR-R1-2.

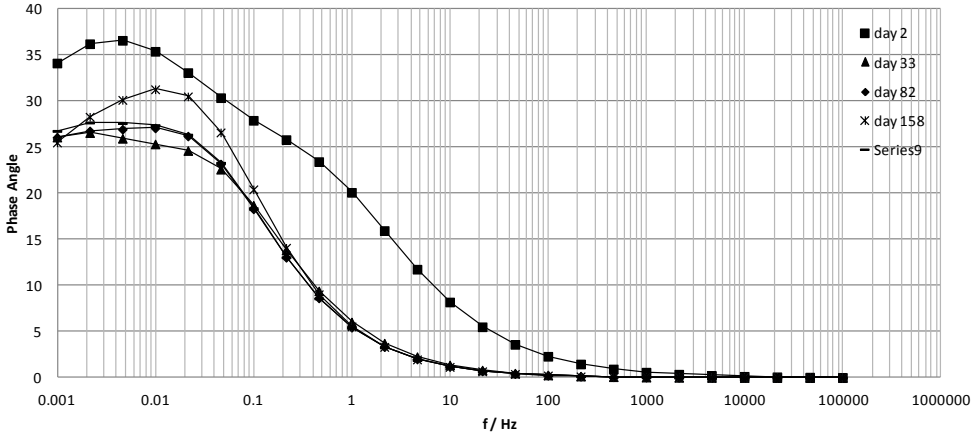

Figure B.6 EIS Phase Angle Bode Diagram. Test Sample FSR-R1-3.

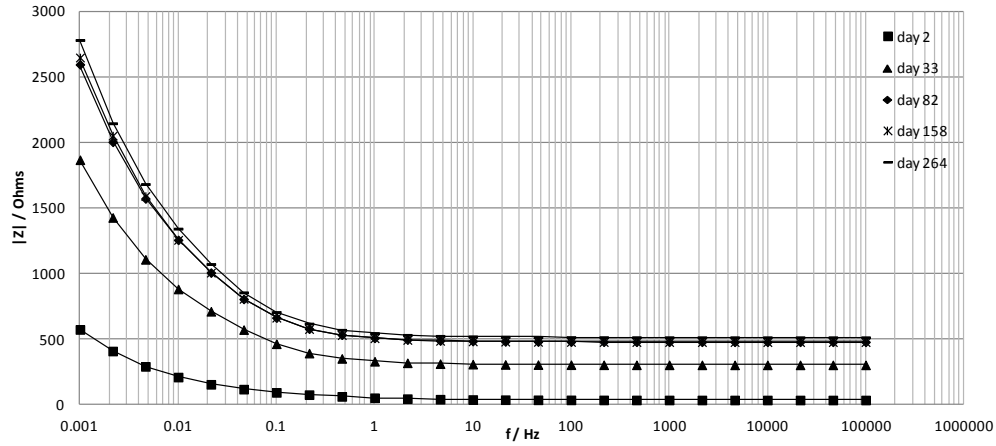

Figure B.7 EIS Modulus Bode Diagram. Test Sample FSR-R1-1.

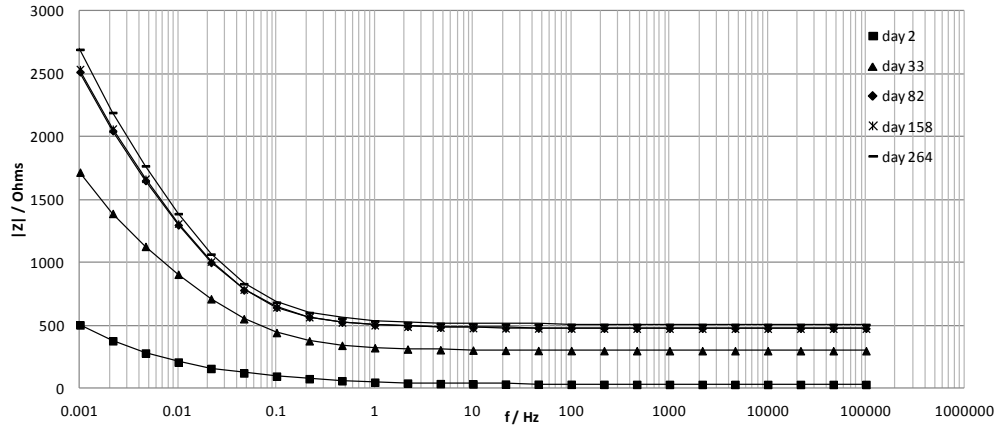

Figure B.8 EIS Modulus Bode Diagram. Test Sample FSR-R1-2.

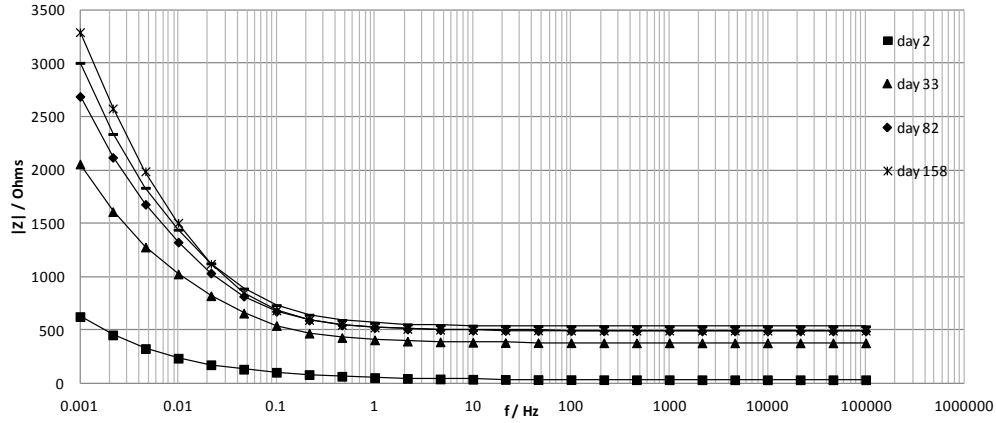

Figure B.9 EIS Modulus Bode Diagram. Test Sample FSR-R1-3.

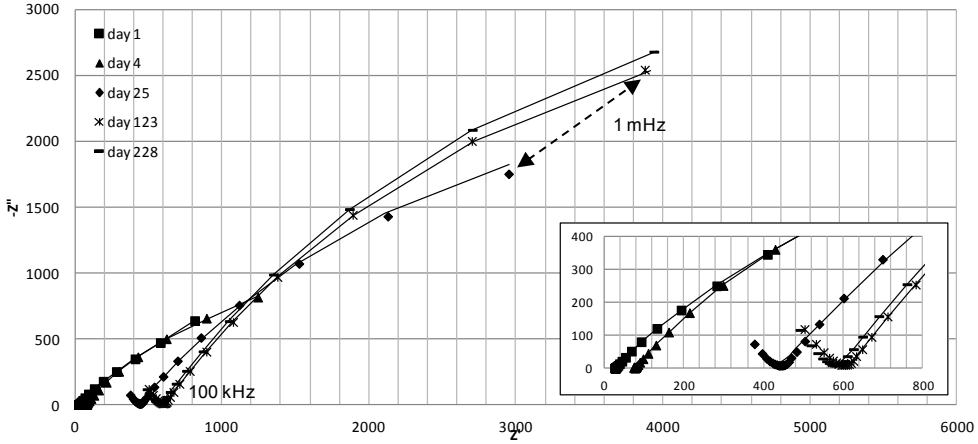

Figure B.10 EIS Nyquist Plot and best fit by Eq. 4.1. Test Sample FSR-R2-1.

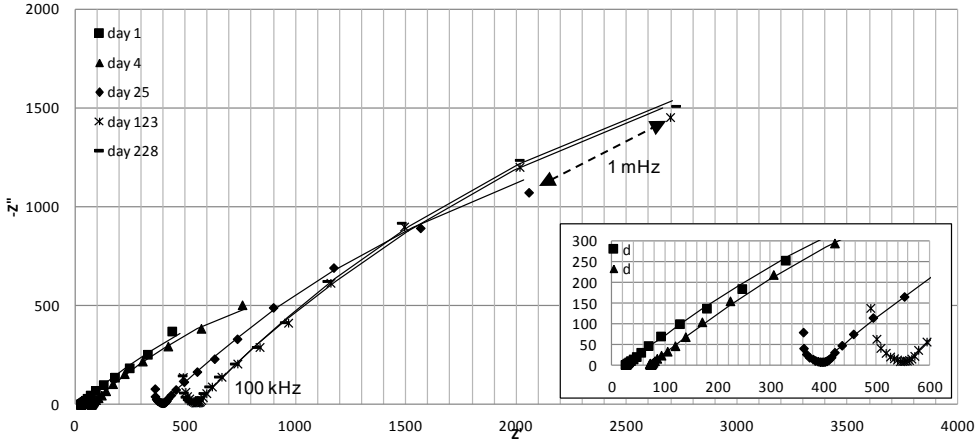

Figure B.11 EIS Nyquist Plot and best fit by Eq. 4.1. Test Sample FSR-R2-2.

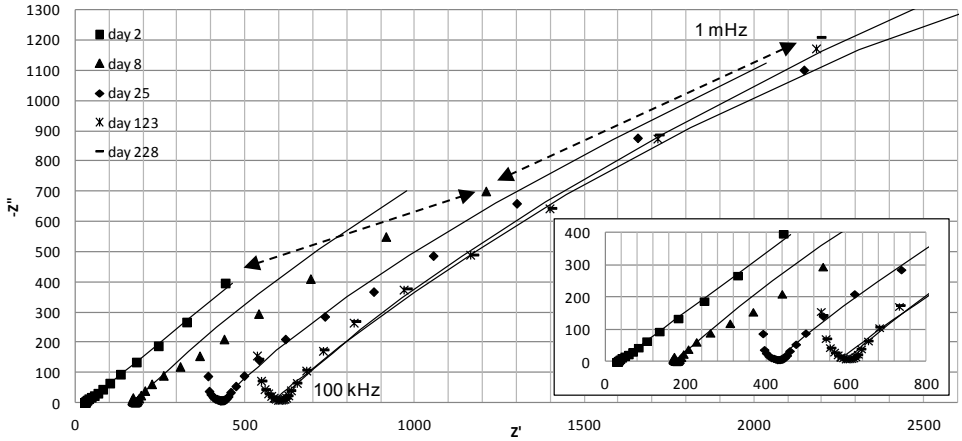

Figure B.12 EIS Nyquist Plot and best fit by Eq. 4.1. Test Sample FSR-R2-3.

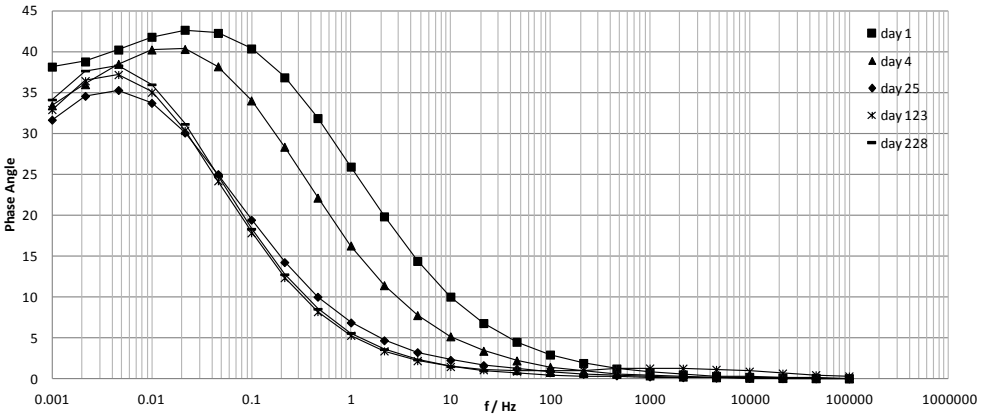

Figure B.13 EIS Phase Angle Bode Diagram. Test Sample FSR-R2-1.

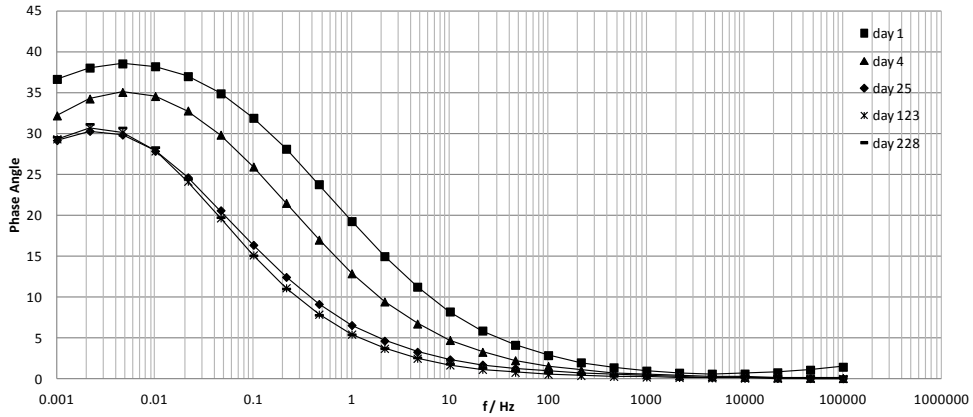

Figure B.14 EIS Phase Angle Bode Diagram. Test Sample FSR-R2-2.

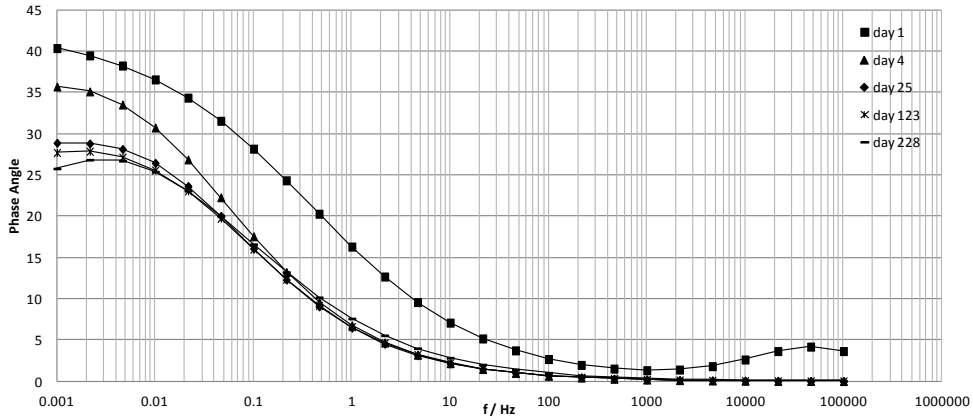

Figure B.15 EIS Phase Angle Bode Diagram. Test Sample FSR-R2-3.

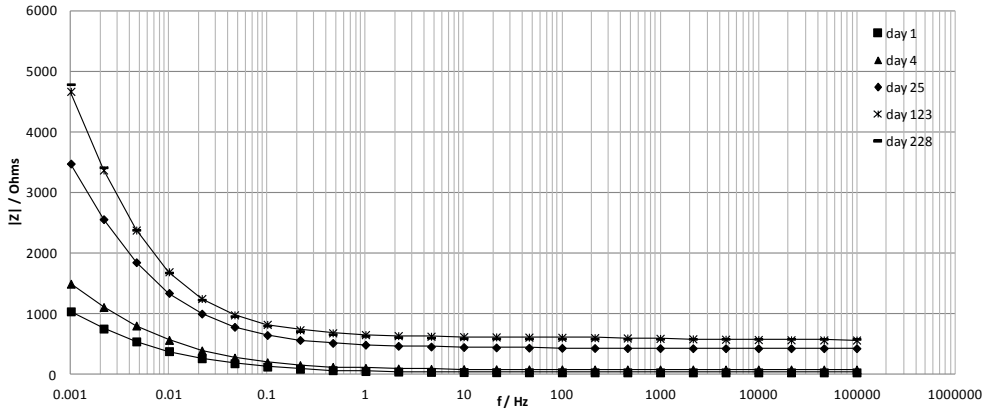

Figure B.16 EIS Modulus Bode Diagram. Test Sample FSR-R2-1.

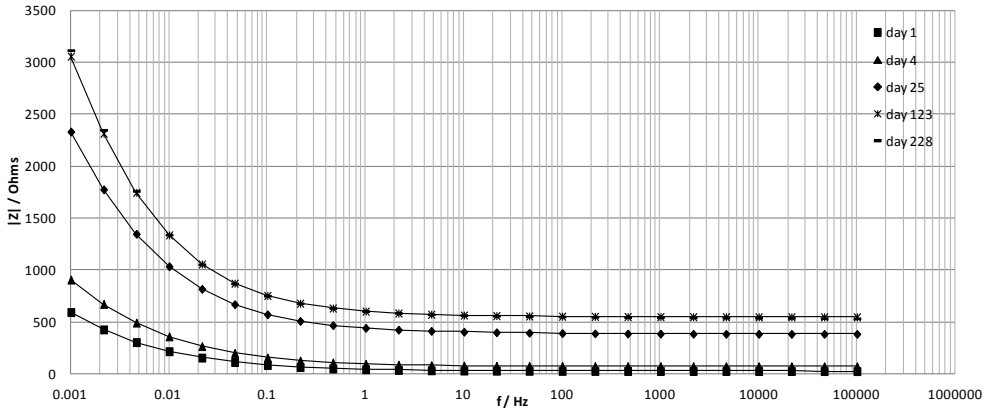

Figure B.17 EIS Modulus Bode Diagram. Test Sample FSR-R2-2.

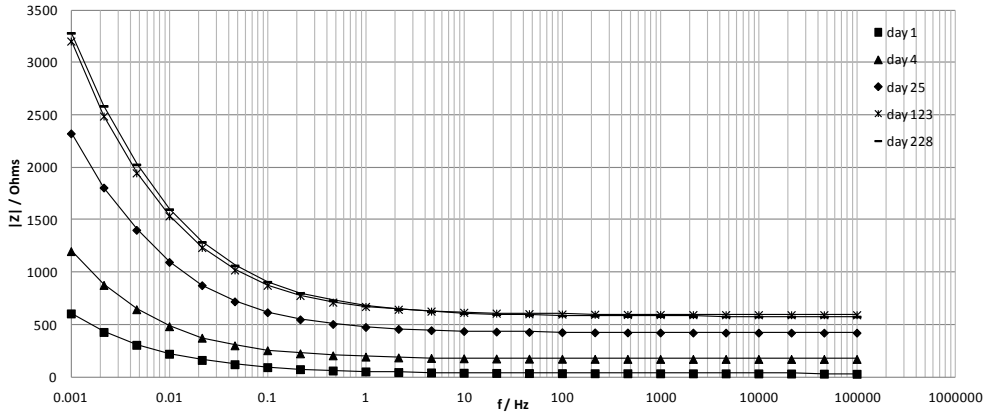

Figure B.18 EIS Modulus Bode Diagram. Test Sample FSR-R2-3.

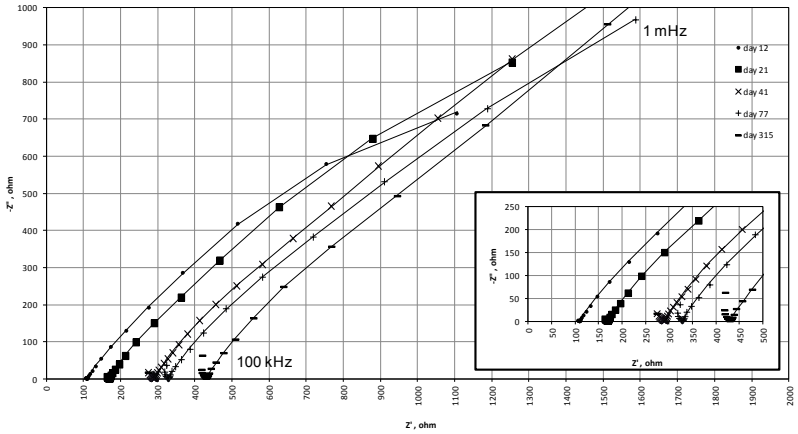

Figure B.19 EIS Nyquist Plot and best fit by Eq. 4.1. Test Sample FS-1.

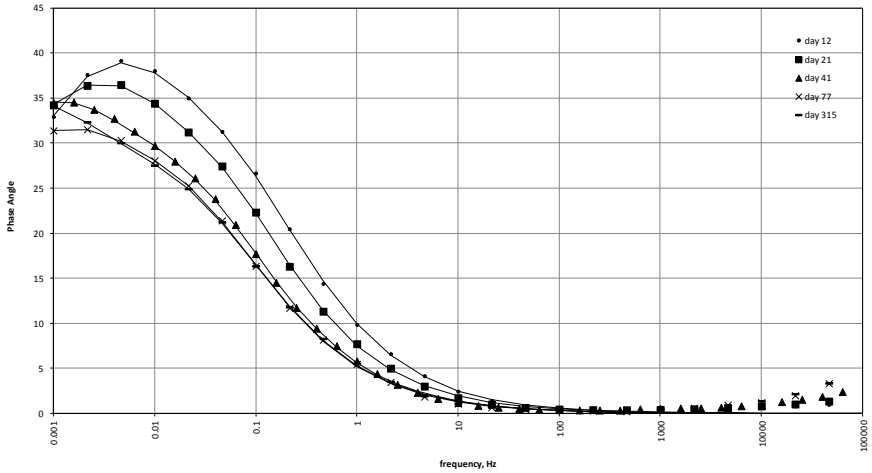

Figure B.20 EIS Phase Angle Bode Diagram. Test Sample FS-1.

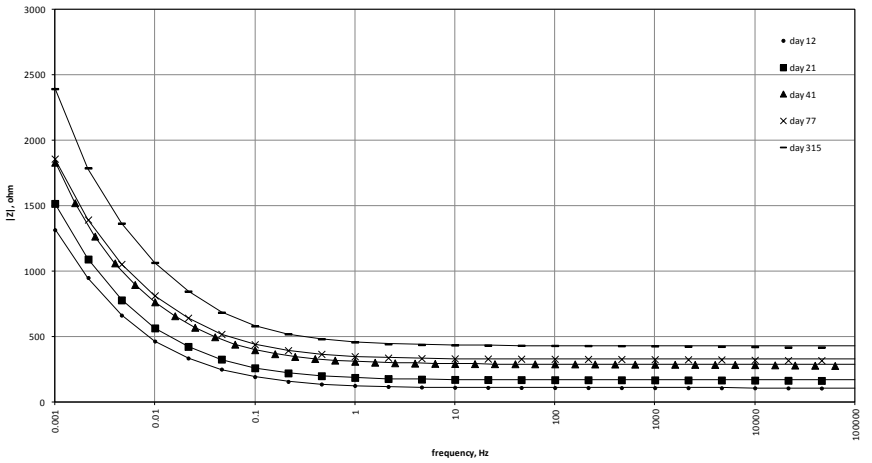

Figure B.21 EIS Modulus Bode Diagram. Test Sample FS-1.

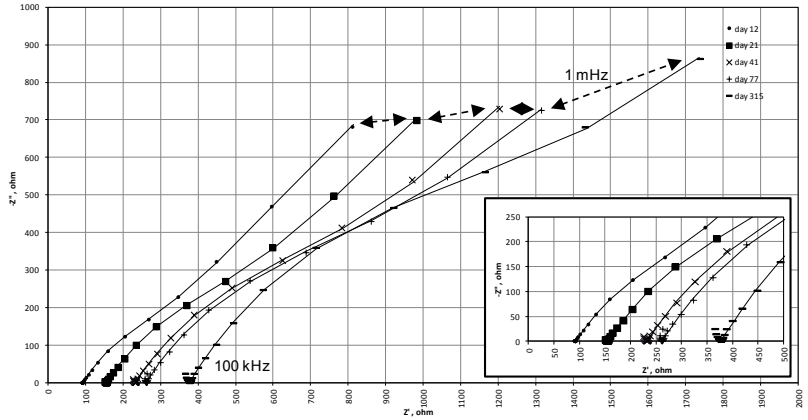

Figure B.22 EIS Nyquist Plot and best fit by Eq. 4.1. Test Sample FS-2.

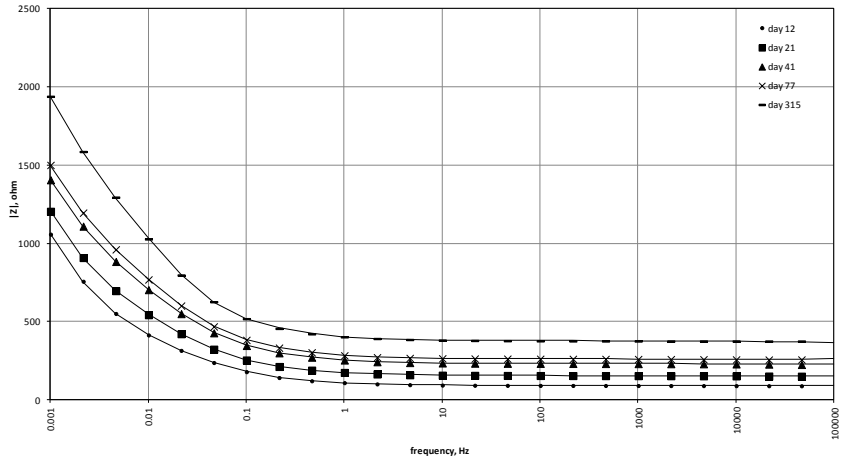

Figure B.23 EIS Phase Angle Bode Diagram. Test Sample FS-2.

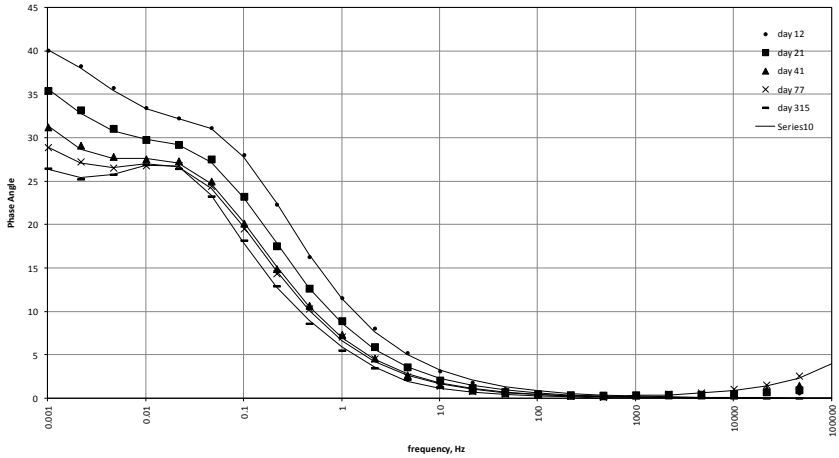

Figure B.24 EIS Modulus Bode Diagram. Test Sample FS-2.

APPENDIX C - RESULTS FLORIDA METHODS (FM) 5-516/X-RAY DIFFRACTION

Florida Department of Transportation
State Materials Office
Corrosion Research Laboratory
5007 NE 39th AVE
Gainesville, FL 32609
Phone: 352-955-6691 Fax: 352-955-6689

FM 5-516 CHLORIDE REPORT

Date Tested: February 22, 2012
Test Performed By: Jason Burchfield

Unit Weight: 3105 lb/yd^3 LIMS #: _____ Lab #: 2012-02-038

Description			Results (lb/yd^3)				Average	
			A	B	C	Range	ppm	lb/yd^3
Standard Solution	**Date:** 2/22/2012	**Expected Value:** 3.0					3.0	
Sample: S-CP-B1, Dissimilar PT Grout Project - Phase 1.								
Grout Material for Testing								
			0.338	0.326	0.332	0.0120	106.9	0.332

Testing performed in accordance with FM5-516
Florida Department of Transportation • State Materials Office • Corrosion Research Laboratory • Gainesville, FL 32609

Florida Department of Transportation
State Materials Office
Corrosion Research Laboratory
5007 NE 39th AVE
Gainesville, FL 32609
Phone: 352-955-6691 **Fax: 352-955-6689**

FM 5-516 CHLORIDE REPORT

Date Tested: February 22, 2012
Test Performed By: Jason Burchfield

Unit Weight: 3105 lb/yd^3 LIMS #: _____ Lab #: 2012-02-039

Description			Results (lb/yd^3)				Average	
			A	B	C	Range	ppm	lb/yd^3
Standard Solution	**Date:** 2/22/2012	**Expected Value:** 3.0					3.0	
Sample: S-CP-R1, Dissimilar PT Grout Project - Phase 1.								
Grout Material for Testing								
			0.335	0.345	0.323	0.0220	107.7	0.334

Testing performed in accordance with FM5-516
Florida Department of Transportation • State Materials Office • Corrosion Research Laboratory • Gainesville, FL 32609

Florida Department of Transportation
State Materials Office
Corrosion Research Laboratory
5007 NE 39th AVE
Gainesville, FL 32609
Phone: 352-955-6691 **Fax: 352-955-6689**

FM 5-516 CHLORIDE REPORT

Date Tested: February 22, 2012
Test Performed By: Jason Burchfield

Unit Weight: 3105 lb/yd^3 LIMS #: _____ Lab #: 2012-02-040

Description			Results (lb/yd^3)				Average	
			A	B	C	Range	ppm	lb/yd^3
Standard Solution	**Date:** 2-22-20012	**Expected Value:** 3.0					3.0	
Sample: S-CP-R2, Dissimilar PT Grout Project - Phase 1.								
Grout Material for Testing								
			0.171	0.171	0.168	0.0030	54.8	0.170

Testing performed in accordance with FM5-516
Florida Department of Transportation • State Materials Office • Corrosion Research Laboratory • Gainesville, FL 32609

Graphics

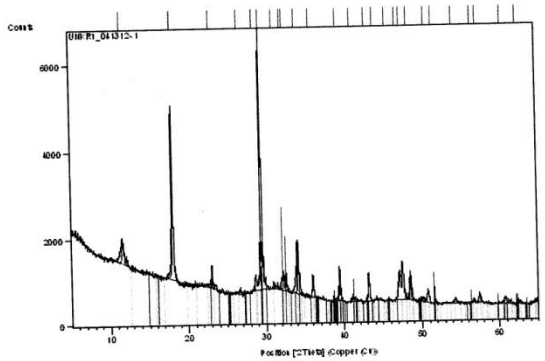

Pattern List

Ref.Code	Compound Name	Chem. Formula
01-086-2334	Calcite	Ca (C O3)
01-076-0571	Portlandite, syn	Ca (O H)2
01-076-1746	Gypsum	Ca S O4 (H2 O)2
00-055-0738	Calcium Silicate	Ca3 Si O5

Peak List

Pos.[°2Th.]	d-spacing[Å]	Rel.Int.[%]	Matched by
11.6561	7.59221	9.30	01-076-1746
18.0468	4.91550	65.21	01-076-0571
23.1026	3.84997	9.09	01-086-2334;00..
26.6287	3.34762	2.10	01-076-1746
28.6741	3.11331	5.41	01-076-0571;01..
29.4300	3.03505	100.00	01-086-2334;01..
31.2370	2.86348	1.31	01-086-2334;01..
32.2368	2.77692	7.16	01-076-1746;00..
32.5699	2.74928	6.94	00-055-0738
34.0815	2.63072	20.45	01-076-0571;00..
36.0109	2.49407	8.33	01-086-2334;01..
39.4356	2.28502	13.91	01-086-2334;01..
41.2022	2.19104	2.99	01-076-1746;00..
43.2075	2.09388	10.75	01-086-2334;01..
44.1415	2.05172	1.29	01-076-1746
45.7413	1.98362	0.79	01-076-1746;00..
47.1199	1.92875	10.50	01-086-2334;01..
47.5632	1.91180	14.80	01-086-2334;01..
48.5361	1.87573	11.05	01-086-2334;01..
50.7942	1.79752	5.17	01-076-0571;01..
51.7470	1.76664	1.48	00-055-0738
54.3366	1.68841	2.10	01-076-0571;01..
56.6839	1.62394	1.21	01-086-2334;01..

Date: 5/3/2012 Time: 2:41:32 PM File: UNKR1_041312~1 User: Chemical Lab

57.4153	1.60498	3.65	01-086-2334;01..
60.6631	1.52660	2.42	01-086-2334;01..
62.6027	1.48266	1.12	01-076-0571;01..

Date: 5/3/2012 Time: 2:41:01 PM File: UNKB1_041312~1 User: Chemical Lab

Graphics

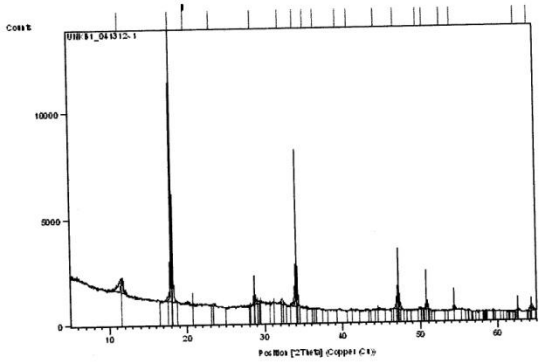

Pattern List

Ref.Code	Compound Name	Chem. Formula
01-076-0571	Portlandite, syn	Ca (O H)2
00-033-0306	Calcium Silicate H..	Ca1.5 Si O3.5 ·x H..
01-070-0982	Gypsum	Ca (S O4) (H2 O..
00-045-0156	Calcium Silicate	Ca Si O3

Peak List

Pos.[°2Th.]	d-spacing[Å]	Rel.Int.[%]	Matched by
11.7123	7.55589	5.18	01-070-0982
18.0710	4.90897	100.00	01-076-0571
20.1503	4.40688	0.48	
23.4181	3.79881	0.67	01-070-0982;00..
28.7262	3.10779	4.64	01-076-0571
32.1988	2.78011	2.25	00-033-0306;01..
34.1145	2.62825	20.44	01-076-0571;00..
35.3709	2.53772	0.68	01-070-0982
36.7205	2.44749	0.36	01-076-0571;01..
39.6732	2.27188	0.39	01-070-0982
41.1132	2.19557	0.56	00-045-0156
44.6194	2.03085	0.27	01-070-0982;00..
47.1329	1.92825	8.84	01-076-0571;01..
50.0149	1.82368	0.66	00-033-0306;01..
50.7823	1.79791	3.82	01-076-0571;01..
53.0558	1.72611	0.37	01-070-0982
54.3510	1.68800	1.99	01-076-0571;01..
62.5407	1.48521	0.75	01-076-0571;01..
64.2854	1.44785	1.73	01-076-0571;01..

Date: 5/3/2012 Time: 2:39:52 PM File: UNK7_47_011312~1 User: Chemical Lab

Graphics

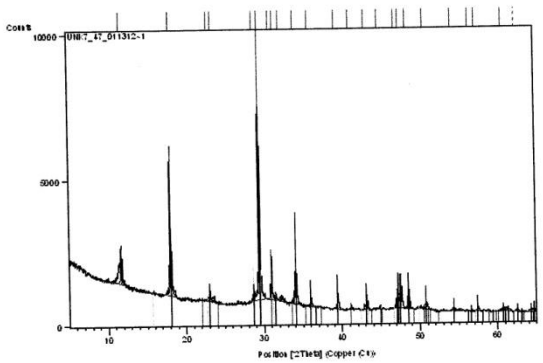

Pattern List

Ref.Code	Compound Name	Chem. Formula
01-086-2334	Calcite	Ca (C O3)
01-076-0571	Portlandite, syn	Ca (O H)2
00-006-0047	Gypsum	Ca S O4 ·2 H2 O
00-036-0426	Dolomite	Ca Mg (C O3)2

Peak List

Pos.[°2Th.]	d-spacing[Å]	Rel.Int.[%]	Matched by
11.7273	7.54623	13.38	00-006-0047
18.0581	4.91245	54.59	01-076-0571
23.0824	3.85328	4.19	01-086-2334
23.5468	3.77833	2.48	00-006-0047
28.7941	3.10061	2.91	01-076-0571
29.4496	3.03308	100.00	01-086-2334
30.9722	2.88735	18.82	00-006-0047;00..
31.5137	2.83897	2.67	01-086-2334
32.2832	2.77304	2.09	00-006-0047
34.1070	2.62881	14.68	01-076-0571
36.0071	2.49433	3.87	01-086-2334;00..
39.4664	2.28331	6.01	01-086-2334
41.1901	2.19165	1.50	00-036-0426
43.2122	2.09367	5.33	01-086-2334
44.9768	2.01554	1.15	00-036-0426
47.1262	1.92850	7.00	01-086-2334;01..
47.5759	1.91132	12.72	01-086-2334
48.5270	1.87606	6.70	01-086-2334;00..
50.8116	1.79695	3.24	01-076-0571;00..
54.3676	1.68752	1.36	01-076-0571;00..
56.6558	1.62468	0.75	01-086-2334;00..
57.4385	1.60439	1.86	01-086-2334;00..
60.9241	1.51943	0.94	01-086-2334;00..

Date: 5/3/2012 Time: 2:39:52 PM File: UNK7_47_011312~1 User: Chemical Lab

Graphics

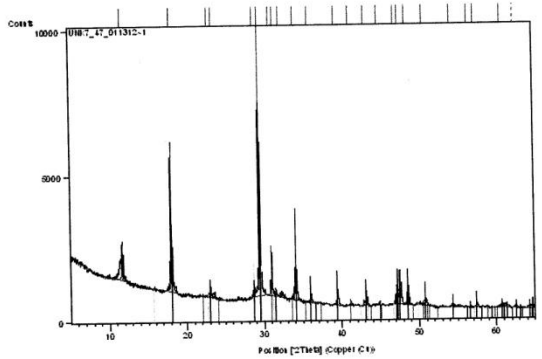

Pattern List

Ref.Code	Compound Name	Chem. Formula
01-086-2334	Calcite	Ca (C O3)
01-076-0571	Portlandite, syn	Ca (O H)2
00-006-0047	Gypsum	Ca S O4 ·2 H2 O
00-036-0426	Dolomite	Ca Mg (C O3)2

Peak List

Pos.[°2Th.]	d-spacing[Å]	Rel.Int.[%]	Matched by
11.7273	7.54623	13.38	00-006-0047
18.0581	4.91245	54.59	01-076-0571
23.0824	3.85328	4.19	01-086-2334
23.5468	3.77833	2.48	00-006-0047
28.7941	3.10061	2.91	01-076-0571
29.4496	3.03308	100.00	01-086-2334
30.9722	2.88735	18.82	00-006-0047;00..
31.5137	2.83897	2.67	01-086-2334
32.2832	2.77304	2.09	00-006-0047
34.1070	2.62881	14.68	01-076-0571
36.0071	2.49433	3.87	01-086-2334;00..
39.4664	2.28331	6.01	01-086-2334
41.1901	2.19165	1.50	00-036-0426
43.2122	2.09367	5.33	01-086-2334
44.9768	2.01554	1.15	00-036-0426
47.1262	1.92850	7.00	01-086-2334;01..
47.5759	1.91132	12.72	01-086-2334
48.5270	1.87606	6.70	01-086-2334;00..
50.8116	1.79695	3.24	01-076-0571;00..
54.3676	1.68752	1.36	01-076-0571;00..
56.6558	1.62468	0.75	01-086-2334;00..
57.4385	1.60439	1.86	01-086-2334;00..
60.9241	1.51943	0.94	01-086-2334;00..

Date: 5/3/2012 Time: 2:39:37 PM File: UNK7_32_041312~1 User: Chemical Lab

Graphics

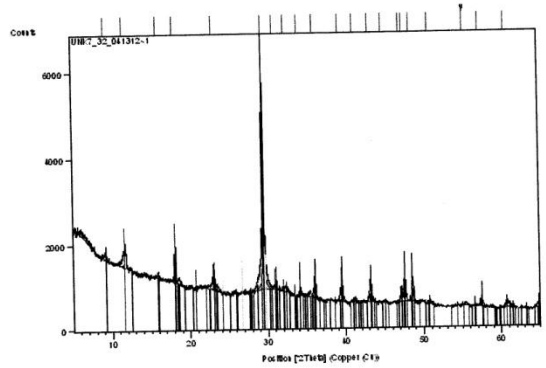

Pattern List

Ref.Code	Compound Name	Chem. Formula
01-085-1108	Calcite, syn	Ca C O3
01-078-0315	Portlandite, syn	Ca (O H)2
00-005-0622	Dolomite	Ca Mg (C O3)2
00-006-0047	Gypsum	Ca S O4 ·2 H2 O
00-046-1360	Thaumasite	Ca3 Si (O H)6 (..
00-023-1044	Calcium Silicate	Ca2 Si O4

Peak List

Pos.[°2Th.]	d-spacing[Å]	Rel.Int.[%]	Matched by
9.1831	9.63051	2.27	00-046-1360
11.7119	7.55617	8.62	00-006-0047
15.9221	5.56632	1.98	00-046-1360;00..
18.1037	4.90019	23.45	01-078-0315;00..
23.1317	3.84519	10.09	01-085-1108
29.4764	3.03038	100.00	01-085-1108
31.0089	2.88402	8.35	00-005-0622;00..
32.3729	2.76555	2.09	00-023-1044
34.1103	2.62856	5.94	01-078-0315
36.0584	2.49090	9.19	01-085-1108;00..
39.4776	2.28269	13.53	01-085-1108;00..
41.1876	2.19178	1.73	00-005-0622;00..
43.2483	2.09200	12.62	01-085-1108;00..
45.0161	2.01387	0.79	00-005-0622
47.1552	1.92739	5.45	01-085-1108;01..
47.6044	1.91024	11.09	01-085-1108;00..
48.5667	1.87462	10.74	01-085-1108;00..
50.8946	1.79421	0.90	01-078-0315;00..
55.4415	1.65735	1.19	
57.4906	1.60306	4.18	01-085-1108;00..
60.7260	1.52391	2.36	01-085-1108;00..

Graphics

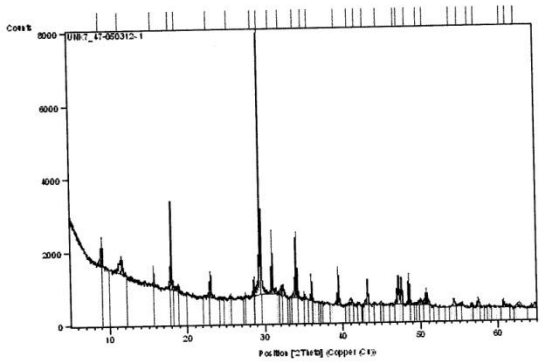

Pattern List

Ref.Code	Compound Name	Chem. Formula
01-086-2334	Calcite	Ca (C O3)
00-044-1481	Portlandite, syn	Ca (O H)2
00-036-0426	Dolomite	Ca Mg (C O3)2
00-041-1451	Ettringite, syn	Ca6 Al2 (S O4)3 ..
01-076-1746	Gypsum	Ca S O4 (H2 O)2

Peak List

Pos.[°2Th.]	d-spacing[Å]	Rel.Int.[%]	Matched by
9.1017	9.71639	10.29	00-041-1451
11.6715	7.58218	5.82	01-076-1746
15.7869	5.61372	4.91	00-041-1451
18.0232	4.92188	33.88	00-044-1481;00..
18.9164	4.69145	2.02	00-041-1451
23.0628	3.85652	9.76	01-086-2334;00..
25.6516	3.47288	1.32	00-041-1451
28.6734	3.11340	7.13	00-044-1481;00..
29.4110	3.03697	100.00	01-086-2334
30.9437	2.88995	23.97	00-036-0426
32.2603	2.77495	4.43	00-041-1451;01..
34.0732	2.63134	25.23	00-044-1481
35.0902	2.55737	1.69	00-041-1451
35.9754	2.49645	9.20	01-086-2334;00..
39.4315	2.28525	14.69	01-086-2334;01..
41.1218	2.19514	2.93	00-036-0426
42.0254	2.15001	0.60	00-041-1451
43.1864	2.09485	10.07	01-086-2334
44.8924	2.01913	0.75	00-036-0426;00..
47.0912	1.92986	11.07	01-086-2334;00..
47.5166	1.91357	10.14	01-086-2334;01..
48.5401	1.87559	11.92	01-086-2334;00..

Date: 5/3/2012 Time: 2:39:21 PM File: UNK7_47-050312~1 User: Chemical Lab

49.9764	1.82500	1.79	00-041-1451;01..
50.7725	1.79824	5.98	00-044-1481;01..
54.3137	1.68907	2.79	00-044-1481;01..
55.2771	1.66189	1.02	00-041-1451;01..
56.5976	1.62621	1.53	01-086-2334;00..
57.4358	1.60445	3.68	01-086-2334;00..
60.6995	1.52577	2.81	01-086-2334;01..
61.4883	1.50808	1.12	01-086-2334;00..
62.6249	1.48219	1.44	00-044-1481;01..

Date: 5/3/2012 Time: 2:37:11 PM File: UNK7_32-050312~1 User: Chemical Lab

Graphics

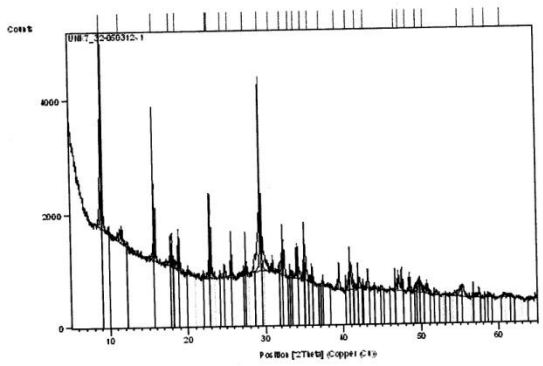

Pattern List

Ref.Code	Compound Name	Chem. Formula
01-086-2334	Calcite	Ca (C O3)
01-087-0673	Portlandite, syn	Ca (O H)2
00-001-0942	Dolomite	Ca O · Mg O ·2 C O2
01-074-1433	Gypsum	Ca (S O4) (H2 O..
00-041-1451	Ettringite, syn	Ca6 Al2 (S O4)3 ..

Peak List

Pos.[°2Th.]	d-spacing[Å]	Rel.Int.[%]	Matched by
9.1250	9.69164	92.39	00-041-1451
11.6228	7.61385	7.45	01-074-1433
15.8474	5.59240	37.37	00-041-1451
18.0500	4.91463	17.00	01-087-0673
18.8980	4.69598	20.38	00-041-1451
22.9321	3.87499	32.15	01-086-2334;00..
23.0375	3.86070	32.62	01-086-2334;00..
24.7672	3.59485	6.06	00-041-1451
25.6561	3.47229	12.72	00-041-1451
27.6166	3.23008	5.63	00-041-1451
29.4243	3.03562	100.00	01-086-2334
30.9428	2.89003	8.48	00-001-0942;01..
32.3180	2.77013	17.52	00-041-1451
33.4340	2.68017	3.59	00-001-0942;01..
34.0798	2.63085	17.79	01-087-0673;00..
35.0133	2.56282	20.11	00-001-0942;00..
36.0121	2.49399	9.52	01-086-2334;01..
37.4063	2.40418	2.98	00-001-0942;01..
39.4577	2.28379	14.69	01-086-2334;01..
40.8542	2.20889	12.00	01-074-1433;00..
42.0538	2.14861	5.41	01-074-1433;00..
43.1785	2.09522	9.72	01-086-2334;01..

Date: 5/3/2012 Time: 2:37:11 PM File: UNK7_32-050312~1 User: Chemical Lab

47.0962	1.92966	10.33	01-086-2334;01..
47.5520	1.91223	11.50	01-086-2334;01..
48.5435	1.87546	9.57	01-086-2334;01..
49.8080	1.83077	6.37	00-041-1451
50.7836	1.79787	7.03	01-087-0673;00..
55.3064	1.66108	5.92	01-074-1433;00..
57.4486	1.60413	4.58	01-086-2334;01..
58.7757	1.57104	1.45	00-001-0942;01..
60.7487	1.52339	1.89	01-086-2334;01..

Date: 5/3/2012 Time: 2:34:57 PM File: UNK7_21_041312~1 User: Chemical Lab

Graphics

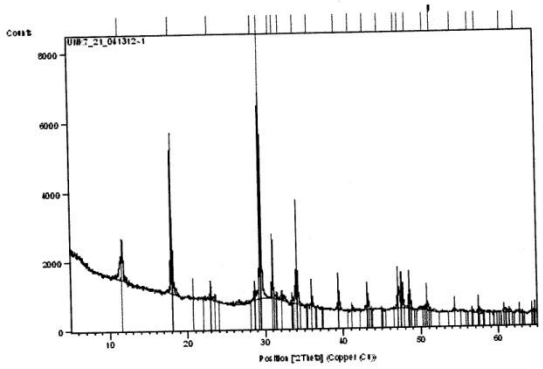

Pattern List

Ref.Code	Compound Name	Chem. Formula
01-086-2334	Calcite	Ca (C O3)
01-087-0673	Portlandite, syn	Ca (O H)2
00-036-0426	Dolomite	Ca Mg (C O3)2
00-006-0047	Gypsum	Ca S O4 ·2 H2 O

Peak List

Pos.[°2Th.]	d-spacing[Å]	Rel.Int.[%]	Matched by
11.7085	7.55831	15.15	00-006-0047
18.0536	4.91368	60.37	01-087-0673
23.0987	3.85061	5.07	01-086-2334
28.6958	3.11102	4.09	01-087-0673
29.4479	3.03325	100.00	01-086-2334
30.9791	2.88673	25.18	00-036-0426;00..
31.4962	2.84051	2.75	01-086-2334
32.2103	2.77914	3.59	00-006-0047
34.1138	2.62830	16.89	01-087-0673
35.9939	2.49521	3.74	01-086-2334;00..
39.4549	2.28395	7.78	01-086-2334
41.1834	2.19199	1.81	00-036-0426
43.1960	2.09441	5.37	01-086-2334
44.9104	2.01836	0.80	00-036-0426
47.1220	1.92867	8.16	01-086-2334;01..
47.5806	1.91114	14.09	01-086-2334
48.5512	1.87518	7.91	01-086-2334;00..
50.8063	1.79712	3.59	01-087-0673;00..
51.7924	1.76520	0.98	
54.3282	1.68865	1.64	01-087-0673;00..
56.6253	1.62548	1.07	01-086-2334;00..
57.5694	1.60105	1.81	01-086-2334;00..
60.7288	1.52510	1.50	01-086-2334;00..

Date: 5/3/2012 Time: 2:32:42 PM File: UNK7_21-050312~1 User: Chemical Lab

Graphics

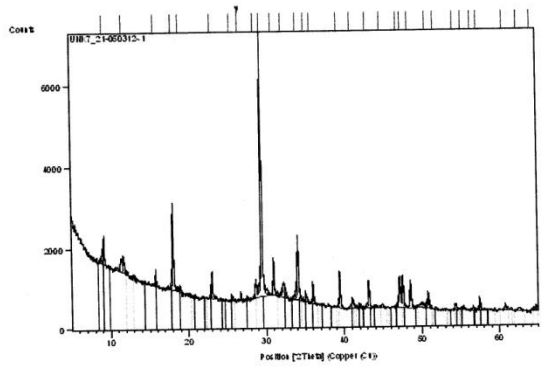

Pattern List

Ref.Code	Compound Name	Chem. Formula
01-086-2334	Calcite	Ca (C O3)
01-087-0673	Portlandite, syn	Ca (O H)2
00-036-0426	Dolomite	Ca Mg (C O3)2
01-072-0596	Gypsum	Ca (S O4) (H2 O..
00-013-0350	Ettringite	Ca6 Al2 (S O4)3 ..

Peak List

Pos.[°2Th.]	d-spacing[Å]	Rel.Int.[%]	Matched by
9.1643	9.65015	10.20	00-013-0350
11.7317	7.54345	5.60	01-072-0596
15.8413	5.59453	4.42	00-013-0350
18.0661	4.91031	33.66	01-087-0673
18.9675	4.67892	2.21	00-013-0350
23.0990	3.85056	10.12	01-086-2334
25.6883	3.46801	1.64	00-013-0350
26.7174	3.33671	2.53	
28.6918	3.11144	7.28	01-087-0673
29.4425	3.03379	100.00	01-086-2334;00..
30.9715	2.88742	14.84	00-036-0426;01..
32.2207	2.77827	6.00	01-072-0596
34.1180	2.62799	25.36	01-087-0673
35.1063	2.55624	2.51	00-013-0350
36.0108	2.49408	8.67	01-086-2334;01..
39.4653	2.28337	14.31	01-086-2334;01..
41.1227	2.19509	3.66	00-036-0426
43.2049	2.09400	10.47	01-086-2334
44.9748	2.01563	1.59	00-036-0426
47.1316	1.92830	11.45	01-086-2334;01..
47.5593	1.91195	12.81	01-086-2334;01..
48.5843	1.87398	10.51	01-086-2334;01..

REFERENCES

American Concrete Institute Committee 423. (2010). *Report on Corrosion and Repair of Grouted Multistrand and Bar Systems (ACI 423.8R-10).* Farmington Hills, MI: American Concrete Institute.

Bentur, A., Diamond, S., & Berke, N. (1997). *Steel Corrosion in Concrete, Fundametals and Civil Engineering Practice.* London: E & FN Spon.

Bertolini, L., & Carsana, M. (2011). *High pH Corrosion of Prestressing Steel in Segregated Grout.* Milano, Italy: Dipartimento di Chimica, Materiali e Ingegneria Chimica "G. Natta", Politecnico di Milano.

Bricker, M. D., & Schokker, A. (2005). *Corrosion from Bleed Water in Grouted Post-Tensioned Tendons.* Skokie, IL: Portland Cement Association.

Brown, J. L. (2002). Landmarks in American Civil Engineering: Sunshine Skyway Bridge. *America Society of Civil Engineers, volume no. 72(11),*, pp. 162-163.

Bushman, J. B. (2012). *Calculation of Corrosion Rate from Corrosion Current (Faraday's Law).* Medina, OH: Bushman & Associates, Inc.

Cabeza, M., Keddam, M., Nóvoa, X., Sánchez, I., & Takenouti, H. (2006). Impedance Spectroscopy to Characterize the Pore Structure During the Hardening Process of Portland Cement Paste. *Electrochemica Acta, 51*, 1831-41.

Cabeza, M., Merino, P., P. Miranda, X. N., & Sánchez, I. (2002). Impedance Spectroscopy Study of Hardened Portland Cement Paste. *Cement and Concrete Research, 32*, 881-91.

Corven Engineering, Inc. (2001). *Mid-Bay Bridge Post-Tensioning Evaluation - Final Report.* Tallahassee, FL: FDOT.

Corven, J. (2001). *Mid Bay Bridge Post Tensioning Evaluation.* Tallahassee, FL: FDOT.

Corven, J., & Moreton, A. (2004). *Post-Tensioning Tendon Installation and Grouting Manual.* Washington, DC: FHWA.

FDOT. (2002). *Sunshine Skyway Bridge Tendons Investigation .* Tallahasse, FL: FDOT.

FDOT. (2002a). *New Directions for Florida Post-Tensioned Bridges.* Tallahassee, FL: FDOT.

FDOT. (2009). Specification 938 POST-TENSIONING GROUT. *Standard Specification for Road and Bridge Construction*, Rev. 4-28-11(FA 6-30-11)(1-12).

FDOT. (2010). *Standard Specifications for Road and Bridge Construction.* Tallahassee, FL: FDOT.

FDOT. (2011). Specification 462 POST-TENSIONING GROUT. *Standard Specification for Road and Bridge Construction*, Rev. 7-21-11(FA 7-28-11)(1-12).

Gamry Instruments. (2010). *Getting Started with Electrochemical Corrosion Measurements.* Warmister, PA: Gamry Instruments.

Gamry Instuments. (2009). *Basics of Electrochemical Impedance Spectroscopy.* Warminster, PA: Gamry Instruments.

González, J., Ramírez, E., Bautista, A., & Feliu, S. (1995). The Behavior of Pre-Rusted Steel in Concrete. *Cement and Concrete Research*, 501-511.

Gouda, V. (1970). Corrosion and Corrosion Inhibition of Reinforcing Steel: I.Immersed in Alkaline Solution. *British Corrosion Journal*, 198-203.

H. Wang, A. S. (2005). *Corrosion of Post-Tensioning Strands.* Tallahassee, FL: FDOT.

Hamilton, H., Schokker, A., Vivas, E., Pacheco, A. R., Brooks, M. A., Shukla, K., . . . Bergin, M. (2006). *Development of a Standard Accelerated Corrosion Test for Acceptance of Post-Tensioning Grouts in Florida.* Gainesville, FL: Department of Civil and Coastal Engineering, Univeristy of Florida.

Hansson, M., Poursaee, A., & Jaffer, S. (2007). *Corrosion of Reinforcing Bars in Concrete.* Skokie, IL: Portland Cement Association.

Hartt, W., & Venugopalan, S. (2002). *Corrosion Evaluation of Post Tensiones Tendons on the Mid Bay Bridge in Destin, Florida.* Tallahassee, FL: FDOT.

Hooton, D., & Thomas, M. D. (2002). *The Use of Limestone in Portland Cements: Effect on Thaumasite Form of Sulfate Attack.* Skokie, IL: Portlan Cement Association.

Jaggi, S., Bohni, H., & Elsener, B. (2001). Macrocell Corrosion of Steel in Concrete - Experiments in Numerical Modeling. *Eurocorr 2001* (pp. 1-11). Riva di Garda, Italy: Associazione Italiana Metallurgica.

Jones, D. A. (1996). *Principles and Prevention of Corrosion, Secon Edition.* Upper Saddle River, NJ: Prentice-Hall, Inc.

Keddam, M., Takenouti, H., Nóvoa, X., Andrade, C., & Alonso, C. (1997). Impedance Measurements on Cement Paste. *Cement and Concrete Research, 27*, 1191-201.

Kingsley Lau, Ivan Lasa, Mario Paredes. (2011). *Corrosion Development of PT Tendons with Defficient Grout: Corroosion Failure in Ringling Causeway Bridge .* Gainesville, FL: Unpublisehd Work.

Lau, K., & Sagües, A. (2007). Coating Condition Evaluations of Epoxy Coated Rebars. *ECS Transactions, 3*, 81-92.

Lau, K., Paredes, M., & Rafols, J. C. (2012). Corrosion Evaluation of Post-Tensioned Tendons with Dissilar Grout. *NACE International Corrosion 2012* (pp. 1-16). Salt Lake City, UT: NACE International.

Luca Bertolini, B. E. (2004). *Corrosion of Steel in Concrete.* New Jersey, USA: Wiley-VCH.

Methods of Prestressing in Concrete. (2011). *www.wordpress.com.*

Novak, P., Mala, R., & L.Joska. (2001). Influence of pre-rusting on steel corrosion in concrete. *Cement and Concrete Research*, 589-593.

Parsons Brinckerhoff Quade and Douglas, Inc. (2001). *Sunshine Skyway Bridge Post-Tensioned Tendons Investigation.* Tallahassee, FL: FDTO.

Popov, B. N. (2002). *Basic of Corrsosion Measurements.* Retrieved from Univesity of North Carlona, College of Engineering and Computing, Chemical Engineering: http://www.che.sc.edu/faculty/popov/drbnp/ECHE789b/Corrosion%20Measurements.pdf

Portland Cement Association. (2012). *Concrete Technology - Durability*. Retrieved from www.cement.org: http://www.cement.org/tech/cct_dur_corrosion.asp

Post-Tensioning Institute. (2003). *Specification for Grouting of Post-Tensioned Structures .* Farmington Hills, MI: Post-Tensioning Institute.

Powers, R. (1999). *Corrosion Evaluation of Post-Tensioned Tendons on the Niles Channel Bridge.* Tallahassee, FL: FDOT.

Sagües, A. (2005). *Corrosion of Post-Tensioning Strands.* Tallahassee, FL: FDOT.

Sagües, A. A. (1993). Corrosion Measurement Techniques for Steel in Concrete. *NACE Corrosion 1993* (pp. 1-21). Houston, TX: NACE International.

Sagües, A., Karins, F. C., & Lau, K. (2011). *Corrosion Characteristics of Post-Tensioned Strands in Ungrouted Ducts.* Tampa, FL: FDOT.

Salas, R., Schokker, A., West, J., Breen, J., & Kreger, M. (2004). *Conclusions, Recommendations and Design Guidelines for Corrosion Protection of Post-Tensioned Bridges.* Austin, TX: FHWA.

Schokker, A. J., Koester, B., Breen, J. E., & Kreger, M. E. (1999). *Development of High Performance Grouts for Bonded Post-Tensioned Structures.* Center for Transportation Research, Univeristy of Texas: Asutin, TX.

Segunpta, A., & Devdas, M. (2012). *Prestressed Concrete Structures.* Retrieved from http://nptel.iitm.ac.in/courses/IIT-MADRAS/PreStressed_Concrete_Structures/pdf/1_Introduction/1.2_Advantages_Types%20of%20Prestressing.pdf.

Song, H. W., & Saraswathy, V. (2007). Corrosion Monitoring of Reinforced Concrete Structures - A Review. *International Journal of Electrochemical Science*, 1-28.

Sprinkel, M. M. (2009). *Varina Enon Tendon Failure.* Charlottesville, VA: Virginia Transportation Research Council.

Trejo, D., Hueste, M. B., Gardoni, P., Pillai, R. G., Kenneth Reinsnschmidt, S. B., Hurlebaus, S., . . . Ngo, T. T. (2009a). *Effect of Voids in Grouted, Post-Tensioned Concrete Bridge Construction: Volume*

1 - Electrochemical Testing and Reliability Assesment. Austin, TX: Texas Department of Transportation.

Trejo, D., Im, S. B., Pillai, R. G., Hueste, M. B., Gardoni, P., Hurlebaus, S., & Gamble, M. (2009). *Effect of Voids in Grouted Post-Tesioned Concrete Bridge Construction: Inspection and Repair Manual for External Tendons in Segmental, Post-Tensioned Bridges.* Austin, TX: Texas Transportation Institute.

U.S. Department of Transportation/Fedral Highway Administration. (2000). *Materials and Methods for Corrosion Control of Reiforced and Prestressed Concrete Structures in New Construction.* McLean, VA: FHWA.

Verma, N., & Balasubramanian, R. (2007). *Corrosion of Steel Reinforcements in Concrete.* Kanpur, India: Indian Institute of Tecnology.

Videm, K. (1998). Field and Laboratory Experience with Electrochemical Methods for Assesing Corrosion of Steel in Concrete. *Materials Science Forum*, 3-14.

VSL International, Inc. (2002). *Grouting of Post-Tensioning Tendons.* Lyssach, Switzerland: VSL International, LTD.

VITA

Juan Carlos Rafols was born . He completed his bachelor's degree in civil engineering in 1998 from the University of Puerto Rico, Mayaguez Campus. After working for various construction companies as a project manager, civil engineer, and establishing a construction company, he moved to North Florida in 2008. He started his graduate studies in civil engineering at the University of North Florida in August 2010.

Mr. Rafols is a certified Professional Engineer (PE) by the Puerto Rico Department of State, recipient of the Edgar Danciger fellowship from the University of North Florida in 2011 and member of the Phi Kappa Phi honor society.

Mr. Rafols expects to obtain his Master's of Science in Civil Engineering in 2012.

Part of the work on this thesis was presented and published at the National Association of Corrosion Engineers conference proceedings and technical symposia at the Corrosion 2012 Conference and Expo celebrated in March 2012 in Salt Lake City, Utah.